Sequential ultrasonic spot welding of thermoplastic composites

An experimental study on the welding process and the mechanical behaviour of (multi-)spot welded joints

Zhao, Tian

DOI
10.4233/uuid:b4f772b3-c9ea-4760-b68e-a8c85fd099b6

Publication date
2018

Document Version
Final published version

Citation (APA)
Zhao, T. (2018). *Sequential ultrasonic spot welding of thermoplastic composites: An experimental study on the welding process and the mechanical behaviour of (multi-)spot welded joints*. [Dissertation (TU Delft), Delft University of Technology]. https://doi.org/10.4233/uuid:b4f772b3-c9ea-4760-b68e-a8c85fd099b6

SEQUENTIAL ULTRASONIC SPOT WELDING OF THERMOPLASTIC COMPOSITES

AN EXPERIMENTAL STUDY ON THE WELDING PROCESS AND THE MECHANICAL BEHAVIOUR OF (MULTI-)SPOT WELDED JOINTS

SEQUENTIAL ULTRASONIC SPOT WELDING OF THERMOPLASTIC COMPOSITES

AN EXPERIMENTAL STUDY ON THE WELDING PROCESS AND THE MECHANICAL BEHAVIOUR OF (MULTI-)SPOT WELDED JOINTS

Proefschrift

ter verkrijging van de graad van doctor
aan de Technische Universiteit Delft,
op gezag van de Rector Magnificus prof. dr. ir. T.H.J.J. van der Hagen,
voorzitter van het College voor Promoties,
in het openbaar te verdedigen op maandag 14 mei 2018 om 15:00 uur

door

Tian ZHAO

Master of Science in Engineering Mechanics,
China University of Mining and Technology (Beijing), Beijng, China,
geboren te Yangquan, Shanxi, China.

Dit proefschrift is goedgekeurd door de

promotor: prof. dr. ir. R. Benedictus
copromotor: dr. I. Fernandez Villegas

Samenstelling promotiecommissie:

Rector Magnificus,	voorzitter
Prof. dr. ir. R. Benedictus,	Technische Universiteit Delft
Dr. I. Fernandez Villegas,	Technische Universiteit Delft
Onafhankelijke leden:	
Prof. dr. I. M. Richardson	Technische Universiteit Delft
Prof. dr. M. Rutner	Technische Universität Hamburg, Duitsland
Prof. dr. F. Balle	University of Freiburg, Duitsland
Prof. dr. C. Dransfeld	Fachhochschule Nordwestschweiz, Zwitserland
Prof. dr. C. Bisagni	Technische Universiteit Delft, reservelid

Keywords: Thermoplastic composites, Ultrasonic spot welding, Mechanical behaviour, Fractographic analysis

Printed by: ProefschriftMaken || www.proefschriftmaken.nl

Front & Back: Sequential ultrasonic multi-spot welding on the front cover, and the comparison of the fracture surfaces between spot welded and mechanically fastened joints on the back cover.

ISBN 978-94-6295-916-3

An electronic version of this dissertation is available at
http://repository.tudelft.nl/.

To my family and my belief

Tian Zhao

SUMMARY

The popularity of thermoplastic composites (TPCs) has been growing steadily in the last decades in the aircraft industry. This is not only because of their excellent material properties, but also owing to their fast and cost-effective manufacturing process. Fusion bonding, or welding, is a typical joining method for TPCs due to the intrinsic properties of thermoplastic polymers. Among different welding technologies, ultrasonic welding has been regarded as one of the most promising techniques for the assembly of TPC components. Ultrasonic welding is by nature a spot welding technique. As it is known that a series of problems result from using mechanical fasteners for joining composite structures, e.g. breaking fibres during drilling and extensive labour work, ultrasonic spot welding can be considered as a promising alternative from the perspective of fast manufacturing cycle. However, fundamental understanding is still lacking to achieve application of ultrasonic spot welding in composite structures to be achieved:

- An appropriate welding procedure is deemed necessary to be defined for ultrasonic spot welding. With the consideration of welding large composite structures, this procedure is expected to provide welded spots with consistent quality in sequential multi-spot welding process.
- The mechanical behaviour and the failure mechanisms of spot welded joints are still unknown. Less is known regarding the comparison of these properties between spot welded and mechanically fastened joints.

Consequently, the focus of this thesis is to systematically investigate ultrasonic spot welding of TPCs and the mechanical behaviour of the spot welded joints. The research started from the definition of a welding procedure for single-spot welded joints and a preliminary investigation of their mechanical behaviour and failure mechanisms. These two characteristics were compared with welded joints and mechanically fastened joints assembled with a single fastener. After that, towards the development of the high-quality multi-spot welded (MSW) joints, it was investigated how changes in the boundary conditions would affect the proposed welding procedure and thereby the quality of the welded joints. A welding procedure which is less sensitive to the changing boundary conditions was proposed. This procedure was further assessed in producing double-spot welded joints. As a final step, effects of geometric parameters on the strength of MSW joints were assessed.

A procedure for ultrasonic spot welding was defined by using spot energy directors and a specific sonotrode. Single-spot welded joints were produced using energy-controlled welding. Regarding the mechanical evaluation, both in-plane and out-of-plane mechanical behaviours of the welded joints were investigated through double-lap shear and pull-through tests, respectively. The same tests were also carried out on mechanically fastened joints with similar size. Welded samples showed similar shear

strength, but less peel strength in comparison to their mechanically fastened counterparts. Failure in welded joints was only found in the outermost layer of the adherends whereby no damage was found within the laminates. In contrast, mechanically fastened joints showed severe laminate failure due to the contact between the fastener and the adherends.

As an initial step towards the development of the high-quality MSW joints for large composite structures, the impact of different boundary conditions provided by different welding jigs on the proposed welding procedure was assessed. This procedure showed a dependence on the various boundary conditions, featured by different optimum welding energy (i.e. the energy resulting in the maximum weld strength) for different jigs. Another welding procedure based on displacement control produced welds with consistent quality under the same optimum sonotrode displacement in different jigs, showing a feasible alternative to energy-controlled welding.

The applicability of displacement-controlled and energy-controlled welding was subsequently assessed for the production of double-spot welded joints. Two welded spots with consistent quality were produced under the same displacement value when using displacement-controlled welding. On the contrary, the first welded spot created in energy-controlled welding was found to affect the energy required for the second one to obtain the same quality. Finally, in comparison to sequential welding, it was found that producing multi-spots within a single-step was more sensitive to the boundary conditions and was susceptible to secondary welding.

The effects of different geometric parameters, e.g. distance between welded spots and numbers of welded spots, on the mechanical behaviour of MSW single-lap joints was studied. The load-carrying capability of the welded joints was improved when increasing the distance between welded spots and the number of welded spots in a fixed overlap. A comparative study was performed between the MSW joints and the mechanically fastened joints with multi-fasteners, which showed that the welded joints showed a comparable load-carrying capability to the mechanically fastened counterparts.

In conclusion, knowledge gaps in ultrasonic spot welding in TPCs were filled by using the conclusions from each chapter. To facilitate the application of this technique, further research is still required regarding different aspects, such as the automation for placing of spot energy directors and the mechanical characterization of a multi-row, multi-column joint.

SAMENVATTING

In de vliegtuigindustrie is de populariteit van thermoplastische composieten (TPC) gestaag gegroeid in de afgelopen decennia. Dit is niet alleen dankzij hun excellente materiaaleigenschappen, maar ook dankzij de toepasbaarheid van snelle en kosteneffectieve productieprocessen. Verbinden door middel van samensmelting of lassen, is een typische verbindingsmethode voor TPC dankzij de intrinsieke eigenschappen van thermoplastische polymeren. Van de verschillende lastechnieken, wordt ultrasoon lassen beschouwd als één van de meest veelbelovende technieken voor het assembleren van TPC-componenten. Ultrasoon lassen is van nature een puntlastechniek. Meerdere problemen kunnen ontstaan bij het gebruik van mechanische verbindingsmethodes voor composiet constructies, waaronder het breken van de vezels door boren en de benodigde intensieve arbeid. Hierdoor kan ultrasoon puntlassen worden gezien als een veelbelovend alternatief vanuit het perspectief van een snelle productiecyclus. Echter, de fundamentele kennis om ultrasoon puntlassen te kunnen toepassen op composiet constructies ontbreekt nu nog:

- Het definiëren van een geschikte lasprocedure wordt noodzakelijk geacht voor ultrasoon puntlassen. Voor het lassen van grote composiet constructies, wordt verwacht dat deze procedure resulteert in puntlasverbindingen met eenzelfde kwaliteit door middel van een sequentieel multi-puntlasproces.
- Het mechanische gedrag en de faalmechanismen van puntlasverbindingen zijn nog steeds onbekend. Dit geldt ook voor de vergelijking van deze eigenschappen tussen puntlasverbindingen en mechanische verbindingen.

Hierdoor is de focus van dit proefschrift het systematisch onderzoeken van ultrasoon puntlassen van TPC en het mechanische gedrag van puntlasverbindingen. Het onderzoek begon met de definitie van een lasproces voor enkelvoudige puntlasverbindingen en een vooronderzoek naar hun mechanische gedrag en faalmechanismen. Deze twee laatste karakteristieken werden vergeleken voor gelaste verbindingen en mechanische verbindingen met een enkele mechanische bevestiger. Voor de ontwikkeling van hoge kwaliteit multi-puntlasverbindingen (MPL-verbindingen), werd hierna onderzoek gedaan naar hoe veranderingen in randvoorwaarden de lasprocedure en de hieruit voortgekomen laskwaliteit beïnvloedden. Hieruit kwam een lasprocedure voort die minder gevoelig is voor veranderingen in de randvoorwaarden. Deze gewijzigde procedure werd gevalideerd door het vervaardigen van dubbele puntlasverbindingen. Als laatste stap werden de effecten van geometrische parameters op de sterkte van MPL-verbindingen geanalyseerd. Een procedure voor ultrasoon puntlassen met een energierichter en een specifieke sonotrode werd gedefinieerd. Enkelvoudige puntlasverbindingen werden gemaakt met behulp van energie-gestuurd lassen. Het mechanische in-het-vlak en uit-het-vlak gedrag van de gelaste verbindingen werd onderzocht door middel van respectievelijk dubbele overlapafschuiftesten en doortrektesten. Dezelfde serie experimenten werd

uitgevoerd voor mechanische verbindingen met dezelfde afmetingen. De gelaste proefstukken gaven eenzelfde afschuifsterkte, maar een lagere afpelsterkte in vergelijking met de mechanisch verbonden proefstukken. De gelaste verbindingen faalden alleen in de buitenste laag van het composiet waarbij geen beschadiging werd gevonden in het laminaat zelf. In de mechanisch verbonden proefstukken werd daarentegen ernstige laminaatschade geobserveerd door het contact tussen het mechanische bevestigingsmiddel en de laminaten.

Als eerste stap in de ontwikkeling van hoge kwaliteit MPL-verbindingen voor grote composiet constructies, werd de impact van verschillende randvoorwaarden op de voorgestelde lasprocedure getest door het gebruik van verschillende klemsystemen. Deze procedure bleek afhankelijk te zijn van verschillende randvoorwaarden gekenmerkt door verschillende optimale energie hoeveelheden (d.w.z. de hoeveelheid energie die benodigd is om de hoogste sterkte te behalen) bij het gebruik van verschillende klemsystemen. Een andere lasprocedure gaf een mogelijk alternatief voor energie-gestuurd lassen. Deze procedure is gebaseerd op verplaatsing-gestuurd lassen en gaf een consistente kwaliteit bij dezelfde optimale diepteverplaatsing voor verschillende klemsystemen.

De toepasbaarheid van het verplaatsing- en energie-gestuurd lassen werd beoordeeld voor het maken van dubbele puntlassen. Met verplaatsing-gestuurd lassen werden twee spotlassen gemaakt met een consistente kwaliteit onder dezelfde optimale verplaatsingswaarde. Voor het energie-gestuurd lassen werd echter ontdekt dat de eerste puntlas de benodigde hoeveelheid energie voor het maken van een tweede zelfde kwaliteit las beïnvloedde. Tenslotte, in vergelijking met sequentieel lassen, werd gevonden dat het produceren van multi-puntlassen in één enkele stap gevoeliger is voor de randvoorwaarden en secundair lassen.

De invloed van verschillende geometrische parameters, bijvoorbeeld de afstand tussen de puntlassen en het aantal lassen, op het mechanische gedrag van een enkele MPL-overlapverbinding werd onderzocht. Een hoger lastvermogen werd behaald door de afstand tussen twee puntlassen te vergroten en door meer puntlassen per overlap te creëren. Een vergelijkende studie was uitgevoerd tussen MPL-verbindingen en mechanische verbindingen met meerdere mechanische bevestigers. Hieruit bleek dat de gelaste verbindingen een vergelijkbaar lastvermogen hebben als de mechanisch verbonden tegenhangers.

Samenvattend kan worden geconcludeerd dat kennishiaten in ultrasoon lassen van TPC zijn opgevuld met de conclusies van elk hoofdstuk. Om de toepasbaarheid van deze technologie te kunnen bevorderen is meer onderzoek nodig naar verschillende aspecten, zoals de automatisering van het plaatsen van de energierichters en de mechanische karakterisering van multi-rij en multi-kolom verbindingen.

CONTENTS

LIST OF FIGURES

LIST OF TABLES

1

INTRODUCTION

Owing to an increasing demand of reducing the weight and the manufacturing cost of aircraft, high-performance thermoplastic composites (TPCs) are drawing more and more attention in the aircraft industry. In line with new material applications, advanced joining techniques should be developed for achieving better performance and faster manufacturing of the aircraft structures. In order to propose a robust and fast joining technology for TPCs, it is not only deemed necessary to understand the process but also crucial to gain insight of the mechanical behaviour and failure mechanisms of the joints, which provides important guidance for the structural design. This thesis presents a series of investigations on manufacturing and mechanical characterization of ultrasonic spot welded joints in TPCs.

1

It is recognised that aircraft provides a fast, reliable mode of transportation with no comparable alternative for long distance travel. However, the aviation activities also cause climate change, as well as noise and air pollution. As indicated by the European Aviation Safety Agency (EASA) [1], the number of flights has increased by 80 % from 1990 to 2014 and is expected to have a further growth by 45 % during the next 20 years. Moreover, CO_2 and NO_x emissions, owing to fuel combustion, have increased by around 80 % and 100 %, respectively, between 1990 and 2014 and will both continuously increase by about 45 % by the end of 2035 [1]. Therefore, large numbers of research programmes have been established involving industry, government and academia in the past decades, aiming at exploring breakthrough technologies for further reduction of fuel consumption of aviation and thus, lower environmental footprint.

It is well known that a key factor for reducing fuel burn and hence aircraft emissions is the aircraft empty weight. Owing to high strength- and stiffness-to-weight ratios, advanced composite materials are therefore becoming increasingly popular for new generation aircraft, such as Airbus A350 XWB and Boeing 787 aircraft [2]. However, conventional thermoset composites are not only suffered from their high material costs, but more importantly, they are limited by the high manufacturing cost (e.g. the expensive autoclave) and time (e.g. long curing cycles) [3]. As a result, improvements in manufacturing technology should be given more consideration. Advanced manufacturing technology is capable of achieving a reduction in manufacturing costs as well as the structural weight, thus reducing the emissions for existing and new aircraft.

1.1. THERMOPLASTIC COMPOSITES FOR AIRCRAFT

THE appeal of Thermoplastic composites (TPCs) for the aircraft industry initiated from the second half of the 1980s [3]. Compared to their thermoset counterparts, which have been extensively used in aircraft structures (e.g. over 50 % of structural mass in the Airbus A350 XWB), the increasing usage of TPCs in the recent years is mainly due to their rapid and cost-effective manufacturing process. Without cross-linked polymer chains, thermoplastic polymers can be melted when they are heated to a certain temper-

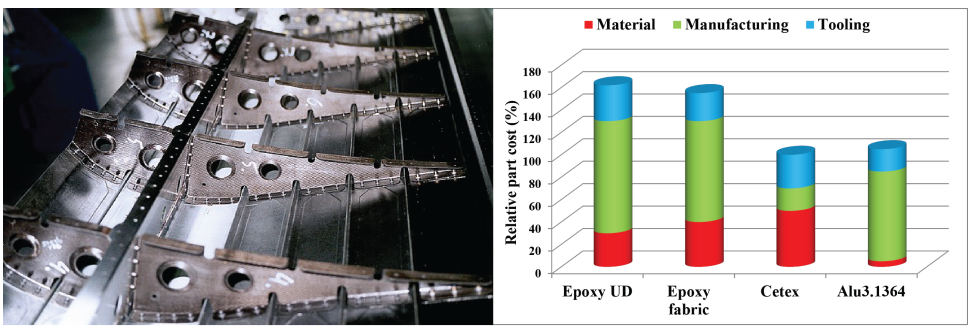

Figure 1.1: (a) Thermoplastic composite ribs and (b) their manufacturing cost by using different materials. Source: TenCate Advanced Composites.

ature and retain their original properties after cooling down. This characteristic provides TPCs with reheatability and reformability and allows them to be manufactured and assembled by cost-effective technologies, such as press forming and fusion bonding or welding. Despite the higher material cost, the manufacturing cost can be significantly reduced compared to thermoset composites (TSCs) by eliminating the autoclave curing, as shown in Fig. 1.1. Apart from that, TPCs also offer advantages such as high damage tolerance, good fracture toughness, excellent environmental and chemical resistance, low storage requirement, and infinite shelf life [3, 4].

TPCs are increasingly used in the current generation of aircraft, in particular for interiors, secondary and semi-structural parts, such as the press-formed ribs of the Dornier 328, press-formed brackets, clips and cleats of the Boeing 787 and the Airbus A350 (Fig. 1.2a) [5], the resistance welded wing fixed leading edges of the Airbus A340 and A380 with Cetex Glass fibre reinforced polyphenylene sulfide (GF/PPS) (Fig. 1.2b), and the induction welded Carbon fibre reinforced PPS rudder and elevators of the Gulfstream G650 business jet [6]. However, more efforts are continuously put in to extend the application of TPCs to primary structures of aircraft. The Thermoplastic Affordable Primary Aircraft Structures (TAPAS) project is one of the most well-known collaborations between the aerospace industry and the academic research for reaching this goal. In this project, a skin panel of a torsion box has been successfully manufactured with Carbon fibre reinforced polyetheretherketone (CF/PEEK) through automated fibre placement, press forming and welding. The test results showed that, owing to higher toughness of TPCs, thinner laminates were allowed for TPC parts which finally resulted in 10 % weight saving compared to conventional TSCs [7].

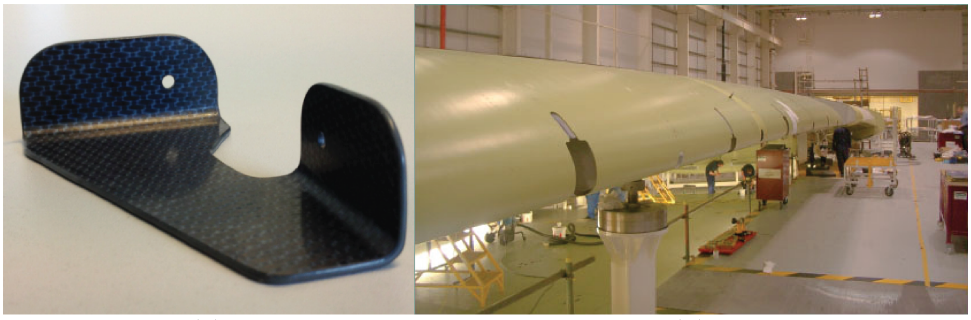

(a) (b)

Figure 1.2: Applications of thermoplastic composites in aircraft structures: (a) press-formed clips; (b) resistance welded fixed wing leading edges of Airbus A380. Source: (a) Tencate Advanced composites, (b) Fokker Aerostructures.

1.2. JOINING TECHNIQUES FOR TPCS

IDEAL structures would be expected to be designed and manufactured without joints, since joints are in most cases the weak points and may result in weight penalty [8, 9]. However, due to the limitations of present manufacturing techniques, aircraft structures with complex geometries are difficult to be produced as integral parts. Therefore, joining

is a necessary step for the manufacturing of structural components. This is particularly the case for fibre reinforced TPC parts which currently are mainly used in secondary structures of aircraft, such as brackets and ribs. Fast and reliable joining techniques, which have direct influence on mechanical performance of the created joints and manufacturing costs, are vitally important for assembly and promotion of TPCs applied in large components.

Traditional joining methods, e.g. mechanical fastening, are proven to not be well-suited for direct application to composites [8, 10–12]. Stress concentrations created by the riveted or bolted holes and damage on fibres due to drilling are most typical drawbacks of the application of mechanically fastened joints in composite structures. In addition, mechanical fasteners unavoidably provide additional weight and their installation is time and labour consuming. In contrast, adhesive bonding benefits from its continuous joint configuration, which effectively prevents stress concentration present in the case of mechanically fastened joints [13]. Nevertheless, it is difficult to apply on some high performance TPCs, such as polyetheretherketone (PEEK) and polyphenylene sulphide (PPS), due to their low surface energy [14]. Furthermore, extensive surface preparation and long curing cycles also make adhesive bonding slow and labour intensive [8, 12, 15].

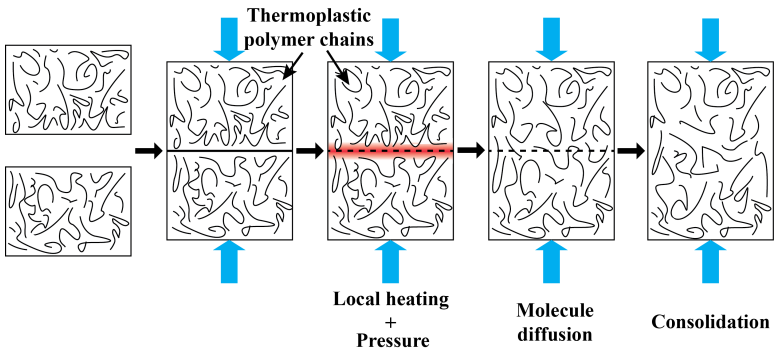

Figure 1.3: Schematic of fusion bonding/welding process of thermoplastic polymers [16].

Fusion bonding or welding is considered as a specific joining technique for TPCs since its working mechanism is correlated to the inherent properties of thermoplastic polymers, which can be softened or melted when heated and retain their original properties after solidification [17]. As schematically shown in Fig. 1.3, prior to the initiation of welding, the surfaces of two parts to be welded are put into contact by applying pressure. Local heating is introduced at the interface by different mechanisms, achieving an intimate contact between the two surfaces. With the increase of temperature, thermoplastic polymer chains around the interface start to flow and inter-diffuse. After the heating stage, thermoplastic polymers are solidified by cooling down to room temperature under constant pressure. In this way, welding shows a potential superiority on joining TPCs in comparison to other traditional techniques [12]. According to the report from Defence and Space Group of the Boeing Company in 1996 [18], welding techniques achieved over 61 % savings in labour work for assembling a composite wing structure

compared to bolting. Based on different heating mechanisms, welding techniques can be basically classified as thermal welding, friction welding and electromagnetic welding, as summarized in Fig. 1.4. Among them, ultrasonic welding, induction welding and resistance welding are regarded as the three most promising technologies (highlighted in Fig. 1.4), owing to a series of advantages, such as limited heat affected zones, excellent weld strength and possibility for large-scale welding, etc. [8, 12, 17].

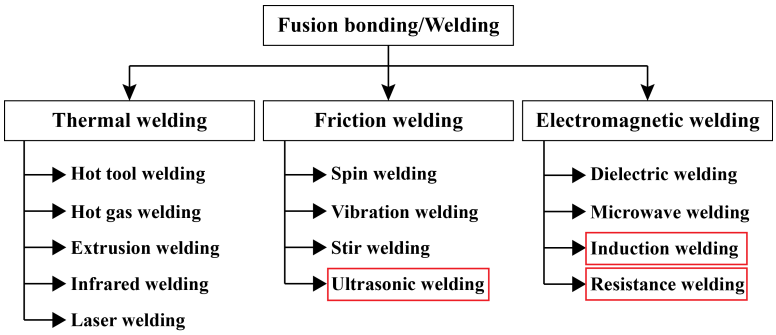

Figure 1.4: Classification of welding techniques for thermoplastics based on different mechanisms of heat generation [12].

1.3. ULTRASONIC WELDING IN TPCS

ULTRASONIC welding is an interesting joining technique for both unreinforced thermoplastics and thermoplastic composites with some typical advantages, such as very fast welding process (less than 1 second), absence of foreign materials, e.g. metal mesh or metal particles, at the welding interface, possibility of in-situ monitoring and excellent weld strength [17, 19–23]. As shown in Fig. 1.4, ultrasonic welding belongs to the friction welding category since heating is driven by interfacial and intermolecular (viscoelastic) friction [24, 25]. The entire welding process can be divided into two stages, namely vibration and consolidation. The vibration phase is triggered by a pre-defined welding force, which is provided by a pressure actuator. Electric generator normally transforms the main line current into controlled high-frequency (typically between 20 and 40 kHz for output) current. This electrical signal is converted to a high-frequency (20 - 70 kHz) and low-amplitude (10 - 250 μm peak-to-peak) vibration through a piezoelectric converter, as schematically shown in Fig. 1.5, and is amplified and transferred to the work pieces to be welded through the booster and the sonotrode. Artificial surface asperities, namely energy directors, or susceptors, are normally sandwiched between the adherends to be welded to concentrate heating at the interface. They are usually made of the same material as the composite matrix and can be either placed at the welding interface or moulded onto the adherends in different geometries, typically with configurations shown in Fig. 1.5. Once the vibration is initiated, energy directors will be deformed and preferentially heated owing to their lower compressive stiffness as compared to that of the composite adherends [26]. When the temperature exceeds their melting temperature, energy directors will melt, flow and transfer heat into the first layer of the laminates.

As a consequence, resin on the surfaces of adherends is also melted and results in diffusion and entanglement of polymer chains at the interface [21]. Subsequently, vibration is stopped and welded parts are kept under pressure to complete consolidation and form a welded joint. Unlike induction and resistance welding [27, 28], ultrasonic welding has not been industrially applied for joining TPCs, even though it is widely used in the plastics industry [29].

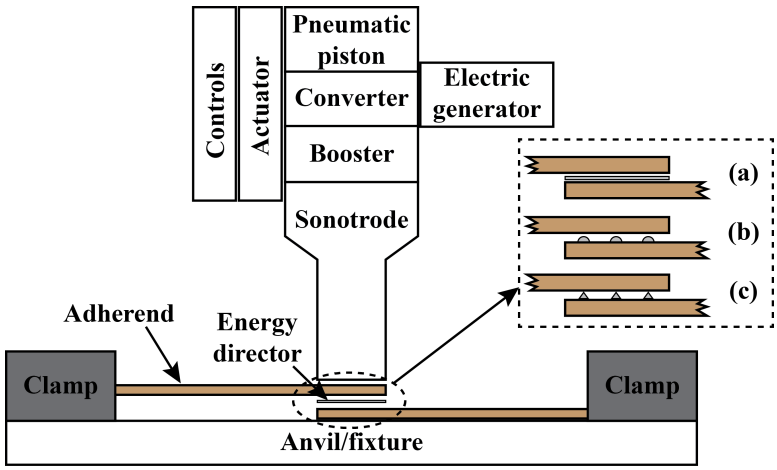

Figure 1.5: Schematic of ultrasonic welding setup [30] and energy director. The magnified part shows different energy director configurations: (a). flat, (b). triangular, (c). semicircular.

One obstacle for industrialization of ultrasonic welding for joining TPCs is that, owing to the fast welding process and small welded area, some fundamental knowledge, like the heating and melting process, of this technique is sill less known and is also hardly observed using existing techniques [25]. Therefore, extensive efforts have been devoted by researchers to gain insight on the process and some inspiring progress has been achieved in recent decades. Both analytical [21, 31, 32] and numerical [22, 23, 33, 34] models were developed to understand the heating mechanisms and the melting of energy directors during the ultrasonic welding process. Apart from that, experimental investigations were also carried out to analyse and optimize the process through in-situ monitoring [19, 20, 35] and evaluate the quality of welded joints [17, 26, 36–39, 41]. Since ultrasonic welding is well-suited for small areas, the quality of welded joints is mostly assessed by single lap-shear tests [17, 19, 20, 26, 30, 35]. Some other tests, but very limited, have been also performed, e.g. double-lap shear tests [39], double cantilever beam tests [36, 37] and end-notched flexural tests [36].

1.4. RESEARCH MOTIVATION

CURRENT research on ultrasonic welding of TPCs mainly focuses on the joint configuration with fully welded overlap, which is created within a single-step. This is however not a feasible way to scale it up for joining large size structures, e.g. the fuselage of aircraft, since substantial power input and pressure will be required for producing a con-

tinuous welding seam like what induction or resistance welding does. It is encouraging that a continuous ultrasonic welding technique for TPCs has been developed by Villegas and her group [42], which provides possibilities for creating continuous weldlines. A continuous welded seam is enabled by a sonotrode with a combination of vibration in the vertical direction and movement in the horizontal direction. Although this technique is currently still in the primary stage, it contributes a significant step for the upscaling of ultrasonic welding in TPCs. Apart from this novel approach, as it is known that ultrasonic welding is a typical spot welding technique for polymer composites, the most straightforward way, for its upscaling is sequential welding of consecutive spots resulting in a multi-spot welded (MSW) joint. Although the concept of sequential ultrasonic welding was already proposed by Lu and Benatar [39], no details in the process were provided in their study. More recently, some investigations were performed by Balle et al. [40] regarding ultrasonic spot welding for joining metal and TPCs. Besides that, little to no research was reported with respect to ultrasonic spot welding in TPCs, in particular for the sequential welding. In contrast to the limited research in TPCs, ultrasonic spot welding is however more mature in joining metals and their alloys. Extensive studies, including both experimental [43–48] and numerical [49–53] work, have been carried out on the process optimization and mechanical characterization. A variety of mechanical testing methods are adopted, including both static [43–45, 53] and fatigue tests [54–56], to evaluate the quality of the welded joints. Although ultrasonic spot welding in metals is fundamentally different from that of TPCs, these studies can provide references for the current work.

As indicated in the previous section, TPCs are predominantly used in the secondary loading parts, e.g. clips and brackets, on existing aircraft. Consecutive multi-spot welded joints enabled by sequential ultrasonic welding are expected to be a fast and cost-effective solution for the assembly of these parts on composites or even metallic aircraft fuselage [57]. More importantly, it can be regarded as a composite-friendly alternative to mechanical fastening, which is still applied as the major joining technique on composite parts. On the other hand, similar to mechanically fastened joints, spot welded joints are also susceptible to stress concentration due to their discrete configuration. This however grants them the potential of crack arrest and crack retardation as opposed to adhesive bonded and continuous welded joints.

1.5. OBJECTIVE FOR THIS RESEARCH

THE objective of this work is to gain deeper knowledge on ultrasonic sequential multi-spot welding of thermoplastic composites and hence to facilitate its application, in particular as an alternative to conventional mechanical fastening, in composite structures. This objective is expected to be met by achieving the following sub-objectives:

- Define a procedure for manufacturing of (multi-)spot welded joints with consistent quality.
- Gain insight into the mechanical behaviour and failure mechanisms of (multi-)spot welded joints in different loading conditions as compared to that of mechanically fastened joints.

As indicated in the previous section, ultrasonic welded joints in TPCs are mostly produced with a fully welded overlap in the literature [19, 20, 30, 35, 39]. In contrast to that, an ultrasonic spot welded joint is defined as a welded area smaller than its respective overlap. The spot welding process is significantly different from full-overlap weld. For instance, the flow fronts of the molten energy director will be squeezed in between the surfaces of the adherends in ultrasonic spot welding rather than squeezed out of the overlap edge. This potentially has an influence on the strategies to control the welding process. Therefore, a welding procedure might need to be defined for ultrasonic spot welding to produce welded spots with consistent quality and high weld strength. As the boundary conditions of the sequential welding process are likely to change with each new spot, the applicability of this procedure on sequential multi-spot welding is assessed. Accordingly, an optimum welding procedure for sequential welding, which is insensitive to change in boundary conditions, should be defined.

Regarding the mechanical evaluation, single-lap shear test is the most commonly used testing method for characterizing the mechanical behaviour of welded joints. However, it is known that secondary bending will occur in this type of joints once they are subjected to a tensile load [58], which results in a mix-mode (peel and shear) load condition. Therefore, it is necessary to first understand the mechanical behaviour of ultrasonic spot welded joints in both (i.e. pure shear and pure peel) loading conditions. On this basis, to improve the mechanical performance of the (multi-)spot welded joints in single-lap configuration, the effects of some geometric parameters, e.g. the distance between welded spots and the number of welded spots, on the joint strength is assessed. Therefore, in order to achieve the above-mentioned objectives step-by-step, a series of scientific questions should be answered to fill in the current knowledge gaps:

1 How to define a procedure which is well-suited to produce a single spot?

2 What is the in-plane (shear) and out-of-plane (peel) mechanical behaviour and failure modes of the created single-spot welded joints?

3 How are the above-mentioned mechanical behaviour and failure modes of spot welded joints compared to those of mechanically fastened joints with a single fastener?

4 What is the optimum welding procedure to obtain multi-spot welded joints with consistent quality taking into account the change in boundary conditions introduced by every new spot in the sequential welding process?

5 In multi-spot welded single-lap joints, what are the effects of different distance between spots and numbers of welded spots in a fixed overlap on the joint strength?

6 How is the mechanical performance of multi-spot welded joints compared to mechanically fastened joints with multiple fasteners in a single-lap configuration?

1.6. THESIS OUTLINE

CONSIDERING the objectives of this work, this thesis is divided into 6 chapters. Each chapter will address one issue mentioned in the scientific questions. A comprehensive study on ultrasonic spot welding in thermoplastic composites will be systematically

provided, as shown in Fig. 1.6. Research starts from single-spot welded joints (Chapter 2 and 3) to double-spot welded (Chapter 4) and finally to multi-spot welded joints (Chapter 5). Chapters 2 and 5 mainly focus on the mechanical characterization of spot welded joints and a comparative study between spot welded joints *vs.* mechanically fastened joints will be performed. Chapters 3 and 4 will provide a two-step study on the development of high-quality multi-spot welded joints with sequential ultrasonic welding. Final conclusions and recommendations for future work are given in Chapter 6.

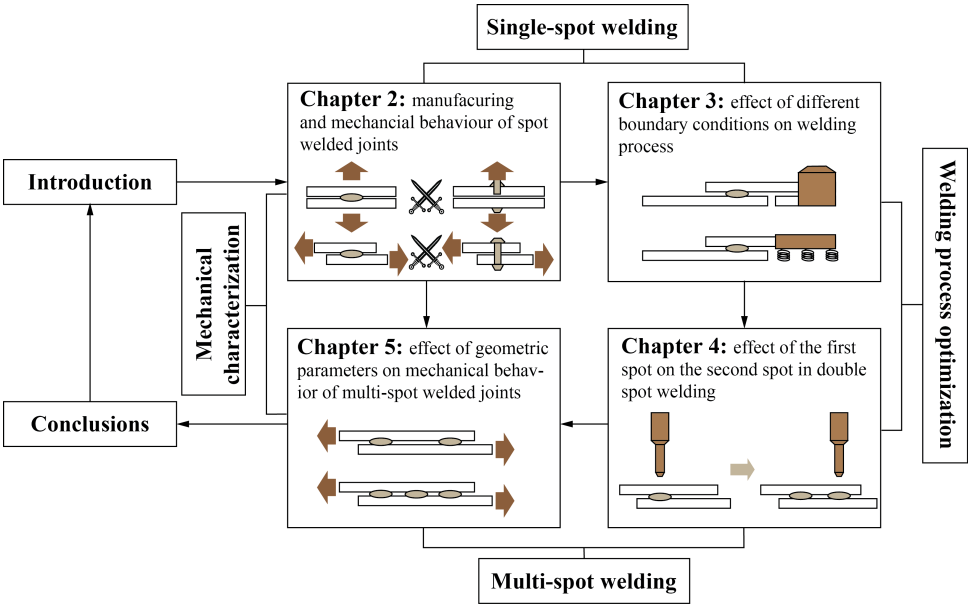

Figure 1.6: Schematic of the structure of this thesis.

- **Chapter 2 - Manufacturing and mechanical behaviour of spot welded joints**. The first three scientific questions will be addressed in this chapter: (a) a procedure will be defined to weld single-spot welded joints within a (bigger) overlap as compared to that of the traditional full-overlap welded joints, (b) the strength and failure modes of single-spot welded joints will be assessed under pure shear and pure peel loading, and (c) the strength and failure modes of the single-spot welded joints will be compared to mechanically fastened joints with a single fastener.

- **Chapter 3 - Effect of boundary condition on welding process**. The fourth scientific question will be discussed in this chapter in two sub-steps: (a) the effect of different boundary conditions on the spot welding procedure defined in Chapter 2 will be assessed, and (b) based on the results, an alternative welding procedure which is insensitive to the change in boundary conditions will be proposed.

- **Chapter 4 - Double-spot welding**. The results obtained in Chapter 3 will be assessed for the production of double-spot welded joints. This chapter will provide

a further investigation on the effects of the change in boundary conditions introduced by the first welded spot on the welding process of the second spot.

- **Chapter 5 - Mechanical behaviour of multi-spot welded joints**. In this chapter, the last two questions will be addressed: (a) the effects of different geometric parameters, i.e. the distance between welded spots (for double-spot welded joints) and the number of welded spots (for multi-spot welded joints), on the mechanical behaviour of multi-spot welded single-lap joints will be assessed, and (b) a comparative study will be carried out on the load-carrying capability between multi-spot welded joints and mechanically fastened joints assembled by multi-fastener.
- **Chapter 6 - Conclusions and recommendations**. Each scientific question mentioned in Section 1.5 will be addressed in this chapter. Recommendations will then be given for future work.

REFERENCES

[1] European aviation enviromental report. European Aviation Safety Agency, the European Environment Agency, and EUROCOMTROL, 2016.

[2] ICAO environmental report: Aviation and climate change. Environmental Branch of the ICAO, 2016.

[3] A.R. Offringa. Thermoplastic composites - rapid processing applications. *Composites Part A: Applied Science and Manufacturing*, 27(4 PART A):329–336, 1996.

[4] M. Hou, L. Ye, and Y.W. Mai. Manufacturing process and mechanical properties of thermoplastic composite components. *Journal of Materials Processing Technology*, 63(1):334 – 338, 1997.

[5] A. Offringa, J.W. van Ingen, and A. Buitenhuis. Butt-joined, thermoplastic stiffened-skin concept development. *SAMPE Journal*, 48(2):7–15, 2012.

[6] A. Offringa. New thermoplastic composite design concepts and their automated manufacture. *JEC Composites magazine*, 58:45–49, 2010.

[7] *http://www.tapasproject.nl*.

[8] C. Ageorges, L. Ye, and M. Hou. Advances in fusion bonding techniques for joining thermoplastic matrix composites: A review. *Composites - Part A: Applied Science and Manufacturing*, 32(6):839–857, 2001.

[9] M. Hou, L. Ye, and Y.W. Mai. An experimental study of resistance welding of carbon fibre fabric reinforced polyetherimide (cf fabric/pei) composite material. *Applied Composite Materials*, 6(1):35–49, Jan 1999.

[10] V.K. Stokes. Joining methods for plastics and plastic composites: An overview. *Polymer Engineering & Science*, 29(19):1310–1324, 1989.

[11] A.B. Strong. High performance and engineering thermoplastic composites. *Technomic Pub.Co*, 1993.

[12] A. Yousefpour, M. Hojjati, and J.P. Immarigeon. Fusion bonding/welding of thermoplastic composites. *Journal of Thermoplastic Composite Materials*, 17(4):303–341, 2004.

[13] J.R. Vinson. Mechanical fastening of polymer composites. *Polymer Engineering & Science*, 29(19):1332–1339, 1989.

[14] S.J. Shaw, J. Comyn, and L. Mascia. Surface treatment and bonding of thermoplastic composites. In *Agard Conference Proceedings 590 - Bolted/Bonded Joints in Polymer Composites. 83rd Meeting of the AGARD strctures and Materials Panel*, Italy, Sepetember 1996.

[15] E.M. Silverman, R.A. Griese. Joining methods for graphite/peek thermoplastic composites. *SAMPE Journal*, 13:151–156, 1993.

[16] A.C. Loos, M.C. Li. Non-isothermal autohesion model for amorphous thermoplastic composites. *Journal of Thermoplastic Composite Materials*, 7(4):280–310, 1994.

[17] I.F. Villegas, L. Moser, A. Yousefpour, P. Mitschang, and H.E.N. Bersee. Process and performance evaluation of ultrasonic, induction and resistance welding of advanced thermoplastic composites. *Journal of Thermoplastic Composite Materials*, 26(8):1007–1024, 2013.

[18] A.R. Wedgewood, P.E. Hardy. Induction welding of thermoset composite adherends using thermoplastic interlayers and susceptors. volume 28, pages 850–861, 1996.

[19] I.F. Villegas. Strength development versus process data in ultrasonic welding of thermoplastic composites with flat energy directors and its application to the definition of optimum processing parameters. *Composites Part A: Applied Science and Manufacturing*, 65:27–37, 2014.

[20] I.F. Villegas. In situ monitoring of ultrasonic welding of thermoplastic composites through power and displacement data. *Journal of Thermoplastic Composite Materials*, 28(1):66–85, 2015.

[21] A. Benatar, T.G. Gutowski. Ultrasonic welding of peek graphite apc 2 composites. *Polymer Engineering & Science*, 29(23):1705–1721, 1989.

[22] A. Levy, S.L. Corre, and I.F. Villegas. Modeling of the heating phenomena in ultrasonic welding of thermoplastic composites with flat energy directors. *Journal of Materials Processing Technology*, 214(7):1361–1371, 2014.

[23] A. Levy, S.L. Corre, and A. Poitou. Ultrasonic welding of thermoplastic composites: A numerical analysis at the mesoscopic scale relating processing parameters, flow of polymer and quality of adhesion. *International Journal of Material Forming*, 7(1):39–51, 2014.

[24] M.N. Tolunay, P.R. Dawson, and K.K. Wang. Heating and bonding mechanisms in ultrasonic welding of thermoplastics. *Polymer Engineering and Science*, 23(13):726–733, 1983.

[25] Z. Zhang, X. Wang, Y. Luo, Z. Zhang, and L. Wang. Study on heating process of ultrasonic welding for thermoplastics. *Journal of Thermoplastic Composite Materials*, 23(5):647–664, 2010.

[26] I.F. Villegas, B.V. Grande, H.E.N. Bersee, and R. Benedictus. A comparative evaluation between flat and traditional energy directors for ultrasonic welding of cf/pps thermoplastic composites. *Composite Interfaces*, 22(8):717–729, 2015.

[27] A. Offringa, D. Myers, and A. Buitenhuis. Redesigned a340–500/600 fixed wing leading edge (j-nose) in thermoplastics. In *Proceedings of the SAMPE Europe Conference*, Paris, France, March 2001.

[28] J.W. Van Ingen, A. Buitenhuis, M. van Wijngaarden, and F. Simmon III. Development of the gulfstream g650 induction welded thermoplastic elevators and rudder. 2010.

[29] D. Grewel, A. Benatar, and J. Park. Plastics and Composites Welding Handbook. *Hansen Gardner Publications*, 2003.

[30] I.F. Villegas and H.E.N. Bersee. Ultrasonic welding of advanced thermoplastic composites: An investigation on energy-directing surfaces. *Advances in Polymer Technology*, 29(2):112–121, 2010.

[31] N.P. Nesterenko and I.K. Senchenkov. Current state and prospects of improvement of ultrasound welding of polymers and thermoplastic composite materials. *Welding International*, 17(3):232–238, 2003.

[32] A. Levy, S.L. Corre, A. Poitou, and E. Soccard. Ultrasonic welding of thermoplastic composites: Modleing of the process using time homogenization. *International Journal for Multiscale Computational Engineering*, 9(1):53–72, 2011.

[33] A. Levy, S.L. Corre, N. Chevaugeon, and A. Poitou. A level set based approach for the finite element simulation of a forming process involving multiphysics coupling: Ultrasonic welding of thermoplastic composites. *European Journal of Mechanics - A/Solids*, 30(4):501 – 509, 2011.

[34] X. Wang, J. Yan, R. Li, and S. Yang. Fem investigation of the temperature field of energy director during ultrasonic welding of peek composites. *Journal of Thermoplastic Composite Materials*, 19(5):593–607, 2006.

[35] G. Palardy, I.F. Villegas. On the effect of flat energy directors thickness on heat generation during ultrasonic welding of thermoplastic composites. *Composite Interfaces*, 24(2):203–214, 2017.

[36] B. Harras, K.C. Cole, and T. Vu-Khanh. Optimization of the ultrasonic welding of peek-carbon composites. *Journal of Reinforced Plastics and Composites*, 15(2):174–182, 1996.

[37] E.C. Eveno, J.W. Gillespie Jr. Experimental investigation of ultrasonic welding of graphite reinforced polyetheretherketone composites. In *Proceedings of 21st International SAMPE Technical Conference*, 21:923–934, Atlantic City, USA, 1989.

[38] A.B. Strong, D.P. Johnson, and B.A. Johnson. Variables interactions in ultrasonic welding of thermoplastic composites. *S.A.M.P.E. quarterly*, 21(2):36–41, 1990.

[39] H.M. Lu, A. Benatar, and F.G. He. Sequential ultrasonic welding of peek/graphite composites plates. In *Proceedings of the annual technical conference ANTEC*, 15:2523–2526, Montreal, 1991.

[40] F. Balle, G. Wagner, and D. Eifler. Ultrasonic metal welding of aluminium sheets to carbon fibre reinforced thermoplastic composites. *Advanced Engineering Materials*, 11(1-2):35–39, 2009.

[41] S.J. Liu, I.T. Chang, and S.W. Hung. Factors affecting the joint strength of ultrasonically welded polypropylene composites. *Polymer Composites*, 22(1):132–141, 2001.

[42] F. Senders, M. van Beurden, G. Palardy, and I. F. Villegas. Zero-flow: a novel approach to continuous ultrasonic welding of CF/PPS thermoplastic composite plates. *Advanced Manufacturing: Polymer & Composites Science*, 2(3-4):83-92, 2016.

[43] V.K. Patel, S.D. Bhole, and D.L. Chen. Ultrasonic spot welding of lightweight alloys. In *Proceedings of 13th International Conference on Fracture*, pages 1–10, Bijing, China, June 2013.

[44] P. Prangnell, H. Haddadi, and Y. C. Chen. Ultrasonic spot welding of aluminium to steel for automotive applications—microstructure and optimisation. *Materials Science and Technology*, 27:617–624, 2011.

[45] V. K. Patel, S.D. Bhole, and D.L. Chen. Microstructure and mechanical properties of dissimilar welded mg–al joints by ultrasonic spot welding technique. *Science and Technology of Welding and Joining*, 17:202–206, 2012.

[46] A. Macwan, V.K. Patel, X.Q. Jiang, C. Li, S.D. Bhole, and D.L. Chen. Ultrasonic spot welding of al/mg/al tri-layered clad sheets. *Materials and Design (1980-2015)*, 62:344 – 351, 2014.

[47] V.K. Patel, S.D. Bhole, and D.L. Chen. Influence of ultrasonic spot welding on microstructure in a magnesium alloy. *Scripta Materialia*, 65(10):911 – 914, 2011.

[48] D. Bakavos and P.B. Prangnell. Mechanisms of joint and microstructure formation in high power ultrasonic spot welding 6111 aluminium automotive sheet. *Materials Science and Engineering: A*, 527(23):6320 – 6334, 2010.

[49] N. Shen, A. Samanta, H. Ding, and W.W. Cai. Simulating microstructure evolution of battery tabs during ultrasonic welding. *Journal of Manufacturing Processes*, 23:306–314, 2016.

[50] S. Elangovan, S. Semeer, and K. Prakasan. Temperature and stress distribution in ultrasonic metal welding—an fea-based study. *Journal of Materials Processing Technology*, 209(3):1143 – 1150, 2009.

[51] A. Siddiq and A. Ghassemieh. Theoretical and fe analysis of ultrasonic welding of aluminum alloy 3003. *Journal of Manufacturing Science and Engineering*, 131:1–11, 2009.

[52] C. Doumanidis and Y. Gao. Mechanical modeling of ultrasonic welding. *Welding Journal (Miami, Fla)*, 83(4):140–S–146–S, 2004.

[53] B. Zhou, M.D. Thouless, and S.M. Ward. Predicting the failure of ultrasonic spot welds by pull-out from sheet metal. *International Journal of Solids and Structures*, 43(25):7482 – 7500, 2006.

[54] T.J. Rinker, J. Pan, M. Santella, and T.Y. Pan. Fatigue behavior of dissimilar ultrasonic welds in lap-shear specimens of az31 and steel sheets. *Engineering Fracture Mechanics*, 2017.

[55] V.K. Patel, S.D. Bhole, and D.L. Chen. Fatigue life estimation of ultrasonic spot welded mg alloy joints. *Materials & Design (1980-2015)*, 62(Supplement C):124 – 132, 2014.

[56] W. Lai, J. Pan, Z. Feng, M. Santella, and T. Pan. Failure mode and fatigue behavior of ultrasonic spot welds with adhesive in lap-shear specimens of magnesium and steel sheets. *SAE International Journal of Materials and Manufacturing*, 6(2):279–285, apr 2013.

[57] F. Balle, F. Staab, and J. Born. Joining of light metals to fiber reinforced polymer composites by power ultrasonics. In *Proceedings of 17th International Conference on Composite Materials*, Munich, Germany, June, 2016.

[58] J. Schijve and G. Campoli and A. Monaco. Fatigue of structures and secondary bending in structural elements. *International Journal of Fatigue*, 31(7):1111–1123, 2009.

2

A Preliminary Comparison of Mechanical Behaviour of Spot Welded and Mechanically Fastened Joints

The in-plane and out-of-plane mechanical behaviour of both ultrasonically spot welded and mechanically fastened joints was investigated by double-lap shear and pull-through tests, respectively. Spot welded specimens showed comparable onset failure load and significantly higher joint stiffness compared to mechanical fasteners when carrying shear load. The failure modes and the damage within specimens were analysed after mechanical tests. Intralaminar failure and very limited damage on the out-most ply were found for welded specimens, whereas catastrophic through-the-thickness failure was observed for mechanically fastened joints. Based on the experimental outcomes, the mechanical performance and failure mechanisms of spot welded joints were critically assessed in comparison to the mechanical fasteners.

This chapter has been published in Composites Part B: Engineering **112**, 224-234 (2017). [1]

2.1. INTRODUCTION

In the latest decades, thermoplastic composites (TPCs) have become increasingly interesting for their use on aircraft structures owing to the superior strength- and stiffness-to-weight ratios in comparison to metals and cost-effective manufacturing process in comparison to thermoset composites (TSCs) [2–4]. Apart from these benefits, TPCs can be welded. This is due to the intrinsic property of thermoplastic resins that they can be melted when being heated and retain their original mechanical properties after cooling down [4–6]. On one hand, welding techniques can be classified based on the heating mechanisms [4], namely friction welding, thermal welding and electromagnetic welding. On the other hand, based on the welded area, welding techniques can be generally divided into two groups, i.e. continuous welding and spot welding. The well-known induction and resistance welding are typically continuous welding techniques. They are currently applied in the aerospace industry for the joining of thermoplastic composite parts [7, 8] as a composite-friendly alternative to mechanically fastened joints [4–6, 9]. Similarly to adhesively bonded joints, continuously welded seams in thermoplastic composite structures do not require drilling of holes in the adherends and avoid stress concentrations resulting from point load introduction. Contrarily to adhesive bonding, welding relies on polymer autohesion at the welding interface and hence it does not depend on adhesion mechanisms of difficult inspectability. Ultrasonic welding is also known as a very interesting technique for joining thermoplastic composites with a number of advantages over resistance and induction welding, such as very short welding times, very low energy consumption, highly concentrated heat generation and potential for in-situ process monitoring [7, 10, 11].One of its main limitations is that it is traditionally a spot welding technique and, hence, as opposed to continuous welding techniques it does not avoid point load introduction in the welded joint. On the positive side, spot welding could be expected to decrease assembly times as well as to provide joints with a crack arresting nature.

Spot welded joints are current practice in metallic constructions/structures such as automotive industries. The main metal spot welding techniques are resistance spot welding (RSW), friction stir spot welding (FSSW) and ultrasonic spot welding (USW). Both RSW and FSSW have been extensively used and studied by many researchers for decades [12, 13]. RSW was attractive because of its ease of operation and low costs and was regarded as the predominant process for joining conventional pressed steel [12, 14, 15]. FSSW was developed in 1991 and was first used for the joining of aluminium and its alloys. It is energy efficient and is capable of joining components of any shapes and dissimilar materials [13, 14]. Compared to FSSW and RSW, USW was shown to have even shorter welding cycles (typically < 0.4 s), less energy consumption and higher efficiency. Therefore, USW has been of increased interest for many researchers and numerous research has been carried out on its application on the assembly of steels and alloys [14–18]. Apart from that, a couple of investigations were carried out on applying spot welding on joining metal and thermoplastic composites. An experimental research was performed by P. Mistschang [19] on metal (Steel DC01 and Aluminium Al/Mg3) and carbon fibre reinforced polymer composites (CFRPC). Induction spot welding was used to bond the metal/CFRPC and the mechanical performance of welded joints was characterized by single-lap tests. The experimental outcomes showed that the lap-shear strength

(LSS) of welded joints created by induction spot welding reached around 85 % of the adhesive bonded joints in the same condition and highlighted the short welding process (< 2 min). However, the results also indicated that the weld strength of induction spot welding was greatly influenced by the pre-treatments on the metal substrates. Besides, the welding time of ultrasonic welding, normally less than 10 s, is significantly shorter than induction welding. More recently, F. Balle [20] investigated the lap-shear mechanical properties and failure modes of hybrid joints consisting of different aluminium alloy (AA1050, AA5754 and AA2024) and thermoplastic composites (CF/PA66 and CF/PEEK) created by ultrasonic spot welding. The test results showed high quality welded joints between metal and CFRPC. There is however very little knowledge on spot welding of thermoplastic composite structures, both in terms of manufacturing process and mechanical performance. This knowledge gap needs to be overcome to facilitate the future industrial application of TPC spot welding.

As the basis for further research and development on the topic, this chapter focuses on the static in-plane and out-of-plane behaviour of single-spot welded joints as compared to joints with a single mechanical fastener. Following usual procedures in composite mechanically fastened joints [21–24], the in-plane behaviour is characterized via double lap shear tests and the out-of-plane behaviour via pull-through tests. The damage affected zones (DAZ) are assessed using cross-section microscopy [23] and ultrasonic inspection [24]. Cross-section microscopy and fractography are used to analyse the failure mechanisms.

2.2. EXPERIMENTAL

2.2.1. MECHANICAL TESTING AND EVALUATION

DOUBLE-LAP shear (DLS) tests were performed to evaluate the in-plane failure and mechanical performance of both spot welded and mechanically fastened joints as the effect of out-of-plane bending can be effectively diminished in this configuration [21, 22]. Specimens were comprised of four composite plates (114.4 × 25.4 mm^2) with a square overlap area of 25.4 × 25.4 mm^2, as shown in Fig. 2.1. Therefore, both a spot welded and a mechanically fastened joint could be created in the central point of the overlap. The tests were carried out on a Zwick/Roell 250 kN universal testing machine. Specimens were clamped with hydraulic grips and loaded until failure with a crosshead speed of 1.3 mm/min in accordance with ASTM D3528-96 [25]. To guarantee a safe failure mode and avoid an over distortion of the specimens, tests were stopped when a 30 % load drop from the maximum attained value was found [26]. Five specimens were tested for both types of joints.

The out-of-plane performance of both welded and mechanically fastened joints was evaluated with pull-through (PT) tests following ASTMD7332-09 [27]. Specimens consisting of two square composite plates assembled with either a spot weld or a mechanical fastener were placed in between a pair of loading fixtures (see Fig. 2.2). The size of the composite plates is shown in Fig. 2.2. To accommodate the test fixture, four holes were drilled on each plate prior to the assembly and the top plate was joined at a 45° angle with respect to the bottom one. A compressive load was applied on the fixture with a Zwick/Roell 250 kN universal testing machine, which resulted in a tensile force on the

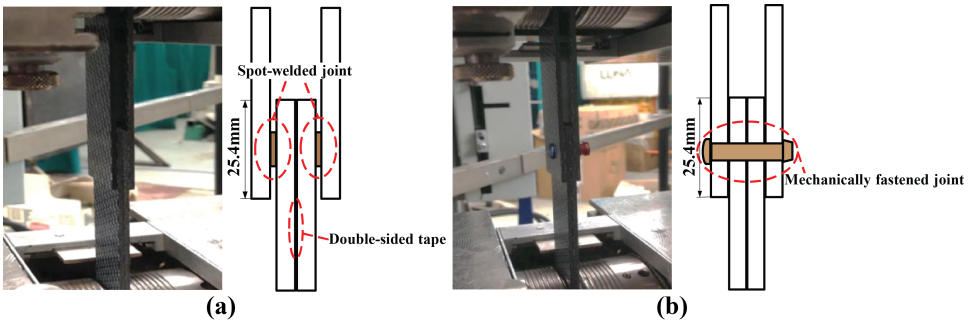

Figure 2.1: Loading fixture and specimen configurations for DLS tests: (a) spot welded specimen; (b) mechanically fastened specimen.

joints. Specimens were loaded with a crosshead displacement rate of 0.5 mm/min and the tests were stopped following the 30 % load drop principle as well. Five specimens were tested for both types of joints.

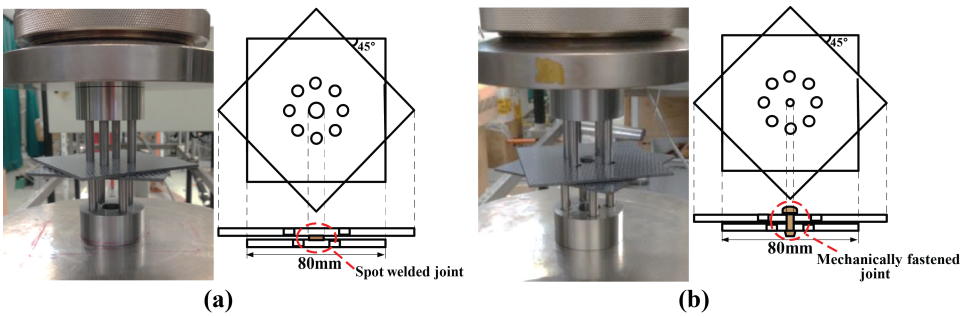

Figure 2.2: Loading fixture and specimen configurations for PT tests: (a) spot welded specimen; (b) mechanically fastened specimen.

Load-displacement (L-D) curves recorded during the tests were utilized to characterize the mechanical behaviour of both types of joints. As illustrated in Refs. [21, 24, 28], the loading process of the mechanically fastened specimens normally shows two failure points, namely onset failure and ultimate failure. In this study, both of the load values on these two points were noted, hereafter mentioned as onset failure load (OFL) and ultimate failure load (UFL), to evaluate the load-carrying capability of the joints. The OFL was calculated by the bilinear approximation method, which is commonly used in numerical modelling to characterize the structural failure and proved to provide good fits to the experimental L-D curves [29, 30]. An example is shown on representative DLS (a) and PT (b) L-D curves for mechanically fastened joints in Fig. 2.3. Linear fitting was performed on the stages before and after the stiffness reduction and the OFL was located at the intersection of two fitting lines. According to the statement in ASTM D7332 [27], OFL of specimens in PT tests is regarded as the first peak load during the loading process in correspondence with a significant load drop (more than 10 %). However, the first obvi-

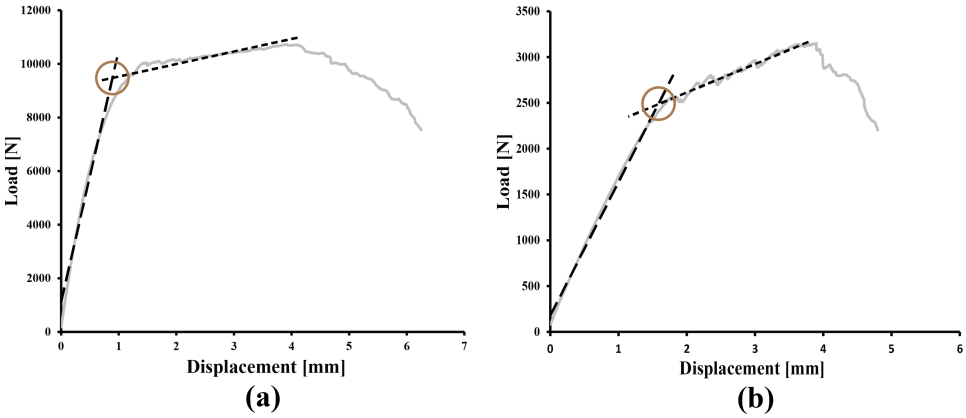

Figure 2.3: Bilnear approximation (dashed lines) for the OFL of mechanically fastened joints in DLS (a) and PT (b) tests. OFL is indicated by the circles on the intersection of two fitting lines.

ous load drop for all mechanically fastened specimens was found to be lower than 10 %, which will be mentioned in Section 2.3.2. Therefore, to keep consistent with the results in DLS tests, the OFL of the mechanically fastened joint is also calculated by using the bilinear approximation method. The UFL is recorded by the maximum load point on the L-D curves. Additionally, the linear fitting of the initially elastic stage of L-D curves corresponds to the joint stiffness (JS), which is another interesting mechanical property for the comparison between the welded and the mechanically fastened joints in this study.

Fracture surfaces were inspected using a Zeiss Stereo Microscope. Further fracture analysis was carried out on welded specimens with a JSM-7500F Scanning Electron Microscope (SEM). Finally, the Damage Affected Zone (DAZ) as well as the through-the-thickness failure within specimens were evaluated via a C-scan and also cross-sectional optical microscopy.

2.2.2. LAMINATES

The material used in this study was 5 harness satin fabric CF/PEEK (carbon fibre reinforced poly-ether-ether ketone), which was supplied by TenCate Advanced Composites, The Netherlands, owing to its excellent weld strength [31]. Six-ply laminates with dimensions of 580 mm × 580 mm and with a $[0/90]_{3s}$ stacking sequence, were consolidated in a hot-platen press. The preimpregnated stacks were sandwiched between two aluminium plates and were compression moulded at 385 °C and 1 MPa for 20 min. The final thickness of the laminates was approximately 1.90 mm, which is the typical thickness used for the TPC laminates in aerospace applications. Afterwards, specimens were cut into the required dimensions according to the test procedures, i.e. DLS and PT tests, with a water cooled diamond saw.

2.2.3. ASSEMBLY TECHNIQUES

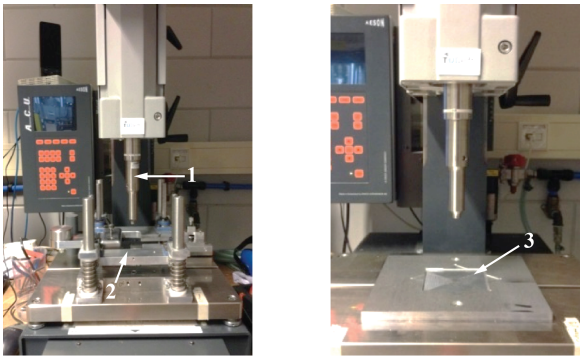

Figure 2.4: Ultrasonic welder and welding jigs used in this study.1: circular sonotrode with a diameter of 10 mm, 2: welding jig for DLS specimens, 3: welding jig for PT specimens.

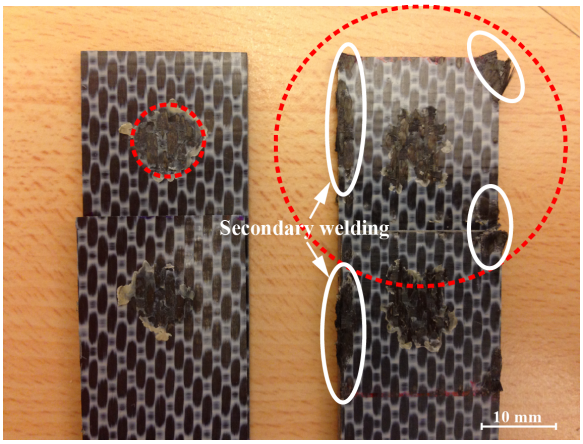

Figure 2.5: Ultrasonic spot welded joints created by the 10 mm-diameter sonotrode (left) and by the 40 mm-diameter sonotrode (right) at 600 J energy, 1500 N welding force and 60.8 μm (left) and 51.8 μm (right) peak-to-peak amplitude. The dotted lines indicate the overlap-area of the corresponding sonotrodes. Secondary welding is found at the overlap edge of the joints created by the latter sonotrode.

ULTRASONIC SPOT WELDING

A 20 kHz Rinco Dynamic micro-processor controlled ultrasonic welder was employed in this study to weld individual specimens. Fig. 2.4 shows the welding set-up equipped with a 10 mm-diameter cylindrical sonotrode. The 40 mm-diameter sonotrode which was commonly used for producing welded joints with fully-welded overlap [7, 10, 11], was proven to be not well-suited for spot welding in this study. This was attributed to its big cross-section, which covered the entire overlap of the welded samples and resulted in secondary welding at the overlap edges, as shown in Fig. 2.5. In contrast, the 10 mm-diameter sonotrode was shown to effectively prevent secondary welding since the circumference of its cross-section was away from the overlap edge of the welded samples. Two different custom-made welding jigs were utilized to accommodate the specimen

configurations for either the DLS or the PT tests, as shown in Fig. 2.4(a) and (b), respectively. Specifically in this study, adherends were first single-lap welded on the welding jig in Fig. 2.4(a). Then, the DLS specimens were created with a pair of single-lap specimens by using double-sided tape, as shown in Fig. 2.1(a).

An energy-controlled welding mode was adopted in this research for the spot welding process. This welding control strategy is however not supposed to be a robust technique for producing welds with consistent quality since during the welding process, energy is not only used to create welds but it is also dissipated into the surroundings, such as adherends and fixtures [32]. Villegas [11] proposed another welding control strategy, namely displacement-controlled welding, in her research on ultrasonic welding of full overlaps. The duration of the vibration phase of this welding procedure is controlled by a pre-defined displacement of the sonotrode. She also provided evidence which indicated that this procedure was more suitable to produce welds with consistent weld strength than energy-controlled welding. However, as depicted in Fig. 2.6, in ultrasonic spot welding, the sonotrode displacement (indicated by the grey line) was found to reach a plateau before the optimum stage of the welding process, which is represented by the second plateau of the power curve [11]. Therefore, displacement-controlled welding could not be adopted in this study and energy-controlled welding was used instead. Based on knowledge gathered from preliminary experimental results, 600J input energy with 1500 N welding force and 60.8 μm peak-to-peak amplitude were used as the welding parameters to define the vibration phase during the welding process in this study. According to observations during the experiments, the combination of the selected welding force (1500 N) and the amplitude (60.8 μm peak-to-peak) led to a stable welding process. Therefore, this parameter combination will be also used in the experiment series in the following chapters. Afterwards the vibration phase, the joints were allowed to consolidate at 1500 N for 4.0 s.

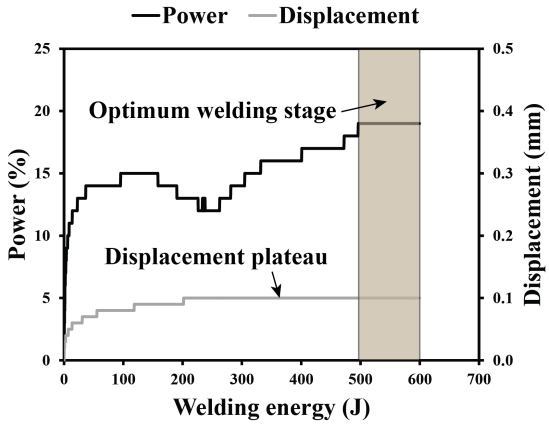

Figure 2.6: Displacement plateau in the ultrasonic spot welding process, occurring before the optimum welding stage.

Spot flat energy directors, made of a neat resin film, were used to create the spot

welded joints in this study, as shown in Fig. 2.7. To keep consistent with the pin diameter of the mechanical fasteners, 4 mm-diameter-circular energy directors (EDs) were used, as cut from the PEEK film with a nominal thickness of 0.25 mm. Prior to the welding process, the spot EDs were manually fixed on the bottom adherend with a Rinco hand-held ultrasonic welder. The ED melted, flowed and created a bigger spot welded joint (approximately 10 mm in diameter) during the welding process, which will be illustrated in detail in Section 2.3.1.

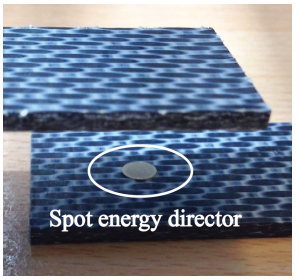

Figure 2.7: Spot energy director fixed on composite adherend prior to welding process.

MECHANICAL FASTENING

Titanium Hi-Lok® fasteners HL10V6 and HL12V6 (protruding head for both) were used to join the composite adherends for the DLS and PT tests, respectively. As indicated in Fig. 2.8, both of these two models of fasteners have a 4.8 mm-diameter-pin, which is close to the diameter of the spot energy director (4 mm). In addition, the 7 mm length pin of the HL10V6 fastener is well-suited for the installation of four composite adherends, which has an overall thickness of around 7.6 mm. The HL12V6 fastener has a 9.3 mm-diameter-head, which is designed for carrying peel load and approximately equal to the diameter of the spot welds (approximately 10 mm). Hi-Lok® fasteners were manually installed with a ratchet wrench, following [33]. The installation of Hi-Lok® fasteners was completed by the failure of the collar's wrenching device [33], providing a consistent clamping force for all of the mechanically fastened joints.

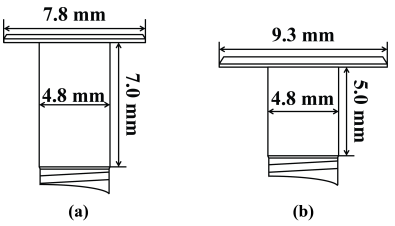

Figure 2.8: Schematic of the Hi-Lok® fasteners utilized in the mechanical tests: (a) HL10V6; (b) HL12V6.

2.3. RESULTS AND DISCUSSION

2.3.1. MECHANICAL BEHAVIOUR OF BOTH TYPES OF JOINTS IN DLS TESTS

A comparison of representative DLS L-D curves between the spot welded and mechanically fastened joints is summarized in Fig. 2.9. The black solid line corresponding to the spot welded specimen exhibits a linear behaviour with a continuous load increase and no obvious reduction of the joint stiffness observed until ultimate failure. On the contrary, the loading history of mechanically fastened specimen with a HL10V6 fastener (the grey dashed line) shows different stages, which is in good agreement with the study in Ref. [21]. Basically, four different stages can be observed from the L-D curve: (1) the load linearly increases in the initial period until the obvious slope/stiffness alternation. Although the load transfer mechanisms are different in this stage, due to the very small change of the stiffness, the first two stages illustrated in Ref. [21] are regarded as one stage; (2) the joint stiffness keeps on decreasing while the load continues to increase due to the presence of bearing damage; (3) the load almost keeps constant until the maximum point (UFL), illustrating the joint slowly losing load-carrying capability with the evolution of bearing damage; (4) the load has a continuous drop which indicates the ultimate failure of the joint.

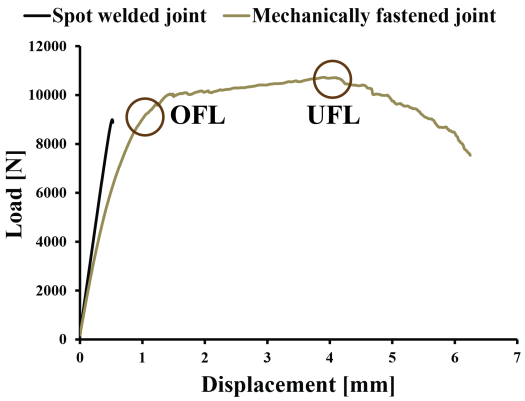

Figure 2.9: Comparison of representative Load-displacement curves between spot welded (solid line) and mechanically fastened (dashed line) joints in DLS tests. The left and right circles indicate the onset and ultimate failure, respectively. The data are adopted from Ref. [34].

Table 2.1 lists the average OFL, UFL and JS of both types of joints, accompanied by the corresponding coefficient of variation (COV) in the parentheses. Since the welded specimens failed immediately after the maximum load was reached, only UFL was represented. As mentioned in Section 2.2.1, the OFL of mechanically fastened joints, which is more important in the structural design rather than the UFL [24], was calculated by using bilinear approximation. It is notable that the OFL of both types of joints in DLS tests are within the same range, which is also indicated by the bar graph in Fig. 2.10. The variation of the load-carrying capability of both types of joints are within standard deviation, which is displayed by the error bars. In contrast, the averaged stiffness of spot welded joints is reported to be substantially higher, by 88 %, than the mechanically fas-

Table 2.1: Experimental results on both types of joints for DLS tests.

Joint type	Average OFL (N) (COV %)	Average UFL (N) (COV %)	Avrage JS (N/mm) (COV %)
Spot welded joints	-	9645.9 (10.6)	17954.4 (3.0)
Mechanically fastened joints (HL10V6)	9190.7 (9.2)	10403.6 (7.5)	9542.5 (7.3)

(OFL: onset failure load, UFL: ultimate failure load, JS: joint stiffness, COV: coefficient of variation).

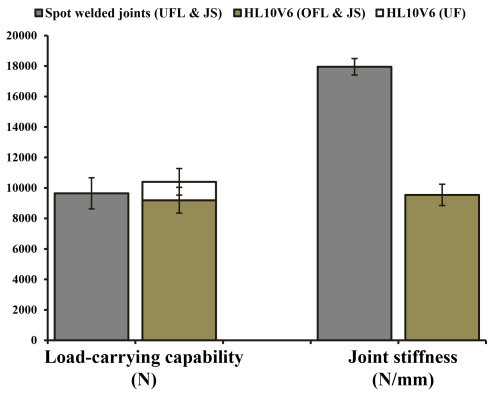

Figure 2.10: Comparison of in-plane mechanical (shear) performance for both types of joints in DLS tests. (OF: onset failure, UF: ultimate failure) The error bars indicate the standard deviation.

tened specimens. In addition, the COV is lower for the spot welded joints.

To figure out the main cause for the stiffness reduction in the mechanically fastened joints, tensile tests were carried out on CF/PEEK composites coupons with and without the central hole. Fig. 2.11 shows the experimental results. It can be noted that, compared to intact composite coupons, the stiffness reduction of central-cut coupon (approximately 12 %) is not as significant as the stiffness difference observed in DLS tests. Therefore, the stiffness degradation observed in the mechanically fastened joints is likely induced by the concentrated pin-load applied on the interior of the circumference of the bolted hole during the DLS tests.

Regarding the fracture surfaces, a post-mortem visual inspection of the welded specimens indicated the presence of a circular welded joint on the overlap, as shown in Fig. 2.12a. The diameter of the spot welded joints was found to be approximately 10 mm on average, which is about 150 % and 108 % in excess of the original ED (4 mm) and the pin of the Hi-Lok® fastener (4.8 mm), respectively. The rest of the overlap remains intact and no further damage is observed. Intralaminar failure was confirmed by the SEM analysis, following the high quality of the bond created during the welding process [35]. This failure mode is represented by tearing of fibre bundles of the out-most laminate ply (Fig. 2.12b) and fibre-matrix debonding (Fig. 2.12c). A further magnification of Fig. 2.12c

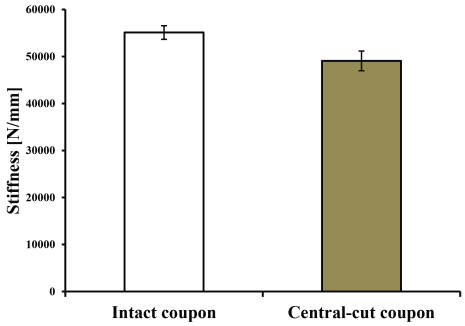

Figure 2.11: Comparison of stiffness between intact and central-cut coupon in tensile test.

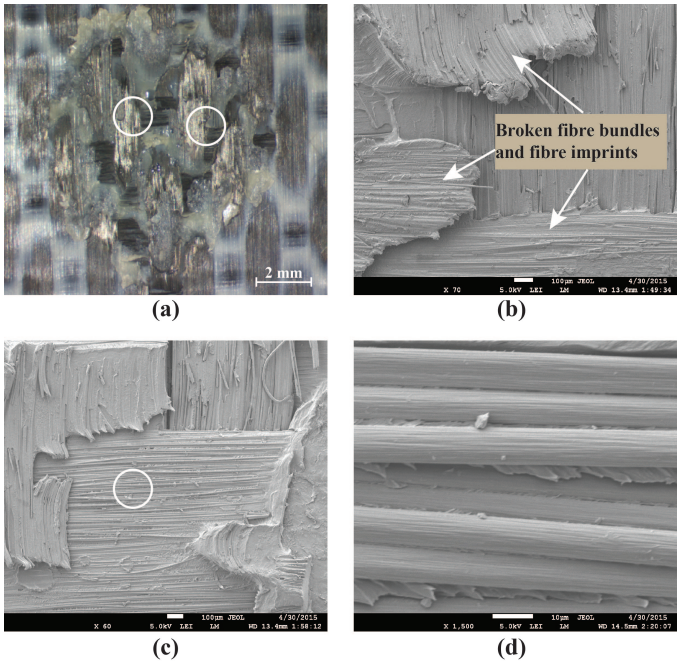

Figure 2.12: Fracture surface (a) and SEM detail (b-d) for spot welded joints after DLS tests. The left and right circles in (a) indicate the approximate locations of (b) and (c), respectively. The circle in (c) indicates the location for (d). Welding parameters: 600 J energy, 1500 N welding force, 60.8 μm peak-to-peak amplitude.

is shown in Fig. 2.12d, providing a better observation on the separation between fibres and thermoplastic resin, indicating the fibre-matrix debonding.

Mechanically fastened specimens after DLS tests are illustrated in Fig. 2.13. Due to the penetration of the fastener during the loading process, a catastrophic bearing failure is found on the composite adherends. Fig. 2.13a and b show the top and bottom sides of the mechanically fastened specimen, respectively. Two cracks are observed on the outer plates, propagating towards the edges of the overlap, indicating that shear-tear out

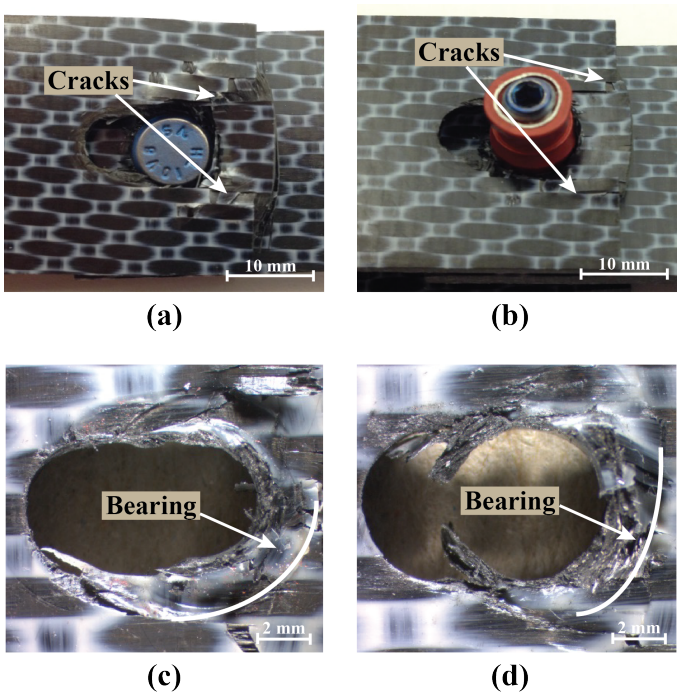

Figure 2.13: The top (a) and bottom (b) view of mechanically fastened joints (HL10V6) after DLS tests and fracture surfaces of outer (c) and inner (d) adherends after removing the fastener.

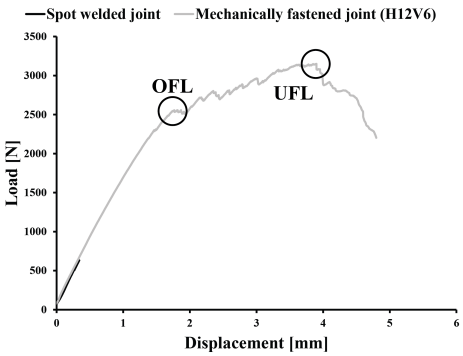

Figure 2.14: Comparison of representative load-displacement curves between spot-welded (solid line) and mechanically fastened (dashed line) joints in PT tests. The left and right circles indicate the onset and ultimate failure, respectively. The data are adopted from Ref. [34].

failure will eventually take place in the composite plates. Fig. 2.13c and d provide a clear view of bearing failure on the adherends after removing the mechanical fastener, which is similar to the observation in Ref. [21]. However, both outer and inner plates show obvious bearing damage together with elongated bolted holes. The possible explanation

could be that the total thickness of the four composite adherends is slightly larger than the pin length of the Hi-Lok® fastener. As a consequence, the head and collar of the fastener marginally penetrated into the outer plates and thus, led to further damage.

2.3.2. MECHANICAL BEHAVIOUR OF BOTH TYPES OF JOINTS IN PT TESTS

Fig. 2.14 shows representative L-D curves for both spot welded and mechanically fastened joints in PT tests. Similar to the DLS tests, spot-welded specimens exhibit a linear behaviour during the loading process without stiffness reduction. The averaged UFL is recorded at approximately 600 N, which is listed in Table 2.2, and is found to be much lower (by 82 %) than the UFL of the specimens joined with HL12V6 fasteners. The OFL of mechanically fastened specimens are calculated by using the bilinear approximation method and the average value is shown in Table 2.2 and Fig. 2.15. The lower UFL of the welded joints is because the mechanically fastened joints relies on the titanium fastener (head) under peel loading, while the resistance to pull-through force of welded joints comes from the interlaminar strength of the composite adherends. As it is known that composite laminates have low transverse properties [23, 24], the observation that load-carrying capability on peel loading of welded specimens is not comparable to the mechanically fastened counterparts is as expected.

Table 2.2: Experimental results on both types of joints for PT tests.

Joint type	**Average OFL (N) (COV %)**	**Average UFL (N) (COV %)**	**Avrage JS (N/mm) (COV %)**
Spot welded joints	-	593.8 (5.1)	1622.8 (4.5)
Mechanically fastened joints (HL12V6)	2455.5 (2.3)	3190.7 (2.4)	1429.3 (6.1)

(OFL: onset failure load, UFL: ultimate failure load, JS: joint stiffness, COV: coefficient of variation).

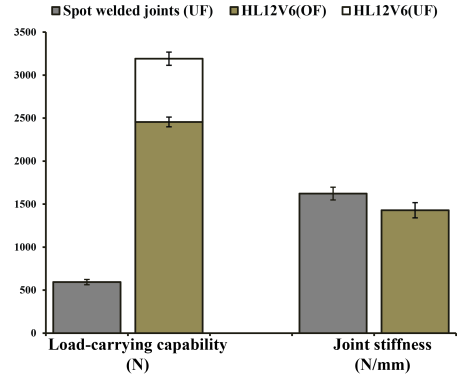

Figure 2.15: Comparison of out-of-plane mechanical (peel) performance for both types of joints in PT tests. (OF: onset failure, UF: ultimate failure) The error bars indicate the standard deviation.

Interestingly, irrespective of the substantial difference regarding load-carrying capability, spot welded specimens show a comparable, even slightly better, joint stiffness to the mechanically fastened specimens. Table 2.2 gives the experimental results of the JS of welded specimens, which is approximately 13 % in excess of that of HL12V6. It is believed that welded specimens are continuous within the joints (Fig. 2.16a), which provide more constraints for the adherend bending with load increase. In contrast, more flexibility is introduced by the clearance of fastener hole, as shown in Fig. 2.16b and c, which leads to a higher displacement and thus a lower stiffness.

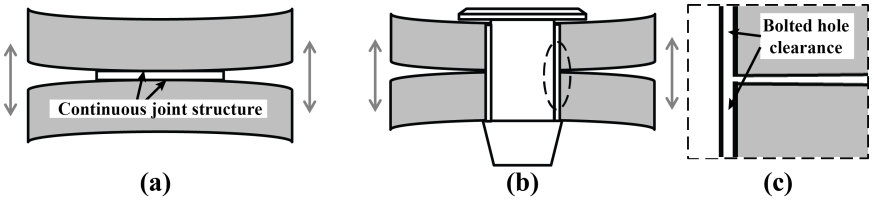

Figure 2.16: Comparison of out-of-plane mechanical (peel) performance for both types of joints in PT tests. (OF: onset failure, UF: ultimate failure) The error bars indicate the standard deviation.

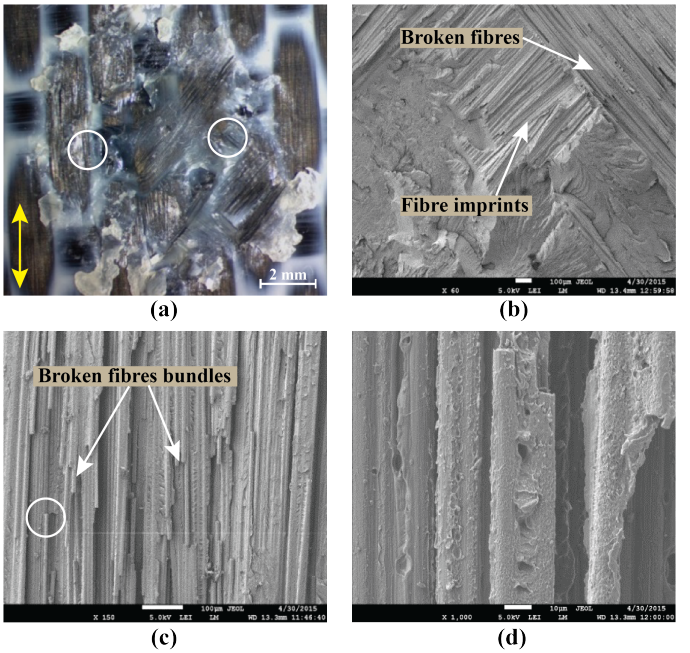

Figure 2.17: Fracture surface (a) and SEM detail (bed) for spot-welded joints after the PT test. The right and left circles in (a) indicate the approximate locations for (b) and (c), respectively. The circle in (c) indicates the location for (d). The apparent fibre orientation of the substrate is indicated by the vertical arrow in (a). Welding parameters: 600 J energy, 1500 N welding force, 60.8 μm peak-to-peak amplitude.

Fig. 2.17 illustrates the fracture analysis performed on the bottom adherend of spot

welded specimens after PT tests. Similar to the observations of the DLS specimens, a circular welded joint with an approximate diameter of 10 mm was found on the fracture surface in Fig. 2.17a. Fig. 2.17b gives SEM details for tearing of the out-most laminate ply. Broken fibres and fibre imprints are observed being distributed with 45° on the fracture surface, indicating they are from the out-most ply of the top adherend. Apart from that, Fig. 2.17c indicates the fibre-matrix debonding, which is shown as broken fibre bundles without little attached resin (Fig. 2.17d) resulted from the peel load. The mechanically fastened specimen in Fig. 2.18a shows the bottom plate is inserted by the Hi-Lok® collar after PT tests, which generates a local force and eventually leads to a bending failure of the laminates (Fig. 2.18b). The bending is found in the vicinity of the bolted hole (Fig. 2.18c) whereas cracks are radially growing away from the hole (Fig. 2.18d), indicating the eventual pull-through laminate failure.

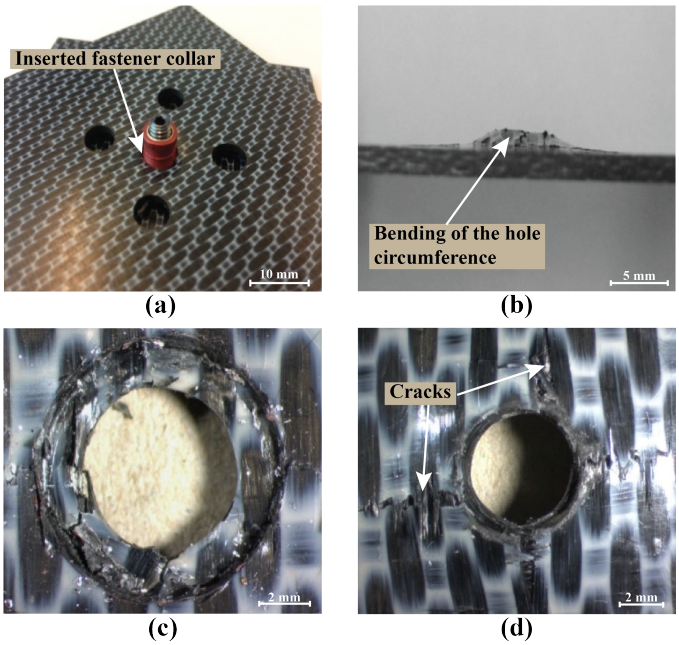

Figure 2.18: The Hi-Lok® collar (HL12V6) after the PT test (a) and the side (b), bottom (c) and top (d) view of fracture surface of bottom adherend after removing the fastener.

2.3.3. DAMAGE AFFECTED ZONE

A combination of ultrasonic C-scan and cross-sectional microscopy was used to assess the internal damage in both the welded and the mechanically fastened joints. To characterize the through-the-thickness damage utilizing a microscope, some selected specimens were cross-sectioned through the central line of the overlap, parallel to the apparent fibre orientation, as indicated in Fig. 2.19. Afterwards, the sectioned specimens were embedded in epoxy and polished. The experimental results are separately shown based on DLS and PT tests.

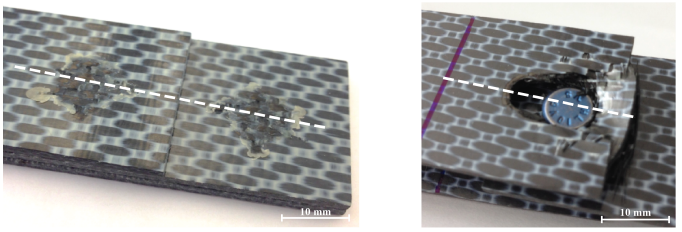

Figure 2.19: Central-cut of both welded (a) and mechanically fastened (b) specimens along the dashed lines for the cross-sectional microscopy.

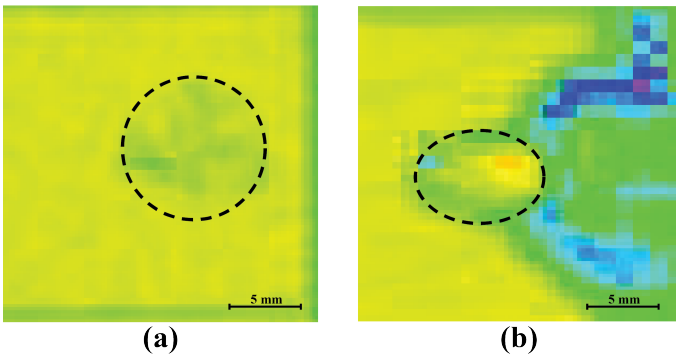

Figure 2.20: Comparison of damaged area of spot welded (a) and mechanically fastened (b) joints after DLS tests. The black dashed lines indicate the welded area (a) and deformed fastener hole (b) after DLS tests, respectively.

DLS TESTS

The C-scan results for the overlap area of both types of joints (welded vs. mechanically fastened) after DLS tests are presented in Fig. 2.20. The size of the damage affected zone (DAZ) in the welded specimen is considerably smaller than the mechanically fastened counterpart. It should be noted that the damaged area captured by C-scan is restricted to the welded area (Fig. 2.20a), in correspondence with the fracture surface in Fig. 2.12a. In contrast, the DAZ in mechanically fastened specimens is not only to be found in the vicinity of the fastener hole, but covers almost half of the overlap (Fig. 2.20b). The area in between the two cracks features a large amount of damage (delamination) in the laminates.

The cross-section micrographs of welded and mechanically fastened specimens provide a better characterization of the through-the-thickness damage, as shown in Fig. 2.21 and Fig. 2.22, respectively. For the welded specimen, naked fibre bundles as well as resin rich pockets are visible on the upper-most ply of the adherend in accordance with the fibre-matrix debonding failure described before. However, this intralaminar damage is exactly limited to the first ply and no damage can be found in the rest of the adherend. Contrastingly, the laminate structure of the mechanically fastened joint is catastrophically damaged in the form of delamination and matrix cracking. The penetration of the

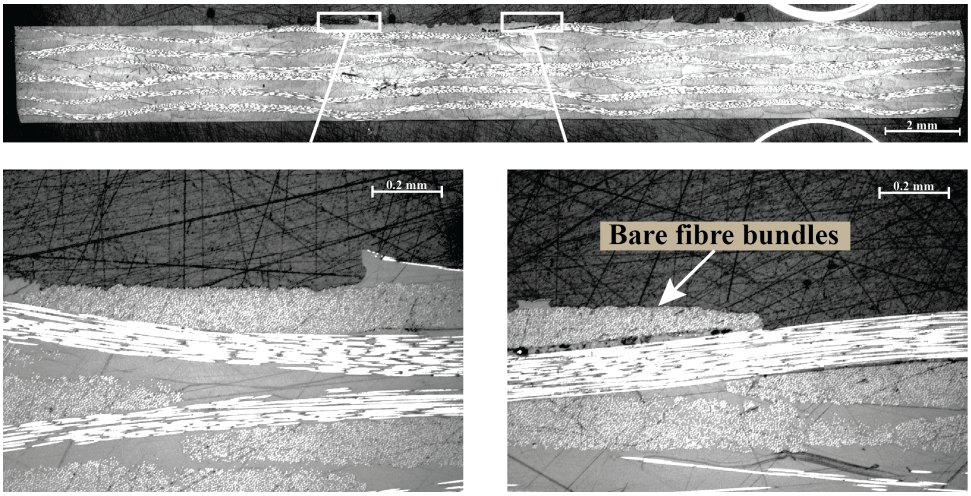

Figure 2.21: Micrographic cross-sections of spot welded joint after DLS tests. The scale bar for 2 mm is shown in the top figure. The bottom image is the magnification of the parts in the white boxes of the top one.

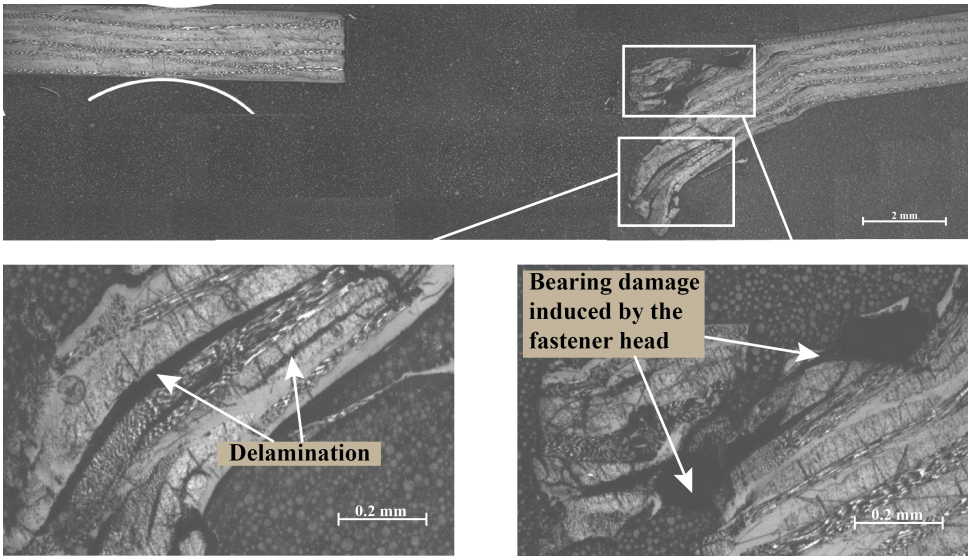

Figure 2.22: Micrographic cross-sections of mechanically fastened joint (HL10V6) after DLS tests. The scale bar for 2 mm is shown in the top image. The bottom images are the magnification of the parts in the white boxes of the top one.

head of the Hi-Lok® fastener results in an obvious deformation on the top. The severe interior damage of the adherend indicates that a relatively big area of material would need to be removed in order to repair the mechanically fastened joints after failure.

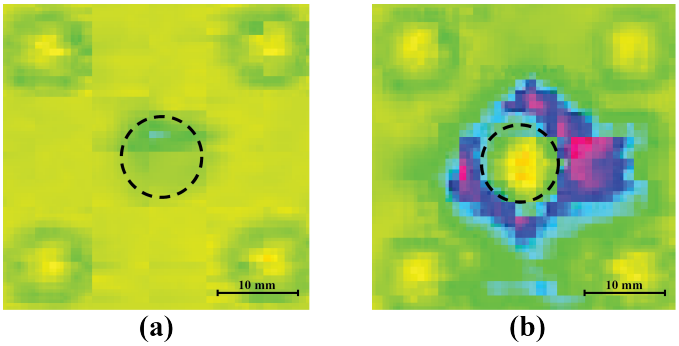

Figure 2.23: Comparison of damaged area of spot welded (a) and mechanically fastened (b) joints after PT tests. The black dashed lines indicate the welded area (a) and bolted hole (b) after PT tests. The four circles at the corners are the drilled holes for loading cylinders in PT tests.

PT TESTS

The comparative analysis of the C-scan images for the two types of joints after the PT tests has similar results to those of the DLS specimens. The images in Fig. 2.23 display a significantly larger DAZ in the mechanically fastened specimen than in the spot welded counterpart. The DAZ of the latter is invariably limited to the welded region. Nevertheless, the internal damage in the mechanically fastened adherends is not only at the periphery of the hole but has a perceptible influence on the surrounding area, which displays a good fits with the result in Ref [24].

Fig. 2.24 shows the cross-section of the welded joint, comprised of a failure taking place both within the post-welded ED on the surface and within bare fibre bundles in the out-most ply. Conversely, matrix rupture is found on the top of the adherend of the mechanically fastened specimen due to the over-bending (Fig. 2.23). Furthermore, as a consequence of the insertion of the Hi-Lok® collar, the laminates are compressed in the vicinity of the fastener hole and hence delaminations are generated.

2.4. CONCLUSIONS

IN this chapter, a series of experimental studies, including two different types of mechanical tests (DLS and PT tests) and fractograpic analysis, were carried out on carbon fibre reinforced PEEK composite specimens. The mechanical behaviour, failure modes and DAZ were characterized and compared between spot welded joints and mechanically fastened joints employing Hi-Lok® fasteners. The spot welds created in both tests were found to be approximately 10 mm in diameter, which was approximately two times bigger than the original EDs as well as the employed Hi-Lok® fasteners. Additionally, based on different tests, the following conclusions can be drawn:

1. DLS tests:

- The spot welded joints achieved a comparable load-carrying capability on shear load to the mechanically fastened joints, ranging from 94 % to 112 % of the average OFL of the mechanically fastened counterparts (HL10V6).

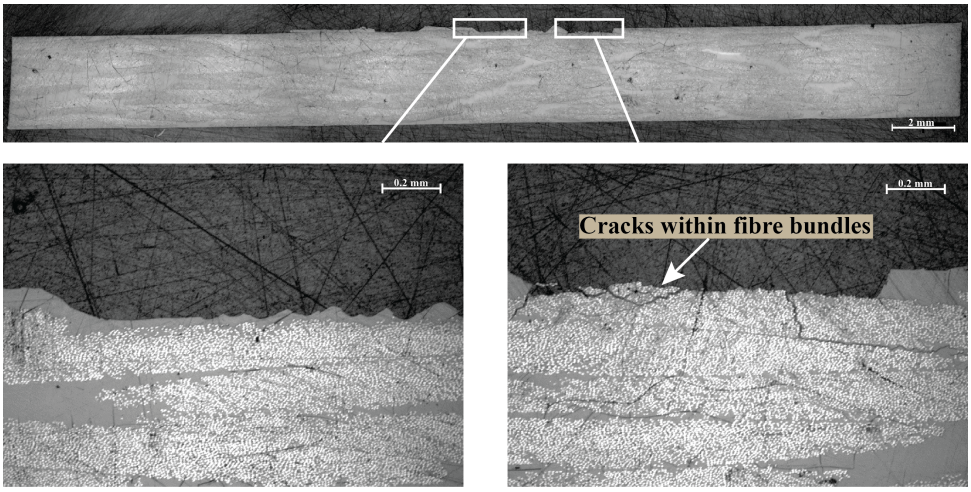

Figure 2.24: Micrographic cross-sections of spot welded joint after PT tests. The scale bar for 2 mm is shown in the top image. The bottom images are the magnification of the parts in the white boxes of the top one.

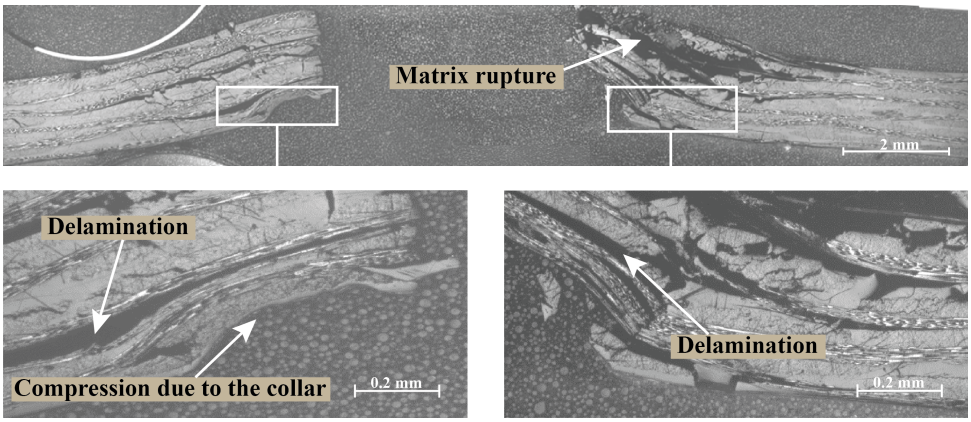

Figure 2.25: Micrographic cross-sections of mechanically fastened joint (HL12V6) after PT tests. The scale bar for 2 mm is shown in the top image. The bottom images are the magnification of the part in the white boxes of the top one.

- The spot welded joints showed an 88 % higher average stiffness as compared to the mechanically fastened joints under shear loading. Extra tensile tests indicated that bearing load applied on the adherend by the fastener pin, rather than the bolted hole, is the main cause for the stiffness reduction of mechanically fastened specimens.

- Intralaminar failure was found to be the major failure mode for spot welded joints, consisting of laminate tearing and fibre-matrix debonding. Further visual inspection by C-scan and optical microscopy indicated that failure in welded specimens

was exactly restricted in the welded area and the outermost ply of the adherend. Conversely, through-the-thickness bearing damage, comprising severe delamination and matrix cracking, was introduced into the composite adherends of mechanically fastened specimens. Moreover, the damaged area was reported to be far beyond the vicinity of the bolted hole.

2. PT tests:

- The load-carrying capability of spot welded joints was found to be inferior to that of the mechanically fastened joints, ranging from 22 % to 24 % of the average onset failure load of HV12V6. This is reasonable since the Hi-Lok® fastener acts as a through-the-thickness reinforcement and hence the mechanically fastened joints do not entirely rely on the through-the-thickness strength of the composite laminate to carry the peel load, as opposed to the welded joints.

- The spot welds showed a slightly higher joint stiffness on average under peel loading, approximately 113.5 % comparing to the mechanically fastened counterparts. A possible explanation is the clearance between the bolted hole and the Hi-Lok® fastener providing more flexibility for the bending of adherends.

- Intralaminar failure was still the major failure mechanism for spot welded joints in PT tests and neither further damaged area on surfaces nor through-the-thickness damage were observed. In contrast, delamination was found inside the adherend of mechanically fastened specimens. Moreover, in the vicinity of the hole, laminates were severely compressed because of the penetration of the Hi-Lok® head and collar during the tests.

In general, the limited damaged area and intact adherends after joint failure for spot weld provide ease of repairing and reusability of welded structural components. In particular, for structures carrying shear load, the comparable load-carrying capability and outstanding joint stiffness provide the possibility for spot welded joints to be a substitute for the conventional mechanical fasteners, although the larger diameter for the welded spots should be taken into account. However, it should be noted that the geometries of both the welded spots and the mechanically fasteners are the most representative for the structural applications. In addition, the load-carrying capability of mechanically fastened joints, in particular under the peel loading, should not be discredited.

REFERENCES

[1] T. Zhao, G. Palardy, I.F. Villegas, C. Rans, M. Martinez, and R. Benedictus. Mechanical behaviour of thermoplastic composites spot-welded and mechanically fastened joints: A preliminary comparison. *Composites Part B: Engineering*, 112:224–234, 2017.

[2] A.R. Offringa. Thermoplastic composites - rapid processing applications. *Composites Part A: Applied Science and Manufacturing*, 27(4 PART A):329–336, 1996.

[3] H. Shi, I.F. Villegas, and H.E.N. Bersee. Strength and failure modes in resistance welded thermoplastic composite joints: Effect of fibre-matrix adhesion and fibre orientation. *Composites Part A: Applied Science and Manufacturing*, 55:1–10, 2013.

[4] A. Yousefpour, M. Hojjati, and J.P. Immarigeon. Fusion bonding/welding of thermoplastic composites. *Journal of Thermoplastic Composite Materials*, 17(4):303–341, 2004.

[5] C. Ageorges, L. Ye, and M. Hou. Advances in fusion bonding techniques for joining thermoplastic matrix composites: A review. *Composites - Part A: Applied Science and Manufacturing*, 32(6):839–857, 2001.

[6] V.K. Stokes. Joining methods for plastics and plastic composites: An overview. *Polymer Engineering & Science*, 29(19):1310–1324, 1989.

[7] I.F. Villegas, L. Moser, A. Yousefpour, P. Mitschang, and H.E.N. Bersee. Process and performance evaluation of ultrasonic, induction and resistance welding of advanced thermoplastic composites. *Journal of Thermoplastic Composite Materials*, 26(8):1007–1024, 2013.

[8] J.W. Ingen, A. Buitenhuis, M. Wijngaarden, and F. Simmons III. Development of the gulfstram g650 induction welded thermoplastic elevators and rubber. In *Proceedings of the international SAMPE symposium and exhibitions*, Seattle, WA, USA, May 2010.

[9] X.R. Xiao, S.V. Hoa, and K.N. Street. Repair of thermoplastic resin composites by fusion bonding. In *Proceedings of the Symposium on Composites Bonding*, pages 30–44, Airport, TX, USA, October 1993.

[10] I.F. Villegas. In situ monitoring of ultrasonic welding of thermoplastic composites through power and displacement data. *Journal of Thermoplastic Composite Materials*, 28(1):66–85, 2015.

[11] I.F. Villegas. Strength development versus process data in ultrasonic welding of thermoplastic composites with flat energy directors and its application to the definition of optimum processing parameters. *Composites Part A: Applied Science and Manufacturing*, 65:27–37, 2014.

[12] S. Fukumoto, I. Lum, E. Biro, R. Boomer, and Y. Zhou. Effects of electrode degradation on electrode life in resistance spot welding of aluminum alloy 5182. *Welding Journal*, pages 307–312, 2003.

[13] N. Afrin, D.L. Chen, X. Cao, and M. Jahazi. Microstructure and tensile properties of friction stir welded az31b magnesium alloy. *Materials Science and Engineering: A*, 472(1):179 – 186, 2008.

[14] V.K. Patel, S.D. Bhole, and D.L. Chen. Ultrasonic spot welding of lightweight alloys. In *Proceedings of 13th International Conference on Fracture*, pages 1–10, Bijing, China, June 2013.

[15] P. Prangnell, H. Haddadi, and Y. C. Chen. Ultrasonic spot welding of aluminium to steel for automotive applications—microstructure and optimisation. *Materials Science and Technology*, 27:617–624, 2011.

[16] V. K. Patel, S. D. Bhole, and D. L. Chen. Microstructure and mechanical properties of dissimilar welded mg–al joints by ultrasonic spot welding technique. *Science and Technology of Welding and Joining*, 17:202–206, 2012.

[17] A. Macwan, V.K. Patel, X.Q. Jiang, C. Li, S.D. Bhole, and D.L. Chen. Ultrasonic spot welding of al/mg/al tri-layered clad sheets. *Materials and Design (1980-2015)*, 62:344 – 351, 2014.

[18] V.K. Patel, S.D. Bhole, and D.L. Chen. Influence of ultrasonic spot welding on microstructure in a magnesium alloy. *Scripta Materialia*, 65(10):911 – 914, 2011.

[19] P. Mitschang, R. Velthuis, and M. Didi. Induction spot welding of metal/cfrpc hybrid joints. *Advanced Engineering Materials*, 15:804–813, 2013.

[20] F. Balle, F. Staab, and J. Born. Joining of light metals to fiber reinforced polymer composites by power ultrasonics. 2016.

[21] T.L. Qin, L.B. Zhao, and J.Y. Zhang. Fastener effects on mechanical behaviors of double-lap composite joints. *Composite Structures*, 100:413 – 423, 2013.

[22] T. D'Antino, L. H. Sneed, C. Carloni, and C. Pellegrino. Effect of the inherent eccentricity in single-lap direct-shear tests of pbo frcm-concrete joints. *Composite Structures*, 142:117 – 129, 2016.

[23] A. Banbury and D.W. Kelly. A study of fastener pull-through failure of composite laminates. part 1: Experimental. *Composite Structures*, 45(4):241 – 254, 1999.

[24] T. Ćwik, L. Iannucci, and M. Effenberger. Pull-through performance of carbon fibre epoxy composites. *Composite Structures*, 94(10):3037 – 3042, 2012.

[25] ASTM D3528-96. Standard test method for strength properties of double lap shear adhesive joints by tension loading, 1996.

[26] ASTM D5961/D5961M-01. Standard test method for bearing response of polymer matrix composite laminates, 2001.

[27] ASTM D7332/D7332M-09. Standard test method for measuring the fastener pull-through resistance of a fiber-reinforced polymer matrix composite, 2009.

[28] G. Catalanotti, P.P. Camanho, P. Ghys, and A.T. Marques. Experimental and numerical study of fastener pull-through failure in gfrp laminates. *Composite Structures*, 94(1):239 – 245, 2011.

[29] A.B. de Morais, A.B. Pereira, M.F.S.F. de Moura, F.G.A. Silva, and N. Dourado. Bilinear approximations to the mixed-mode i–ii delamination cohesive law using an inverse method. *Composite Structures*, 122:361 – 366, 2015.

[30] J.P.H. Belnoue, S. Giannis, M. Dawson, and S.R. Hallett. Cohesive/adhesive failure interaction in ductile adhesive joints part ii: Quasi-static and fatigue analysis of double lap-joint specimens subjected to through-thickness compressive loading. *International Journal of Adhesion and Adhesives*, 68:369 – 378, 2016.

[31] B. Harras, K.C. Cole, and T. Vu-Khanh. Optimization of the ultrasonic welding of peek-carbon composites. *Journal of Reinforced Plastics and Composites*, 15(2):174–182, 1996.

[32] A. Benatar and T.G. Gutowski. Ultrasonic welding of peek graphite apc-2 composites. *Polymer Engineering & Science*, 29(23):1705–1721, 1989.

[33] Hi-Shear. Corporation. hi-lok®;/hi-tigue fastening systems installation instructions. 1991.

[34] T. Zhao, G. Palardy, I. F. Villegas, C. Ran, and R. Benedictus. Comparative analysis of in-plane and out-of-plane mechanical behaviour of spot-welded and mechanically fastened joints in thermoplastic composites. In *Proceedings of 17th European Conference of Composite Materials*, Munich, Germany, June 2016.

[35] I.F. Villegas and H.E.N. Bersee. Ultrasonic welding of advanced thermoplastic composites: An investigation on energy-directing surfaces. *Advances in Polymer Technology*, 29(2):112–121, 2010.

3

Effect of Boundary Conditions on Ultrasonic Spot Welding of Thermoplastic Composites

This chapter focused on assessing the effect of boundary conditions, in particular two different types of clamping jigs, on single-spot ultrasonic welded joints in thermoplastic composites. The research was motivated by the fact that in sequential ultrasonic welding of multi-spot welded joints the boundary conditions for each new spot are influenced by existing spots, which might entail continuous recalculation of welding parameters. The results showed that the welding energy consumed to obtain maximum strength welds was significantly affected by the clamping jig. Contrarily, the displacement undergone by the sonotrode until maximum weld strength was reached was found to be rather insensitive to the clamping jig. Consequently, displacement-controlled welding was preliminary identified as the most promising welding control strategy for sequential ultrasonic welding of thermoplastic composite structures.

Parts of this chapter have been published in Composites Part A: Applied Science and Manufacturing **109**, 355-367 (2018). [1].

3.1. INTRODUCTION

ULTRASONIC welding is an attractive joining technique for thermoplastic composites (TPCs), owing to the short welding times, absence of foreign materials at the weld-line, possibility for in-situ monitoring and ease of automation [2–4]. However, upscaling of the process technique towards configurations with large overlaps is still a challenge [5]. Ultrasonic welding in TPCs is by nature a spot welding technique, hence the most straightforward upscaling route is sequential welding of consecutive spots resulting in a multi-spot welded (MSW) joint. According to our previous research [6], single-spot welded (SSW) thermoplastic composite joints yield similar shear strength as joints with a single mechanical fastener of comparable size. Consequently, sequential multi-spot welding has the potential to become a composite-friendly and fast-processing alternative to mechanical fastening in thermoplastic composite structures.

Unlike ultrasonic spot welding of metallic materials [7–10], ultrasonic spot welding of thermoplastic composites has been barely explored. At the beginning of the 90's, Lu and Benatar [11] reported successful results on sequential ultrasonic welding of thermoplastic composites although they provided no details on the way the process was carried out. To the best of the authors' knowledge, little to no research on the topic has been reported in the open literature since then. One of the main challenges of the sequential ultrasonic welding process is the fact that the boundary conditions of the welding process are likely to change with each new welded spot. In particular, the number of welded spots affects the stiffness of the overlap as well as the clamping scenario and hence has the potential to influence the way in which the ultrasonic vibration is distributed at the welding interface and in the adherends, as shown in Fig. 3.1. Consequently, obtaining welded spots of consistent quality in a MSW joint might require that different welding parameters are used for each spot if the welding process is not adequately controlled.

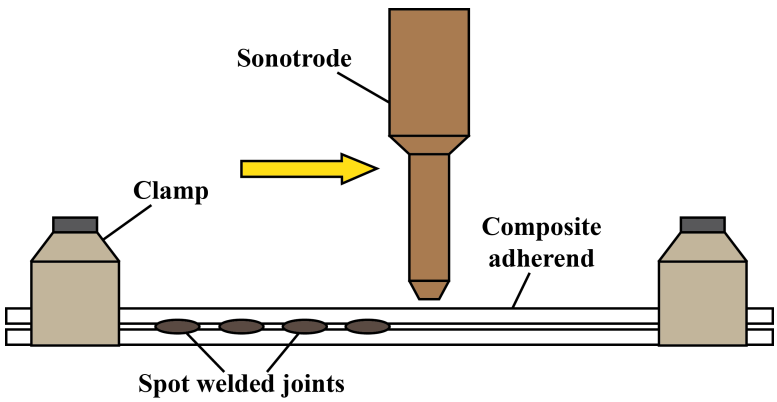

Figure 3.1: Schematic of the sequential ultrasonic spot welding process. The created welds introduce a step-like increase in the stiffness of the overlap, which provides a different boundary condition for the new spot. Dimensions are not to scale.

Microprocessor-controlled ultrasonic welders allow different modes to directly or indirectly control the duration of the vibration phase in the ultrasonic welding process. These control modes are typically based on the vibration time, the consumed energy

or the vertical displacement of the sonotrode. Among these, energy and displacement (i.e. indirect) control are typically preferred over time (i.e. direct) control. Harras *et al.* [12] performed a comparative study between time and energy control modes for the one-shot ultrasonic welding of Mode I and Mode II fracture toughness carbon fibre reinforced polyetheretherketone (CF/PEEK) samples. Their results showed that the maximum critical strain energy release rates (G_{IC} and G_{IIC}) were obtained when a constant welding energy input was used. However, the optimum welding time (i.e. the welding time resulting in maximum G_{IC} and G_{IIC}) was found to depend significantly on the sample configuration. Similarly, different research [13] showed a good correlation between weld strength and input weld energy for samples with different surface roughness. Finally, energy-controlled ultrasonic welding was successfully used in our previous research [6] to manufacture SSW joints in CF/PEEK adherends with consistent strength, failure modes and welded surface area.

Despite these successful results for energy-controlled welding, one needs to consider that the welding energy is not only used to create the weld, but it is also dissipated in the adherends and the clamping jig [14]. Hence, changes in, for instance, the thickness or stiffness of the adherends do have a significant impact in the energy required for the welding process [3]. Consequently, the step-like increase in the stiffness of the overlap together with changes in the clamping scenario caused by each new welded spot can be expected to affect the energy required for welding each spot in a sequential manner. Alternatively, displacement-controlled welding could help circumvent this issue since the vertical displacement of the sonotrode during the welding process is mainly related to physical changes in the weldline and the uppermost layer of the adherends, and hence it is fairly independent of the energy dissipated in the surroundings. The results of our previous research [3] indicated a potential superiority of displacement-controlled with regards to energy-controlled ultrasonic welding, however, no conclusive comparison between the two welding modes was carried out there.

The research presented in this chapter is an initial step of a bigger effort on the development of high-quality sequential ultrasonic welding for MSW thermoplastic composite joints. This chapter focuses on assessing the impact that changes in the boundary conditions of the ultrasonic welding process causes on the welding process itself and on its outcome, i.e. the quality of spot welded joints, for different controlling strategies. Even though geared towards sequential multi-spot welding, this research was performed on single-spot welded joints in order to simplify the experiments and analysis of the results. Two different welding (clamping) jigs were used to introduce different boundary conditions in both displacement-controlled and energy-controlled welding processes. The welding process was analysed through the feedback data, i.e. power and sonotrode displacement, provided by the ultrasonic welder. The quality of the spot welded joints was assessed through mechanical testing and fractographic analysis.

3.2. EXPERIMENTAL

3.2.1. MATERIALS

THE thermoplastic composite material used in this study was 5 harness satin fabric carbon fibre reinforced polyphenylene suphide (CF/PPS) supplied by Ten Cate Ad-

vanced Composites, The Netherlands. The reason for using CF/PPS instead of CF/PEEK composites was, due to the limited power of the ultrasonic welder in this study, the optimum displacement was unable to be reached when using displacement-controlled welding for the latter material. Laminates, consisting of six semi-impregnated fabric layers in a $[0/90]_{3s}$ stacking sequence, were consolidated in a hot platen press at 320 °C and 1 MPa for 20 min. Owing to the relatively lower portion of the thermoplastic resin in the used semi-impregnated pregreg, the resulting laminates had a final nominal thickness of 1.62 mm (less than 1.9 mm in Chapter 2) and, nominally, 58 % fibre volume fraction. Samples were subsequently cut with a water-cooled diamond saw into 101.6 × 25.4 mm^2 dimensions, then spot welded in the centre of a 25.4 × 25.4 mm^2 square overlap, as shown in Fig. 3.2. The main apparent orientation of fibres on the surface of the adherends was parallel to their longitudinal direction.

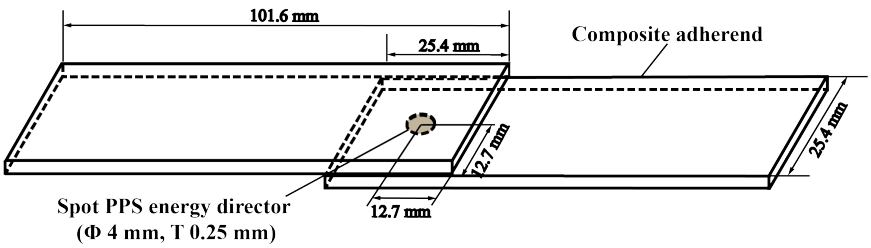

Figure 3.2: Schematic of the configuration of single-spot welded single-lap joints. The grey dashed ellipse indicates the location of the spot energy director (PPS, Φ: diameter, T: thickness) and thus the spot weld. Dimensions are not to scale.

3.2.2. ULTRASONIC WELDING PROCESS

A 20 kHz Rinco Dynamic 3000 microprocessor-controlled ultrasonic welder was used to weld individual SSW joint. As indicated in [3], this ultrasonic welder allows for a series of amplitude values for a fixed sonotrode/booster configuration. In this study, a 10 mm-diameter-circular titanium sonotrode was used for the spot welding process (see Fig. 3.3) similarly to previous research in [6].

In order to investigate the influence of boundary conditions on the welding process, two different custom-designed welding jigs, hereafter referred to as Jig 1 (Fig. 3.3a) and Jig 2(Fig. 3.3b) were used. In Jig 1, two fixed bars were used to clamp the adherends away from the welding overlap. The top adherend partially rested on the bottom adherend (overlap area) and on a 1.5 mm-thick aluminium supporting plate, as schematically shown Fig. 3.4a. Accounting for normal thickness variations in the adherends, such a thin supporting plate was chosen to prevent blocking of the downward movement of the sonotrode during melting and flowing of the ED in any case. As a consequence, the initial angle between the two welding surfaces nominally differed from 0 °. This initial lack of parallelism was subsequently corrected once the sonotrode was compressed against the overlap. However it did cause a non-uniform strain distribution in the ED which, as discussed in the Results and Discussion section, was believed to impact the flow of molten ED. In Jig 2, the top adherend was conversely clamped onto a platform supported by four springs and parallel to the base of the jig (see Fig. 3.4b). As a result

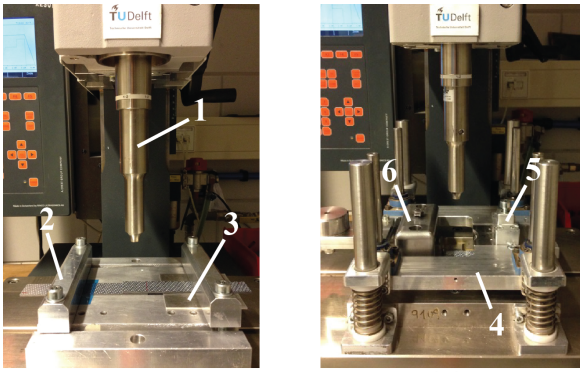

Figure 3.3: Ultrasonic welder, circular sonotrode and welding jigs used in this study: (a) Jig 1 and (b) Jig 2. 1. sonotrode, 2: bar clamp in Jig 1, 3: supporting plate, 4: sliding platform in Jig 2, 5: clamp for the top adherend and 6: clamp for the bottom adherend.

the top and bottom adherends were nominally parallel throughout the welding process. Apart from the geometrical aspects discussed above, the significant differences in the way the top adherend was clamped in Jig 1 and Jig 2 was expected to have a significant influence in the energy dissipated during the welding process.

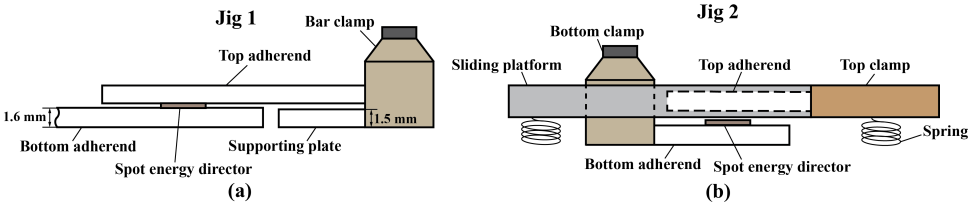

Figure 3.4: Schematic of the clamping situation in (a) Jig 1 and (b) Jig 2. Dimensions are not to scale.

During the vibration phase of the welding process, a mechanical vibration with 60.8 μm peak-to-peak amplitude was introduced in the welding stack. The welding force at the onset of the vibration phase was 1500 N and it was linearly increased at a rate of 1000 N/s throughout the vibration phase. After that, welded joints were consolidated under 1500 N force for 4 s. Either the vertical displacement of the sonotrode or the welding energy was used to indirectly control the duration of the vibration phase in displacement-controlled and energy-controlled welding, respectively. That is to say, the vibration phase was automatically stopped when either the pre-defined sonotrode displacement or the consumed energy value was reached. Following the procedure explained in [3], the optimum displacement (displacement-controlled welding process) or the optimum welding energy (energy-controlled welding process) for Jig 1 and Jig 2 were determined using the power and displacement curves provided by the ultrasonic welder. As described in detail in [4], based on power and displacement data the vibration phase of the welding process can be divided in the five stages depicted in Fig. 3.5. These stages

are related to the physical changes underwent by the ED and adherends and ultimately to the weld strength [3]. Therefore, the power and displacement curves can be used to determine the optimum displacement or the optimum welding energy, i.e. the displacement or energy values that result in maximum weld strength. These have been shown to lie within stage 4, which coincides with the occurrence of a second, relatively wide, power peak (see Fig. 3.5) [3, 4].

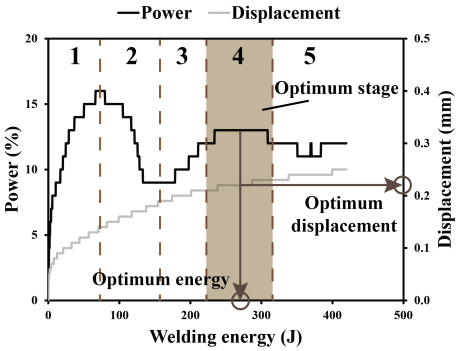

Figure 3.5: Typical calibration power curve for ultrasonic spot welding process. As stated in [3], the entire welding process can be divided into 5 stages and the stage 4 is regarded as the optimum stage since the maximum weld strength was consistently obtained in this stage.

3.2.3. TESTING AND ANALYSIS

The single-lap SSW joints were mechanically tested in a Zwick/Roell 250 kN universal testing machine following the ASTM D1002 standard [15]. The hydraulic grips of the testing machine were offset to ensure parallelism between the load path and the weldline in every sample. The distance between grips was 60 mm. Tests were initiated with a preload of approximately 100 N and performed at a crosshead speed of 1.3 mm/min. Five samples were tested per set of welding conditions. The apparent lap-shear strength (LSS)

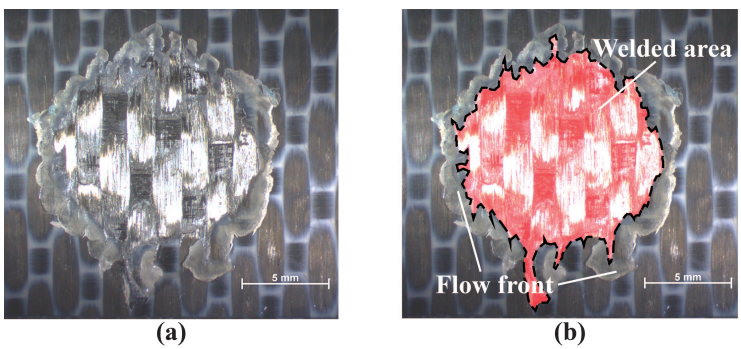

Figure 3.6: (a) Representative fracture surface of SSW joint and (b) definition of the corresponding WA (delimited by the dashed line) without taking into account the flow front of the ED.

was calculated as the maximum load recorded in the tests divided by the welded areas. In accordance with the results in [6], the load-displacement response of SSW joints exhibited a linear behaviour and hence, the maximum load reached in the lap-shear tests, referred to as ultimate failure load (UFL), was an indicator for the load-carrying capability of the spot-welded joints. The final welded areas (WAs) of SSW joints was visually inspected via a Zeiss stereo-microscope and was measured using ImageJ150 (NIH). Fig. 3.6b illustrates the definition of the WA in the SSW joint shown in Fig. 3.6a. It must be noted that, as a general rule in this study, the flow front of the ED was not considered for the measurement of the welded areas, i.e. only the area that showed failure in the composite was considered as welded area. Owing to the fact that adhesive failure was observed at the flow front, its contribution to the total weld strength was considered negligible. The LSS, UFL and WA of the SSW joints were used to gain insight into the influence of the process control on the variability of weld quality.

Fractography was used to evaluate the failure mechanisms of the welded joints by using a high-resolution Zeiss stereo-microscope and a JEOL JSM-7500F scanning electronic microscope (SEM).

3.3. RESULTS AND DISCUSSION

3.3.1. OPTIMUM DISPLACEMENT AND OPTIMUM ENERGY VALUES

THE curves in Fig. 3.7a and Fig. 3.7b show the evolution of the power and the vertical displacement of the sonotrode as a function of the welding energy during the calibration welding processes, i.e. processes used to obtain optimum displacement and energy values, in Jig 1 and Jig 2, respectively. It must be noted that according to the procedure proposed in [3], these samples were welded using displacement control and maximum nominal displacement equal to the initial thickness of the ED (i.e. 0.25 mm). Figs. a and b also show how stage 4 was defined and how the optimum energy and displacement values were taken from around the middle of this stage. This resulted in an optimum sonotrode displacement of 0.23 mm and optimum welding energy of 420 J for Jig 1 (Fig. 3.7a), and optimum sonotrode displacement of 0.23 mm and optimum welding energy of 350 J for Jig 2 (Fig. 3.7b). Table 3.1 summarises the optimum welding parameters for each jig. It must be noted that even though the power curves in Figs. 3.7a and 3.7b did not show a very distinct onset or ending of stage 4, the validity of the optimum values shown in Table 3.1 was further proven by the results shown hereafter.

According to the values in Table 3.1, the optimum displacement seemed to be practically insensitive to the type of welding jig used whereas the optimum welding energy seemed to be significantly affected by the welding jig. In fact Jig 1, which imposed the highest constraints to the movement to the top adherend, was found to require a considerably higher (approximately 20 %) welding energy than Jig 2. Moreover, in the power curves for the samples welded in displacement-controlled mode and under the optimum sonotrode displacement (0.23 mm), the vibration was found to almost consistently stop within the optimum stage of the process, i.e. stage 4 (see Fig. 3.8a for J1/D_{opt} and Fig. 3.8b for J2/D_{opt}). In the case of energy-controlled welding under optimum welding energy (i.e. 420 J for Jig1 and 350 J for Jig 2), the power curves showed that for most of the samples the vibration stopped within stage 4 but displayed more variability than

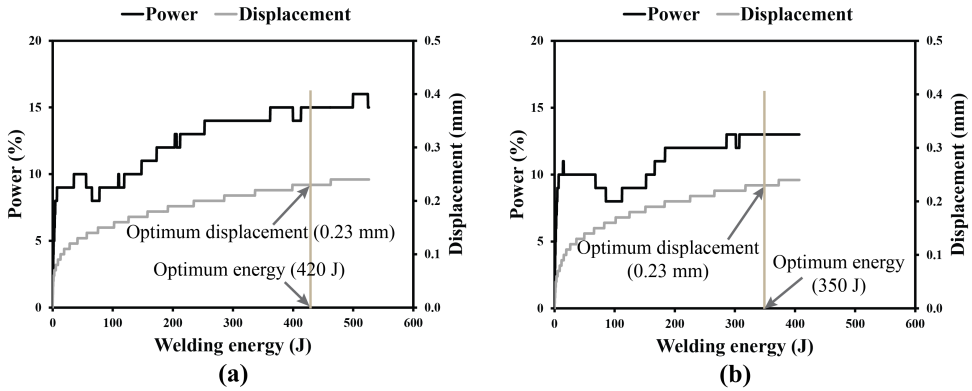

Figure 3.7: Calibration power and displacement curves for displacement-controlled SSW joints obtained in (a) Jig 1 and (b) Jig 2 (60.8 μm peak-to-peak amplitude, 1500 N welding force and 1000 N/s force ramp during the vibration phase, 0.25 mm sonotrode displacement).

Table 3.1: Welding jigs, welding processes and optimum displacement/energy for the SSW joints studied in this research. Welding amplitude was 60.8 μm (peak-to-peak), initial welding force was 1500 N and welding force ramp was 1000N/s in all cases.

Weld reference	Welding jig	Welding porcess	Optimum displacement (mm)	Optimum energy (J)
J1/D_{opt}	Jig1	Displacement-controlled	0.23	-
J1/E_{opt}	Jig1	Energy-controlled	-	420
J2/D_{opt}	Jig2	Displacement-controlled	0.23	-
J2/E_{opt}	Jig2	Energy-controlled	-	350

in displacement-controlled welding (see Fig. 3.9a for J1/E_{opt} and Fig. 3.9b for J2/E_{opt}). This is in line with our previous observations concerning the effect of sample-to-sample variability on the optimum welding energy [3]. Despite this variability, using the optimum welding energy in energy-controlled welding still proved to result in a bigger number of samples in the optimum welding stage than welding in non-optimum conditions. As shown in Fig. 3.10a, samples welded in Jig 1 with the optimum energy for Jig 2 (i.e. 350 J, hence lower than the optimum energy for Jig 1) did not reach the optimum welding stage. Likewise, samples welded in Jig 2 with the optimum energy for Jig 1 (i.e. 420 J, hence higher than the optimum energy for Jig 2) went beyond the optimum welding stage (see Fig. 3.10b).

3.3.2. DISPLACEMENT CEILING

The reader should note that in order to enable displacement-controlled welding of the SSW joints the welding force needed to be continuously increased during the vibration phase of the welding process. Using a constant welding force, which is the common pro-

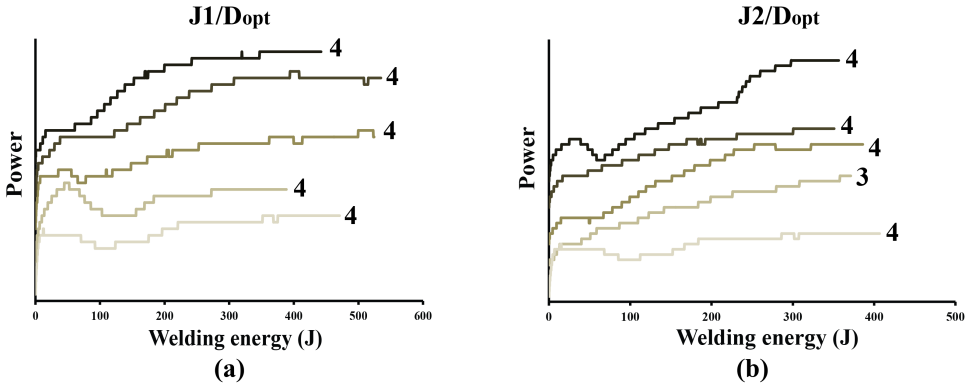

Figure 3.8: Power curves for the optimum displacement-controlled SSW joints obtained in (a) Jig 1 (J1/D_{opt}) and (b) Jig 2 (J2/D_{opt}). The power curves are shifted vertically and the displacement curves are not shown here for clarity. The numbers correspond to the welding stages shown in Fig. 3.5.

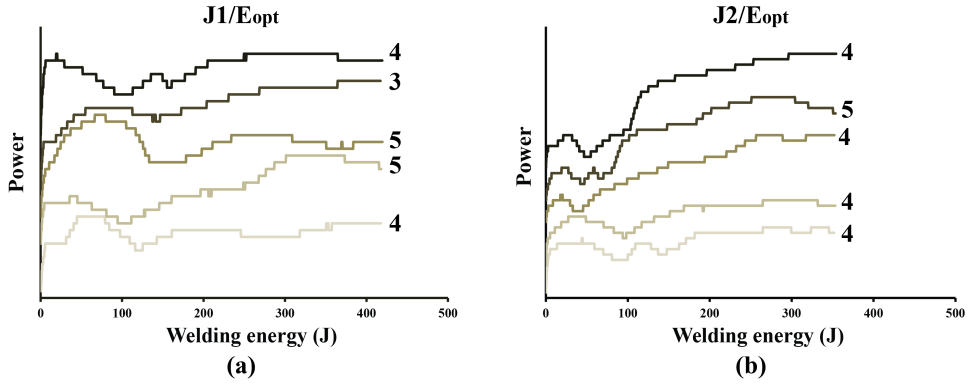

Figure 3.9: Power curves for the optimum energy-controlled SSW joints obtained in (a) Jig 1 (J1/E_{opt}) and (b) Jig 2 (J2/E_{opt}). The curves are shifted vertically for clarity. The numbers correspond to the welding stages shown in Fig. 3.5.

cedure used for displacement-controlled welding of full overlaps [3–5, 16], was however found to result in a displacement plateau as shown in Fig. 3.11a, referred to as "displacement ceiling" hereafter. This displacement ceiling typically occurred before the optimum stage of the process, i.e. stage 4, was reached (Fig. 3.11a) which invalidated using displacement control as the welding strategy for the SSW joints.

The displacement ceiling was observed to occur in this study at around 0.10 mm for a constant welding force of 1500 N. Radial squeeze flow of the molten ED and hence gradual increase of the welded areas was still observed within the displacement ceiling, despite the constant sonotrode displacement. The flow front, which can be distinctly observed on the fracture surfaces in Fig. 3.6, was hence gradually pushed away from the original ED location and towards the colder adherends, which potentially caused it to solidify. The solidified flow front together with the gradually decreasing welding

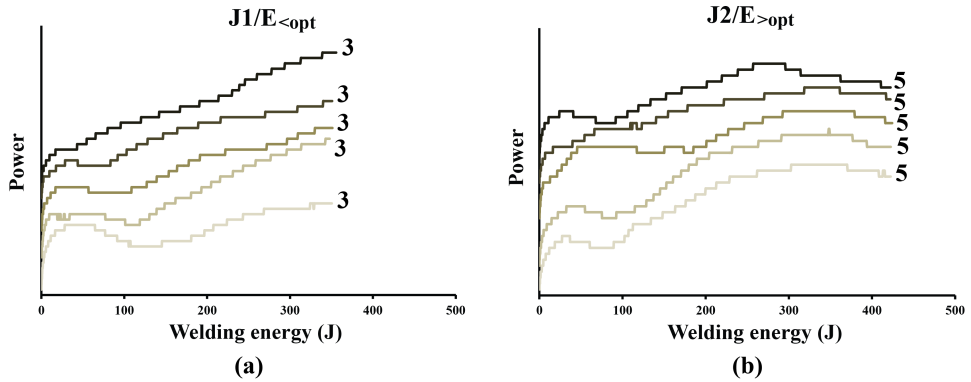

Figure 3.10: Power curves for energy-controlled SSW joints obtained in: (a) Jig 1 at 350 J (J1/E$_{<opt}$), and (b) Jig 2 at 420 J (J2/E$_{>opt}$). The curves are shifted vertically for clarity. The numbers correspond to the welding stages shown in Fig. 3.5.

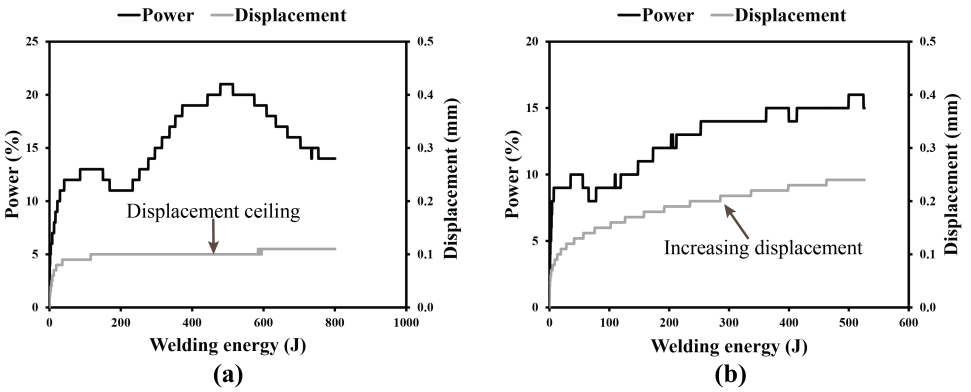

Figure 3.11: Representative power curves for SSW joints obtained under (a) 1500 N constant welding force and (b) increasing welding force (1500 N initial force, 1000 N/s force ramp) (60.8 μm peak-to-peak amplitude).

pressure (owing to constant welding force over gradually increasing welding area) hindered the downward displacement of the sonotrode causing the displacement ceiling. By constantly increasing the welding force during the vibration phase, the solidified flow front could be further compressed resulting in a continuous increase of the sonotrode displacement which eventually enabled displacement-controlled welding of SSW joints [17] (see Fig. 3.11b).

3.3.3. MECHANICAL PERFORAMANCE OF SSW JOINTS

Table 3.2 and Fig. 3.12 show the lap-shear strength (LSS), the ultimate failure load (UFL) and the final welded areas (WAs) of the SSW joints obtained under the optimum sets of conditions in Table 3.1. They also show the LSS, UFL and WA of two non-optimum cases, namely samples welded in Jig 1 at 350 J, i.e. below the optimum energy (J1/E$_{<opt}$), and samples welded in Jig 2 at 420 J, i.e. above the optimum energy (J2/E$_{>opt}$).

Table 3.2: LSS, UFL and WA values (average ± standard deviation) for the SSW joints studied in this research (COV stands for coefficient of variation).

Weld reference (Jig/mode)	Lap-shear strength, LSS (MPa) (COV, %)	Ultimate failure load, UFL (N) (COV, %)	Welded area, WA (mm^2) (COV, %)
$J1/D_{opt}$	37.5 ± 1.3 (3.3)	3578.7 ± 162.3 (4.5)	95.4 ± 7.3 (7.6)
$J1/E_{opt}$	38.3 ± 1.4 (3.8)	3834.1 ± 272.7 (7.1)	100.2 ± 9.1 (9.1)
$J2/D_{opt}$	35.8 ± 1.4 (4.0)	3923.4 ± 242.5 (6.1)	109.7 ± 7.9 (7.2)
$J2/E_{opt}$	36.9 ± 0.9 (2.4)	4240.8 ± 389.9 (9.2)	115.2 ± 12.0 (10.3)
$J1/E_{<opt}$	37.6 ± 0.7 (2.0)	3149.8 ± 213.6 (6.8)	83.7 ± 4.2 (5.0)
$J2/E_{>opt}$	36.0 ± 2.6 (7.2)	4132.8 ± 263.1 (6.4)	115.1 ± 8.6 (7.5)

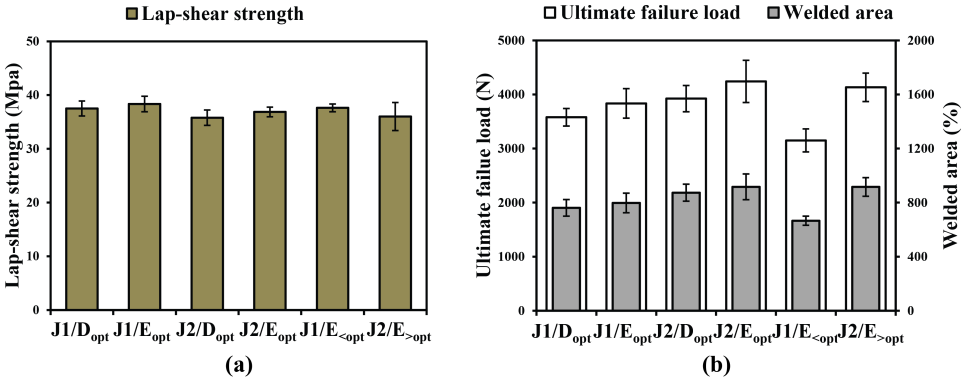

Figure 3.12: (a) LSS and (b) UFL and WA of SSW joints manufactured with displacement-controlled and energy-controlled welding in combination with different clamping jigs. Note that the welded areas are represented relative to the original areas of the spot EDs.

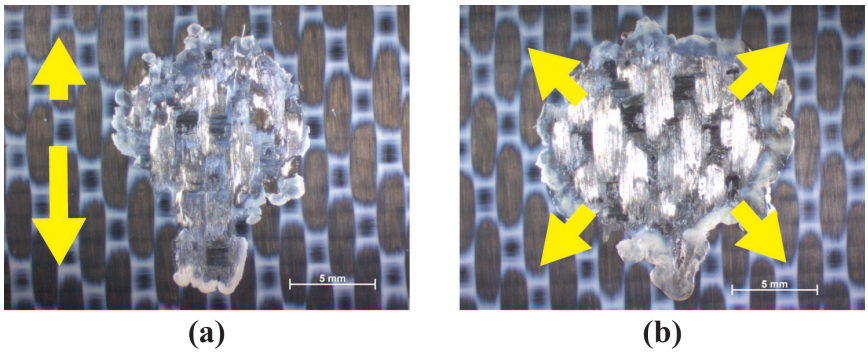

Figure 3.13: Representative fracture surfaces of SSW joints welded in (a) Jig 1 and (b) Jig 2. The arrows indicate the non-uniform flow of the molten ED in Jig 1 and uniform flow of molten ED in Jig 2.

An interesting observation is that all the different types of samples under study, even those welded in non-optimum conditions, yielded similar LSS. The average LSS values

ranged from 35.8 to 38.3 MPa and the scatter was well below 10 %, which are in good agreement with results obtained for CF/PPS welded joints with fully welded overlaps [16]. It should be noted that the way in which the welded area was defined, i.e. only taking into account the area featuring composite failure, also contributed to this result. The amount of welded areas, and hence the ultimate failure load, showed however more variability among different types of welded samples. Considering the SSW joints obtained in the optimum conditions, the WA was slightly smaller in all those welded in Jig 1. As a consequence of this, the average UFL of samples welded in Jig 2 under optimum conditions (energy or displacement) was around 10 % higher than that of samples welded in Jig 1 under optimum conditions (energy or displacement). Fig. 3.13 shows a typical fracture surface of a SSW joint obtained in Jig 1 and one obtained in Jig 2. As seen in this Figure, welds performed in Jig 2 featured a somewhat radial flow of the ED (Fig. 3.13b), whereas the ED flow in Jig 1 showed certain directionality (Fig. 3.13a). This is likely a consequence of the non-uniform initial strain state introduced in the ED by Jig1 owing to lack of parallelism between welding surfaces. This might as well have an impact on the extent of WA and hence the UFL.

3.3.4. FRACTURE SURFACE ANALYSIS

A fractographic analysis was carried out on the fracture surfaces of the SSW joints after mechanical testing. In displacement-controlled welds (optimum displacement), fibre-matrix debonding was consistently found as the main failure mechanism, which is believed to indicate high weld quality [18]. As shown in Fig. 3.14a, the main features on these fracture surfaces were bare fibres, deep fibre imprints on the matrix as well as torn fibres. In energy-controlled welds (optimum energy), fibre-matrix debonding as described above was as well the predominant type of failure (Fig. 3.14b). However, some of the samples showed other secondary types of failure. One of these secondary failure types was characterized by resin-rich fracture surfaces with partially debonded fibres, shallow fibre imprints and fractured resin (Fig. 3.15a). The other secondary failure type showed porosity and significant fibre distortion together with the predominant bare fibres and deep fibre imprints as illustrated in Fig. 3.15b. The resin-rich fracture surfaces (Fig. 3.15a) are believed to correspond to under-welded samples, i.e. those cases where the vibration was stopped before the optimum welding stage was reached (namely occasional samples welded in stage 3, see Fig. 3.9a). Whereas the fracture surfaces with porosity (Fig. 3.15b) are believed to correspond to over-welded samples, i.e those cases where the vibration was stopped beyond the optimum welding stage (namely occasional samples welded in stage 5, see Fig. 3.9b). These results indicate that, even when the same optimum energy is used, the final state or quality of the weld can vary. This relates to the fact that the welding energy is not only invested in creating the welded joint but is also dissipated in the adherends, the welding fixture and the base [14]. Hence the exact energy used to create the weld is unpredictable and scatter in weld quality resulting from energy-controlled welding is unavoidable. It must be noted, however, that owing to the relatively wide processing window characteristic of the ultrasonic welding process [3], the differences in weld quality observed in the fracture surfaces of the energy-controlled welds did not have a significant impact on their resulting LSS in the present study (Table 3.2 and Fig. 3.12a).

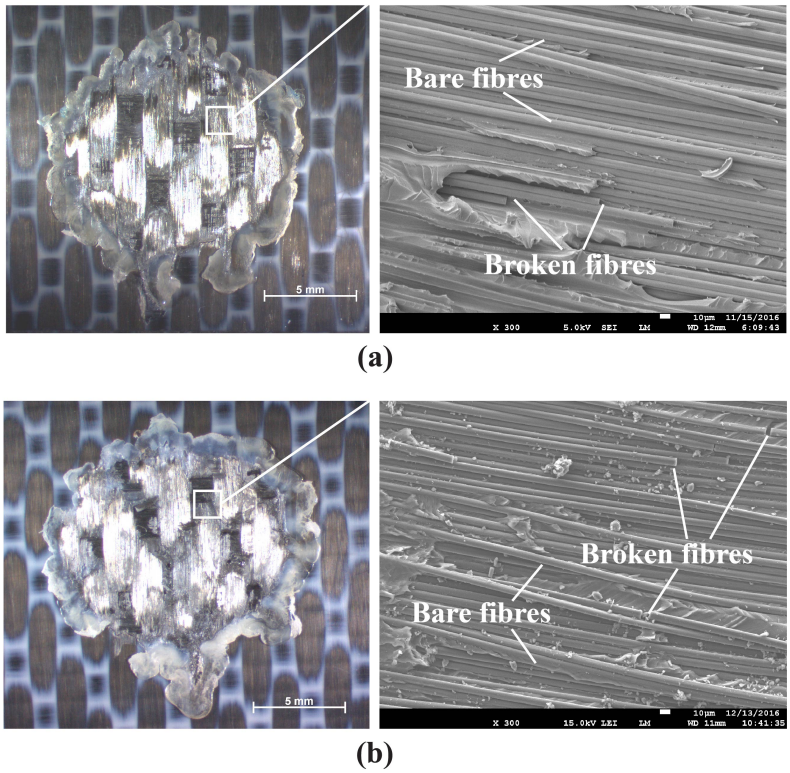

Figure 3.14: Representative fracture surfaces (left) and SEM detail (right) of SSW joints welded at (a) the optimum displacement (displacement-controlled welding) and (b) the optimum energy (energy-controlled welding).The scale bars are 5 mm (for stereo-microscopy) and 10 μm (for SEM). Both samples were welded in Jig 2

Regarding the non-optimum welded samples, resin-rich failure, with the same features as those shown in Fig. 3.15a, was invariably found for samples welded at 350 J in Jig 1, i.e. at an energy value below the optimum. This resin-rich failure is consistent with the smaller welded areas and hence thicker weld lines. In contrast, samples welded at 420 J in Jig 2 mostly showed fracture surfaces with obvious porosity and fibre distortion, similar that shown in Fig. 3.15b. Although fibre distortion and porosity were not proven to significantly decrease LSS in both [3] and this research (see Table 3.2), the high scatter in LSS of these samples could potentially be attributed to these over-heating features.

3.4. CONCLUSIONS

IN this chapter, a series of experimental studies were carried out to evaluate the effect of boundary conditions, in particular two different types of clamping jigs, on displacement-controlled and energy-controlled ultrasonic welding of single-spot welded (SSW) joints. The following main conclusions can be drawn for the results obtained from this research:

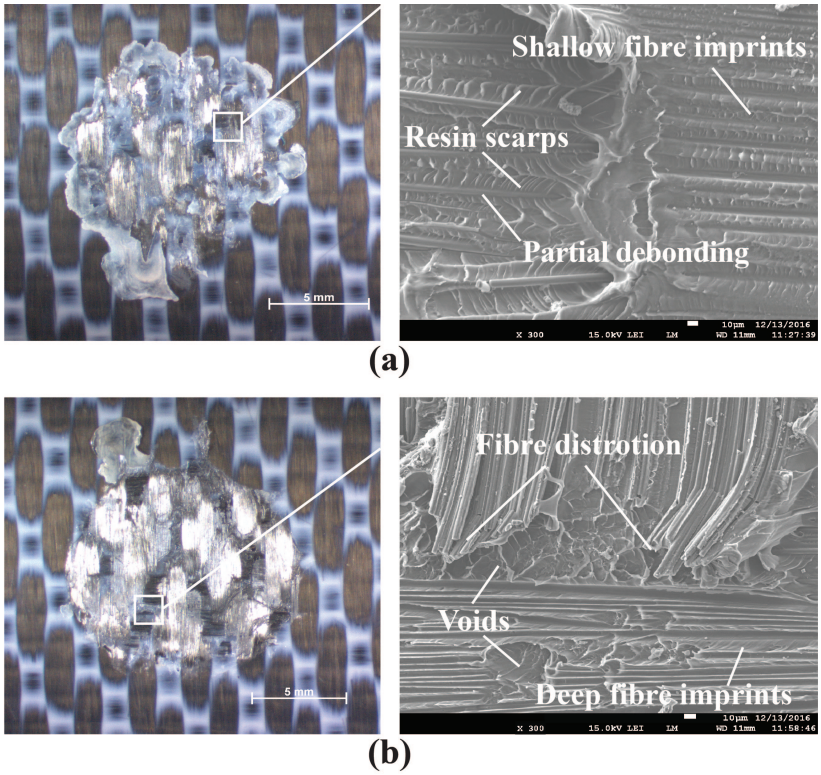

Figure 3.15: Fracture surfaces (left) and SEM details (right) showing secondary failure types in SSW joints welded at the optimum energy in (a) Jig 1 and (b) Jig 2. The SEM micrograph in (a) shows significant presence of resin cusps, indicating shear failure took place in the thermoplastic resin [19]. In contrast, void imprints combined with deep fibre imprints and fibre distortion are found in the SEM micrograph in (b). The scale bars are 5 mm (for stereo-microscopy) and 10 μm (for SEM).

- When displacement-controlled welding was used, the optimum sonotrode displacement (resulting in maximum weld strength) was the same for the two different welding jigs considered in this study. On the contrary, in energy-controlled welding the optimum welding energy was found to be dependent on the welding jig. In this specific study, there was a 20 % difference in the optimum energy values for the two different jigs under consideration.
- Both optimum displacement-controlled and optimum energy-controlled welding processes yielded similar ultimate failure load and similar welded areas. The welded spots underwent mostly intralaminar failure. The samples welded in energy-control mode showed however higher variability on their failure features than the samples welded in displacement-controlled mode.
- Non-optimum energy-controlled welding processes led to either lower ultimate failure load, in the case of welding energy below the optimum, or porosity in the welded joints, in the case of welding energy above the optimum.

- Finally, owing to limitations imposed by the cold adherends to the squeeze-flow of the molten energy directors, displacement-controlled welding of SSW joints was found to only be feasible if the welding force was gradually increased during the vibration phase of the welding process.

Based on these conclusions, welding energy is possibly dissipated into the surroundings (e.g. adherends and clamping jigs, etc.) during the welding process and likely to result in weld with different quality. It might be interesting to observe this point by thermal maeasurement and/or vibration analysis. In addition, the loss of energy is expected to be reduced by the usage of improved and adapted welding jigs or with damping devices. In contrast, displacement-controlled welding has the potential to enable sequential ultrasonic welding of multi-spot welded joints with a fixed set of welding parameters, i.e. avoiding recalculation of the welding parameters for each individual spot. Future research will focus on assessing the applicability of displacement-controlled ultrasonic welding to multi-spot welded joints.

REFERENCES

[1] T. Zhao, C. Broek, G. Palardy, I.F. Villegas, and R. Benedictus. Towards robust sequential ultrasonic spot welding of thermoplastic composites: Welding process control strategy for consistent weld quality. *Composite Part A: Applied Science and Manufacturing*, 109:355–367, 2018.

[2] C. Ageorges, L. Ye, and M. Hou. Advances in fusion bonding techniques for joining thermoplastic matrix composites: A review. *Composites - Part A: Applied Science and Manufacturing*, 32(6):839–857, 2001.

[3] I.F. Villegas. Strength development versus process data in ultrasonic welding of thermoplastic composites with flat energy directors and its application to the definition of optimum processing parameters. *Composites Part A: Applied Science and Manufacturing*, 65:27–37, 2014.

[4] I.F. Villegas. In situ monitoring of ultrasonic welding of thermoplastic composites through power and displacement data. *Journal of Thermoplastic Composite Materials*, 28(1):66–85, 2015.

[5] G. Palardy and I.F. Villegas. On the effect of flat energy directors thickness on heat generation during ultrasonic welding of thermoplastic composites. *Composite Interfaces*, 24(2):203–214, 2017.

[6] T. Zhao, G. Palardy, I.F. Villegas, C. Rans, M. Martinez, and R. Benedictus. Mechanical behaviour of thermoplastic composites spot-welded and mechanically fastened joints: A preliminary comparison. *Composites Part B: Engineering*, 112:224–234, 2017.

[7] V.K. Patel, S.D. Bhole, and D.L. Chen. Ultrasonic spot welding of lightweight alloys. In *Proceedings of 13th International Conference on Fracture*, pages 1–10, Bijing, China, June 2013.

[8] A. Macwan, V.K. Patel, X.Q. Jiang, C. Li, S.D. Bhole, and D.L. Chen. Ultrasonic spot welding of al/mg/al tri-layered clad sheets. *Materials and Design (1980-2015)*, 62:344 – 351, 2014.

[9] Bin Zhou, M.D. Thouless, and S.M. Ward. Predicting the failure of ultrasonic spot welds by pull-out from sheet metal. *International Journal of Solids and Structures*, 43(25):7482 – 7500, 2006.

[10] V. K. Patel, S. D. Bhole, and D. L. Chen. Microstructure and mechanical properties of dissimilar welded mg–al joints by ultrasonic spot welding technique. *Science and Technology of Welding and Joining*, 17:202–206, 2012.

[11] H.-M. Lu, A. Benatar, and F.-G.Cf+ He. Sequential ultrasonic welding of peek/graphite composites plates. In *Proceedings of the annual technical conference ANTEC*, volume 37, pages 2523–2526, 1991.

[12] B. Harras, K.C. Cole, and T. Vu-Khanh. Optimization of the ultrasonic welding of peek-carbon composites. *Journal of Reinforced Plastics and Composites*, 15(2):174–182, 1996.

[13] General Dynamics/Convair Division. Graphite composite truss welding and cap section forming subsystem.

[14] A. Benatar and T.G. Gutowski. Ultrasonic welding of peek graphite apc-2 composites. *Polymer Engineering and Science*, 29(23):1705–1721, 1989.

[15] ASTM D 1002-05. Standard test method for apparent shear strength of single-lap-joint adhesively bonded metal specimens by tension loading (metal-to-metal). *ASTM International*, 2005.

[16] I. F. Villegas, B. V. Grande, H.E.N. Bersee, and R. Benedictus. A comparative evaluation between flat and traditional energy directors for ultrasonic welding of cf/pps thermoplastic composites. *Composite Interfaces*, 22(8):717–729, 2015.

[17] C. Broek. Optimising ultrasonic welding of carbon fibre pekk composites by investigating integrated energy directors, displacement ceilings and displacement-controlled welding strategies. *Master thesis of Delft University of Technology*, 2015.

[18] I.F. Villegas and H.E.N. Bersee. Ultrasonic welding of advanced thermoplastic composites: An investigation on energy-directing surfaces. *Advances in Polymer Technology*, 29(2):112–121, 2010.

[19] E.S. Greenhalgh. Failure Analysis and Fractography of Polymer Composites. *Woodhead Publishing in Materials*, 2009.

4

APPLICATION OF DISPLACEMENT-CONTROLLED WELDING IN DOUBLE-SPOT WELDING

In the research of this chapter, double-spot welded joints, consisting of two single-spot welded joints, were formed in thermoplastic composites by using ultrasonic welding. In the first part, welded joints were sequentially welded via two welding control modes, i.e. displacement- and energy-controlled welding, and the quality of the created welded joints were comparatively investigated. After that, the effects of welding sequences on sequential spot welding were studied. In the last part, the double-spot welded joints were simultaneously manufactured within a single-step and a study was carried out on the welding process and quality of the joints as compared to sequentially welded joints. The experimental results showed that displacement-controlled welding is an appropriate control mode for sequential double-spot welding, featured by consistently producing high-quality spot welded joints with the same sonotrode displacement and insensitivity to the welding sequence. Moreover, sequential welding showed more robustness as compared to simultaneous welding in double-spot welding.

Parts of this chapter have been published in Composites Part A: Applied Science and Manufacturing **109**, 355-367 (2018). [1].

4.1. INTRODUCTION

ULTRASONIC welding is an interesting assembling technique for thermoplastic composites (TPCs), owing to the short welding times, absence of foreign materials at the weldline, possibility for in-situ monitoring and ease of automation [2–5]. It is well-suited for welding small area and therefore, it is intrinsically a spot welding technique [3]. Consequently, in order to realize the industrial application of ultrasonic welding in joining big composite structures, the most straightforward route is sequential welding of consecutive spots, thus resulting in a multi-spot welded (MSW) joint. Our previous research [6] showed that ultrasonically single-spot welded TPC joints yield similar shear strength as joints with a single mechanical fastener of comparable size, while at the same time they introduce much less damage into composite laminates. Consequently, multi-spot ultrasonic welding stands out as a very promising technique and composite-friendly alternative to mechanically fastening for the assembling of mass-produced TPC parts in composite aircraft (such as clips and brackets) or in automotive structures.

However, this welding technique has been barely investigated so far. Although Lu and Benatar [7] reported their work on sequential ultrasonic welding of TPCs, no details on the manufacturing process or on the quality of the resulting welds were provided in that publication. One obstacle for sequential ultrasonic welding is the fact that the boundary conditions for each new spot are likely to be changed by the created spots, as shown in Fig. 4.1. Therefore, the welding parameters are likely to be recalculated for each spot in order to obtain consistent weld quality in TPCs, contrarily to the cases in metal spot welding [8, 9]. The research in Chapter 3 has indicated that the changes in boundary conditions, provided by different clamping jigs, indeed affect the energy required for obtaining a single-welded spot with high quality. Therefore, the optimum welding energy (i.e. the energy required to obtain welds with maximum strength) in manufacturing MSW joints is likely different from spot to spot.

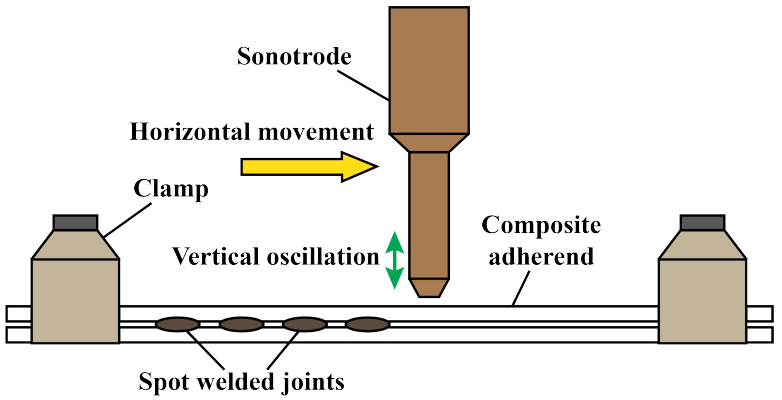

Figure 4.1: Schematic of the sequential ultrasonic spot welding process. The created welds introduce a step-like increase in the stiffness of the overlap, which provides a different boundary condition for the new spot. Dimensions are not to scale.

However, changes in the boundary conditions provided by different clamping jigs are basically different from the scenario in sequential multi-spot welding. For instance,

according to the study in [10], the welding energy is not only input in the welds but also dissipated in the surroundings such as adherends and welding fixtures. Therefore, the longer adherends for multi-spot welding are expected to dissipate more energy during the vibration phase, thus affecting the energy dissipated during the welding process. Therefore, the optimum welding energy required for individual spots in multi-spot welding is expected to differ from that of single-spot welds. As a possible alternative, displacement-controlled welding is controlled by the vertical displacement of the sonotrode. The process is independent of the energy dissipated in the surroundings and provided promising results for single welded spots, as shown in the previous chapter. Therefore, displacement-controlled welding is expected to be a more adequate technique for multi-spot welding.

Towards the manufacturing of high-quality multi-spot welded TPC joints, this chapter goes one step further and provides the results obtained in the investigation carried out on the processing of multi-spot welded joints, specifically double-spot welded joints, referred to as 2SW joints hereafter. The research work can be divided into three parts. Firstly, 2SW joints were sequentially manufactured, i.e. single spots were welded one after the other, using both displacement- and energy-controlled processes. The quality of thus-manufactured welded joints was evaluated and subsequently the applicability of both control strategies was assessed. Secondly, regarding the sequential welding manner, changes in the welding sequence also likely result in various boundary conditions for each new weld. Hence, the 2SW joints were manufactured following a different sequence comparing to that in the previous section. Finally, with the prospect of rapid-manufacturing, simultaneous welding of two spots was proposed. A comparative study between both welding strategies (i.e. sequential vs. simultaneous) was performed. The quality of all the welded joints was assessed through mechanical testing and fractographic analysis.

4.2. EXPERIMENTAL

4.2.1. MATERIALS

CARBON fibre reinforced polyphenylene sulphide (CF/PPS) laminates were used as the adherend material within this study. The laminates were fabricated using semi-impregnated Cetex® CF/PPS, with a five-harness satin fabric reinforcement, supplied by Ten Cate Advanced Composites, The Netherlands. Consolidated laminates with dimensions 580 mm × 580 mm and $[0/90]_{3s}$ stacking sequence were manufactured using a Joos LAP 100 hot platen press. Consolidation temperature, pressure, and time of 320 °C, 1 MPa, and 20 minutes were respectively used. The resulting laminates had a final thickness of approximately 1.6 mm and nominally 58 % fibre volume fraction. After that, adherends with the dimensions indicated in Fig. 4.2 were cut from the laminates using a Proth water-cooled diamond saw. The main apparent fibre orientation on the outer surfaces of the adherends was parallel to the longer side (i.e. loading-direction) of the adherends.

In order to facilitate the spot welding process, circular spot energy directors (EDs) made out of neat resin [6] were manufactured. The EDs were fabricated from three 0.08 mm thick neat Fortron® PPS films, stacked and consolidated in a hot platen press at 260

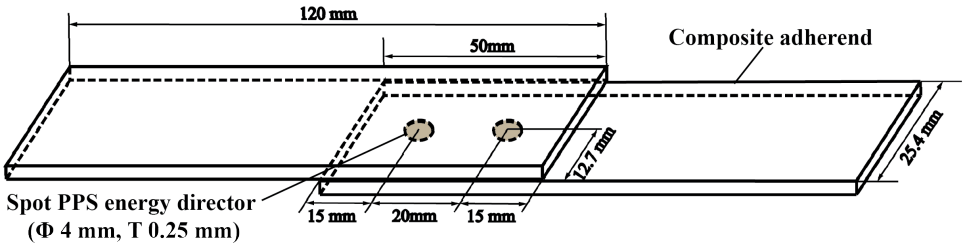

Figure 4.2: Schematic of the double-spot welded single-lap shear joint configurations. The grey dashed ellipse indicates the location of the spot energy director (PPS, Φ: diameter, T: thickness) and thus the spot weld. Dimensions are not to scale.

°C and 2 MPa for 10 minutes, resulting in an approximately 0.25 mm thick film. Spot EDs with a diameter of 4 mm were cut from the resulting consolidated film and secured to the bottom composite adherends to be joined, at the positions indicated in Fig. 4.2, using a Rinco handheld ultrasonic welder.

4.2.2. ULTRASONIC WELDING PROCESS

Individual samples were welded using a 20 kHz microprocessor-controlled Rinco Dynamic ultrasonic welder with a maximum power output of 3000 W. In this study, the two different sonotrodes shown in Fig. 4.3 were used. Sonotrode C (circular base, 10 mm diameter, Fig. 4.3a) was used for single-spot and sequential double-spot welding, while Sonotrode R (rectangular base, 60 mm × 24 mm, Fig. 4.3b) was used for simultaneous (single-step) double-spot welding. The clamping system consisted of two aluminium bars, one on top of each adherend, bolted to a base plate with a torque of 20 Nm, also illustrated in Fig. 4.3. The top adherend partially rested on the bottom adhered (single-lap overlap area) and on a 1.5 mm-thick aluminium supporting plate.

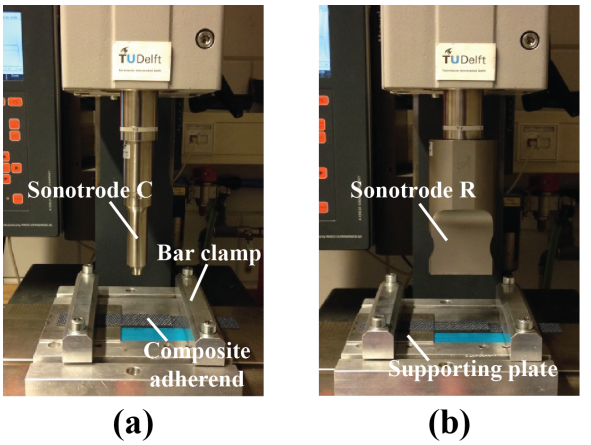

Figure 4.3: Ultrasonic welder including welding jig and (a) Sonotrode C (for sequential double-spot welding) and (b) Sonotorode R(for simultaneous double-spot welding).

The peak-to-peak vibration amplitude used in this study was 60.8 μm and 52.8 μm for sequential (Sonotrode C) and simultaneous (Sonotrode R) double-spot welding, respectively. This difference in amplitude resulted from the different gain factors for the corresponding sonotrode geometries. For both processes an initial welding force of 1500 N was used which was linearly increased at a rate of 1000 N/s during the vibration phase, following the procedure introduced in previous chapter. During cooling down a solidification force of 1500 N was applied for 4 s.

Displacement- and energy-controlled welding control strategies were executed during sequential double-spot welding. The resulting welded joints were referred to as 2SW-D and 2SW-E, for displacement-controlled and energy-controlled welding, respectively. The optimum sonotrode displacement (i.e. 0.23 mm) and the optimum energy (i.e. 420 J) for the single welded spots, which were obtained in Chapter 3, were directly used for the 2SW-D and the 2SW-E joints, respectively. However, as indicated in Section 4.1, the optimum energy for each spot in 2SW joints is potentially different from that of single spots, which will be discussed later on. In the first part of the experiments, both 2SW-D and 2SW-E joints were sequentially welded following the sequence shown in Fig. 4.4, hereafter denoted as Sequence I. In the second part, 2SW joints welded following the sequence in Fig. 4.5, denoted as Sequence II, were used to investigate the effects of welding sequence on the quality of welded joints. Finally, two single-spot were simultaneously welded to create the 2SW joints. All the combinations of different control modes and welding sequences are summarized in Table 4.1.

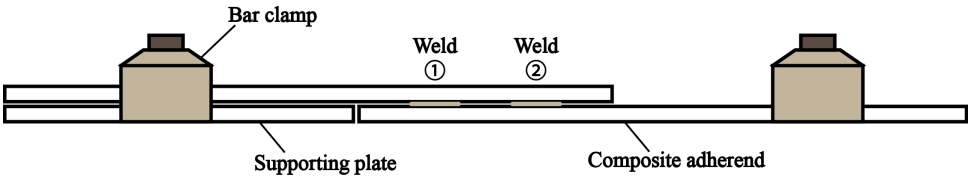

Figure 4.4: Schematic of the welding sequence used in the sequential double-spot welding in the first part of experimental work, denoted as Sequence I. Weld 1 and 2 represent the spot welded in the first and second place, respectively.

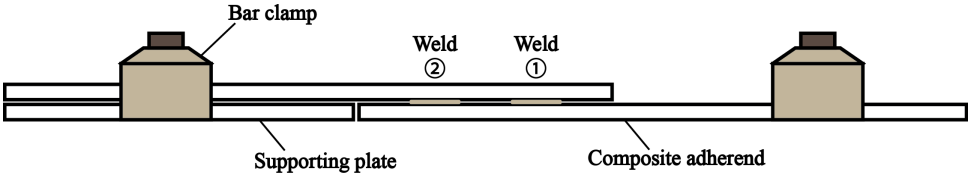

Figure 4.5: Schematic of the welding sequence used in the sequential double-spot welding in the second part of experimental work, denoted as Sequence II. Weld 1 and 2 represent the spot welded in the first and second place, respectively.

Table 4.1: The experimental programme carried out in the research of this chapter

Weld reference (welding strategy)	Control mode	Welding sequence*	Number of samples
2SW-D (sequential)	Displacement	Sequence I	5
2SW-E (sequential)	Energy	Sequence I	5
2SW-D (sequential)	Displacement	Sequence II	5
2SW-D (simultaneous)	Displacement	-	5

(* The welding sequences were indicated in Fig. 4.4 and Fig. 4.5.)

4.2.3. TESTING PROCEDURE AND POT-TESTING ANALYSIS

Testing of the welded samples was performed in accordance with the procedures for single-lap shear sample testing in the ASTM D1002 standard [11]. Samples were tested using a Zwick/Roell 250 kN universal testing machine with a constant crosshead speed of 1.3 mm/min at an initial load of approximately 100 N. Hydraulic grips were used on the testing machine. These grips were offset to ensure parallelism between the load path and the weldline in every sample. The tests were performed at room temperature (20 ± 3 °C) with a relative humidity of 50 ± 5 %. Five samples were tested per set of welding conditions (see Table 4.1). The apparent lap-shear strength (LSS) was calculated as the ratio of the ultimate failure load (UFL) to the total welded areas (WAs) for the two spots. The UFL was recorded as the maximum load value during the tests, which is regarded as an indicator the load-carrying capability of the welded joints.

Post-testing fractographic analysis of all of the tested samples was performed. Firstly, the measurement of the final welded areas was achieved using ImageJ150 (NIH) on images captured by a Zeiss stereo-microscope, following the approach used for single-spot welded joints (previous chapter, as shown in Fig. 3.6). Secondly, different failure modes and mechanisms of welded joints were identified using a Jeol JSM-7500F scanning electron microscope (SEM).

4.3. RESULTS

THIS section presents the major results obtained from the experiments performed. Firstly, regarding the comparison between the displacement- and energy-controlled welding in sequential spot welding, fractographic analysis, mechanical behaviour of the 2SW joints, and outputs obtained from the welding processes are reported. Secondly, the performance of sequential 2SW joints manufactured following two different sequences is shown. Finally, the comparison between sequential vs. simultaneous double-spot welding is presented mainly through the analysis of the fracture surfaces. In order to facilitate a comparative discussion in the next section of this paper, the overall results will be presented in a concise and unbiased manner in the present section.

4.3.1. SEQUENTIAL DOUBLE-SPOT WELDING WITH DIFFERENT MODES

FRACTOGRAPHIC ANALYSIS OF INDIVIDUAL SPOTS IN THE 2SW JOINTS

Fig. 4.6a illustrates the typical fracture surfaces of the two single spots in 2SW-D joints, which feature consistent appearance and spot size. SEM analysis (Fig. 4.6b and c) showed

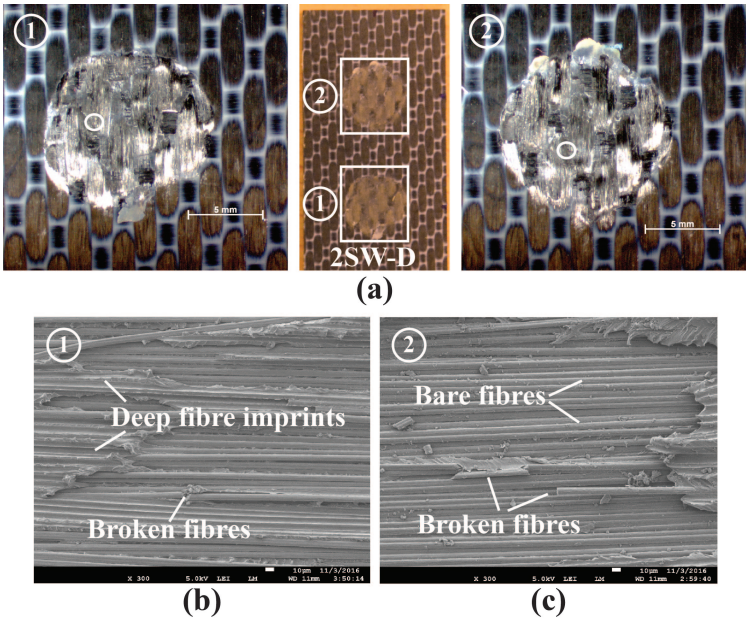

Figure 4.6: (a) Representative fracture surfaces of the 2SW joints sequentially manufactured with displacement-controlled welding process at 0.23 mm displacement, 60.8 μm peak-to-peak amplitude, 1500 N welding force and 1000 N/s increasing force during the vibration phase. The numbers indicate the welding sequence. SEM micrographs (b) and (c) show the details of the areas circled in the fracture surfaces of Weld 1 and Weld 2, respectively. The scale bars are 5 mm (for microscopy) and 10 μm (for SEM).

the occurrence of intralaminar failure in both spots in the form of fibre-matrix debonding (bare fibres and deep fibre imprints on thermoplastic resin) and fibre breakage. On the contrary, 2SW-E joints featured significantly different fracture surfaces for the two welded spots, as shown in Fig. 4.7a. The bottom spot, which was welded in the first place, was apparently bigger than the top one, i.e. the one welded in second place. In addition, the bottom spot showed typical intralaminar failure (i.e. fibre-matrix debonding and torn fibres, see Fig. 4.7b). Differently, the top spot mostly featured a resin-rich fracture features with partially debonded fibres and predominant resin cusps (Fig. 4.7c), related to shear failure of the thermoplastic resin [12]. Fig. 4.8 summarizes the final welded areas measured for each spot in both 2SW-D and 2SW-E joints. Both spots yielded similar values for WA in 2SW joints, which were also comparable with that of single welded spots. To make a clear indication for the number of welded spots, single-spot welded joints are referred to as 1SW joints hereafter. In contrast to that, the spots welded in the second place in 2SW-E joints were smaller in average, by approximately 20 %, than that of the spot welded in the first place. Both of them were also smaller than the ones in the reference 1SW-E joints.

JOINT STRENGTH

Table 4.2 and Fig. 4.9 show the lap-shear strength (LSS), the ultimate failure load (UFL) and the final welded areas (WAs) of sequential 2SW-D and 2SW-E joints. As a reference,

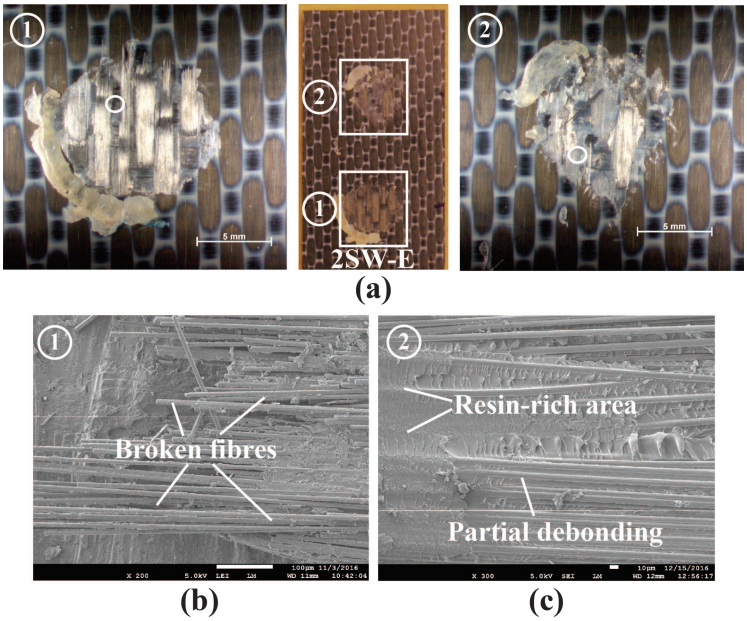

Figure 4.7: (a) Representative fracture surfaces of the 2SW joints sequentially manufactured with energy-controlled welding process at 420 J energy, 60.8 μm peak-to-peak amplitude, 1500 N welding force and 1000 N/s increasing force during the vibration phase. The numbers indicate the welding sequence. SEM micrographs (b) and (c) show the details of the areas circled in the fracture surfaces of Weld 1 and Weld 2, respectively. The scale bars are 5 mm (for microscopy) and 10 μm (for SEM).

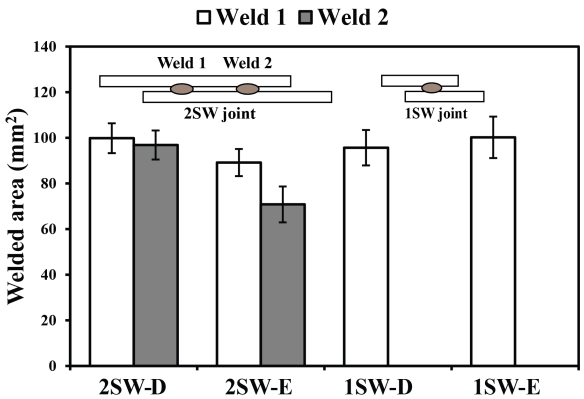

Figure 4.8: Welded areas of individual spots in both 2SW-D and 2SW-E joints. Both types of 2SW joints were sequentially manufactured following Sequence I (Table 4.1). Welded areas of the 1SW-D and the 1SW-E joints are also listed as references.

the LSS, UFL and WA values of the 1SW-D and 1SW-E joints in are also included in Table 4.2 and Fig. 4.9. Essentially, the 2SW-D and 2SW-E joints yielded similar LSS values, which were also comparable to the LSS values yielded by the 1SW-D and the 1SW-E joints

(see Fig. 4.9a). The average LSS values for all types of joints ranged from 35.8 to 38.3 MPa, which are in good agreement with results obtained for CF/PPS welded joints with fully welded overlaps [13]. However, it must be noted that the 2SW-E joints exhibited higher scatter (approximately 9 %) than the 2SW-D joints (below 5 %) and the 1SW-E and the 1SW-D benchmark (below 4 %).

Table 4.2: LSS, UFL and WA values (average ± standard deviation) for both types of the 2SW joints studied in this research and their references of the 1SW joints (COV stands for coefficient of variation). Both types of the 2SW joints were manufactured following Sequence I (Table 4.1)

Weld reference (Type-mode)	Lap-shear strength (MPa) (COV, %)	Ultimate failure load (N) (COV, %)	Welded area* (mm^2) (COV, %)
2SW-D	35.8 ± 1.7 (4.7)	7037.5 ± 467.8 (6.6)	196.3 ± 14.3 (7.3)
2SW-E	36.1 ± 3.2 (8.8)	5838.3 ± 780.0 (13.3)	160.2 ± 8.9 (5.5)
1SW-D	37.5 ± 1.3 (3.3)	3578.7 ± 162.3 (4.5)	95.4 ± 7.3 (7.6)
1SW-D	38.3 ± 1.4 (3.8)	3834.1 ± 272.7 (7.1)	100.2 ± 9.1 (9.1)

(*The average welded area of the 2SW joins is the sum of the welded areas of the two individual spots.)

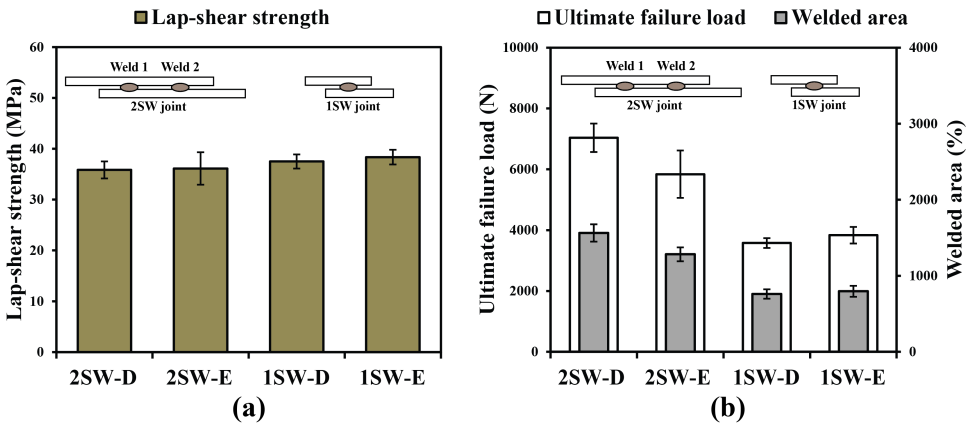

Figure 4.9: (a) LSS and (b) UFL and WA of both types of the 2SW joints manufactured with displacement- and energy-controlled welding at 0.23 mm displacement/420 J energy, 60.8 μm peak-to-peak amplitude, 1500 N welding force and 1000 N/s increasing force during the vibration phase. The 1SW joints welded at the same parameters are also listed as references. Note that the welded areas are represented relative to the original areas of the single-spot EDs. Both types of the 2SW joints were manufactured following Sequence I (Table 4.1).

Regarding the total WA and the UFL of all types of joints, the 2SW-E joints showed smaller total welded areas, around 20 % smaller, than that of the 2SW-D joints. As a consequence, the average UFL of the 2SW-E joints was 20 % lower than their 2SW-D counterparts. Meanwhile, the average UFL of the 2SW-E joints showed significantly higher (around 2 times higher) scatter as compared to that of the 2SW-D joints.

OUTPUT DATA FROM THE WELDING PROCESS

Fig. 4.10 illustrates the welding energy and sonotrode displacement obtained as outputs from the ultrasonic welder for the 2SW-D and the 2SW-E joints. The energy and displacement output values corresponding to the single-spot welding process are also shown in this figure as reference. As depicted in Fig. 4.10a, the average energy value corresponding to displacement-controlled welding of each one of the spots in the 2SW joints was higher than the average energy value dissipated in the spot in the displacement-controlled 1SW joints. Owing to the high dispersion in the results (around 30 % of the corresponding average values), no significant differences could however be reported between the energy dissipated in welding of the first and the second spot.

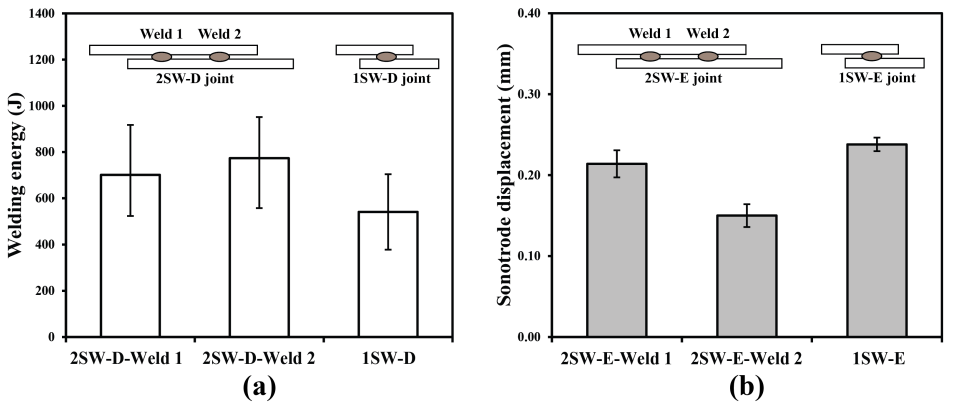

Figure 4.10: (a) Welding energy for each welded spots in the 2SW joints and the 1SW joints produced with displacement-controlled process at 0.23 mm displacement and (b) sonotrode displacement for each welded spots in the 2SW joints and the 1SW joints produced with energy-controlled process at 420 J energy. Both types of the 2SW joints were manufactured following Sequence I (Table 4.1).

Regarding the output data obtained from the energy-controlled welds in the 2SW-E joints (Fig. 4.10b), the average displacement value for Weld 2 was obviously lower than that of Weld 1 and both of them were below the value for the 1SW-E joints, which was approximately equal to the optimum displacement value used for both the 2SW-D and the 1SW-D welded joints. The dispersion in the displacement values was much smaller than the dispersion in energy values, always below 10 % of the corresponding average value.

4.3.2. DIFFERENT WELDING SEQUENCES

The experimental results presented in the previous section were obtained from the sequential 2SW joints welded following Sequence I (Fig. 4.4). This section presents results corresponding to the sequential 2SW joints welded following Sequence II (Fig. 4.5). As indicated in Table 4.1, only displacement-controlled welding was used for this part of the research. Table 4.3 and Fig. 4.11 show the LSS, UFL and WA of the 2SW samples welded following Sequence I and Sequence II. It must be noted that the 2SW-D samples obtained following both sequences yielded similar LSS and WA, thus similar UFL. The corresponding scatter values for all these average values were below 10 %. Additionally,

Fig. 4.12 illustrates the fracture surfaces of joints obtained following Sequence I and Sequence II, featuring consistent spot size and failure mode (i.e. intralaminar failure with fibre-matrix debonding and torn fibres).

Table 4.3: LSS, UFL and WA values (average ± standard deviation) for the 2SW joints manufactured with different sequences (COV stands for coefficient of variation).

Weld reference (Sequence)	Lap-shear strength (MPa) (COV, %)	Ultimate failure load (N) (COV, %)	Welded area* (mm^2) (COV, %)
Sequence I	35.8 ± 1.7 (4.7)	7037.5 ± 467.8 (6.6)	196.3 ± 14.3 (7.3)
Sequence II	35.1 ± 1.9 (5.4)	6957.3 ± 366.8 (5.3)	198.0 ± 17.8 (8.9)

(*The average welded area for the 2SW sample is the sum of the welded areas of the two individual spots.)

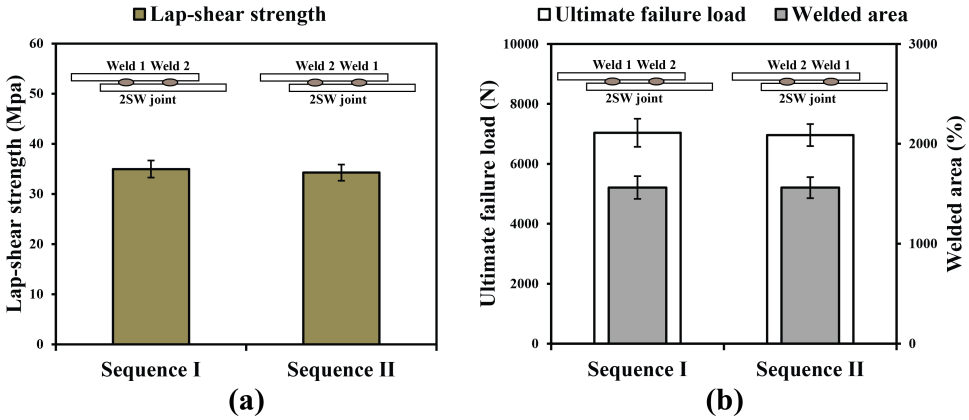

Figure 4.11: (a) LSS and (b) UFL and WA of welded joints manufactured following two different welding sequences at 0.23 mm displacement, 60.8 μm peak-to-peak amplitude, 1500 N welding force and 1000 N/s increasing force during vibration phase. Note that the welded areas are represented relative to the original areas of the sing-spot EDs.

4.3.3. SIMULTANEOUS DOUBLE-SPOT WELDING

Benefiting from the ability of the sonotrode R to cover the entire overlap, two spots could be welded within a single-step welding process. In addition , the welding time was found significantly reduced in comparison to that of sequential welding, as summarized in Table 4.4. However, post-testing inspection revealed that neither of these spots was of good quality. Fig. 4.13a shows considerable different fracture surfaces in a simultaneous 2SW joint obtained at 0.18 mm displacement. Firstly, spot A had a surface area almost double than that of Spot B. Secondly, SEM observations showed that Spot A mainly featured by debonding between fibres and matrix. On the contrary, Spot B showed a resin-rich fracture surface. More importantly, both Spot A and B showed void imprints on their fracture surfaces (see Fig. 4.13a), with the voids in Spot A being apparently larger than

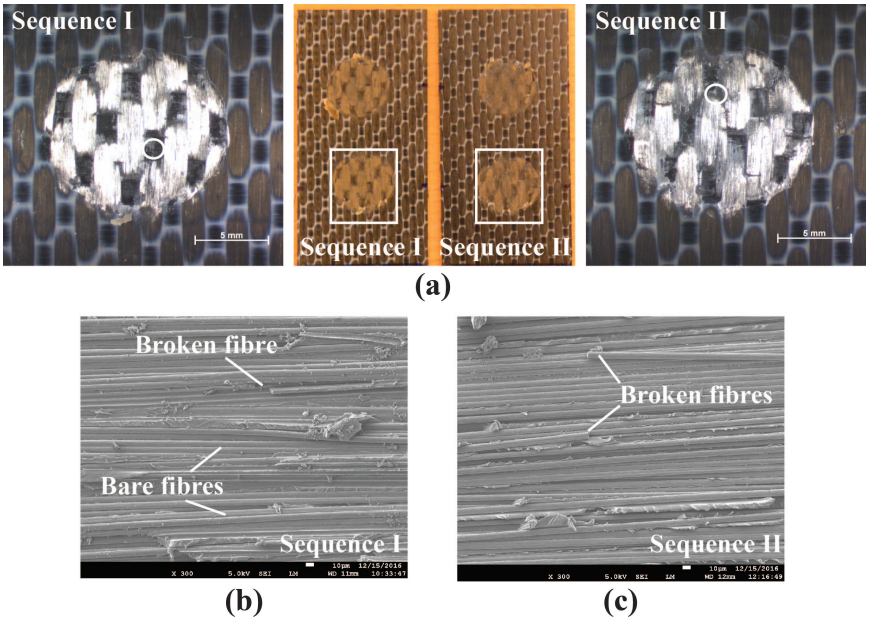

Figure 4.12: (a) Representative fracture surfaces of the 2SW joints manufactured following two different welding sequences at 0.23 mm displacement, 60.8 μm peak-to-peak amplitude, 1500 N welding force and 1000 N/s increasing force during the vibration phase. SEM micrographs (b) and (c) show the details of the areas circled in the fracture surfaces of samples welded following Sequence I and II, respectively. The scale bars are 5 mm (for microscopy) and 10 μm (for SEM).

Table 4.4: Maximum power and vibration time for individual spot in sequential welding at the optimum sonotrode displacement and simultaneous welding at different sonotrode displacements considered in this study. Power is presented as percentage of the maximum available power, 3000 W.

Welding strategy	Sonotrode displacement (mm)	Maximum power (%) (COV, %)	Vibration time (ms) (COV, %)
Sequencial* (Weld 1)	0.23	20.2 ± 4.6 (22.8)	1629.6 ± 361.9 (22.2)
Sequencial (Weld 2)	0.23	17.8 ± 5.3 (29.6)	2060.0 ± 87.8 (4.2)
Simultaneous	0.17	70.6 ± 3.8 (5.4)	412.2 ± 46.9 (11.3)
Simultaneous	0.18	77.2 ± 4.2 (5.5)	584.3 ± 42.3 (7.2)
Simultaneous	0.19	78.6 ± 3.9 (5.0)	746.0 ± 76.8 (10.3)

(*The data for sequential welding was obtained from the 2SW-D joints welded following Sequence I, as shown in Fig. 4.4.)

those in Spot B. Inspection at higher magnification indicated the void imprints in Spot A were located in between the bare fibres (Fig. 4.13b) whereas void imprints in Spot B were mostly present on top of the resin-rich area (Fig. 4.13c).

The welded areas of both spots could be increased by increasing the sonotrode displacement, e.g. 0.19 mm, as shown in Fig. 4.14. However, welding was found to occur

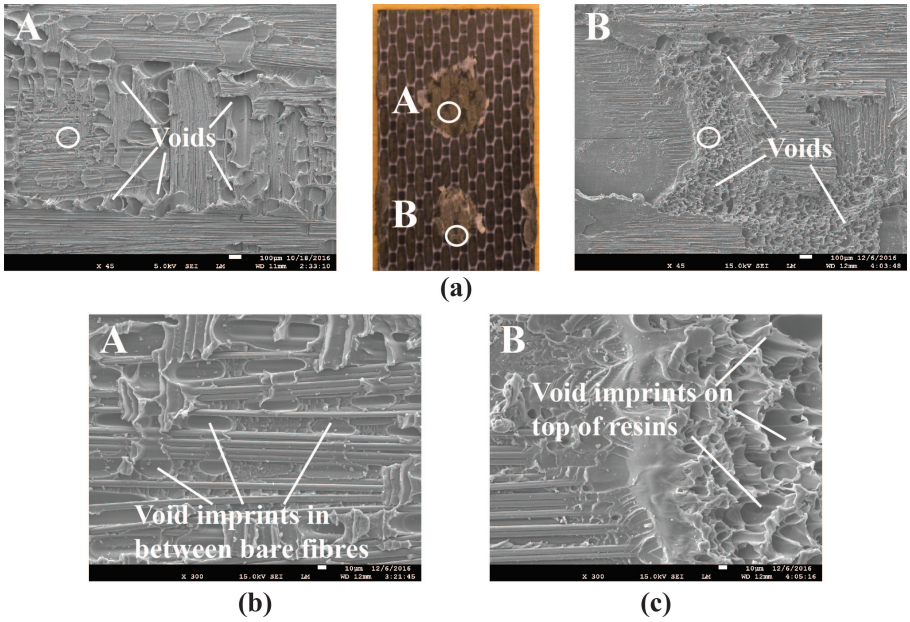

Figure 4.13: (a) Representative fracture surfaces and SEM details of both spots in the 2SW joint simultaneously manufactured at 0.18 mm displacement, 52.8 μm peak-to-peak amplitude, 1500 N welding force and 1000 N/s increasing force during the vibration phase. The SEM micrographs (b) and (c) show further magnification of the circled area in the top SEM images of Spot A and B, respectively. The scale bars are 100 μm, 10 μm and 10 μm for the SEM graphs in a, b and c.

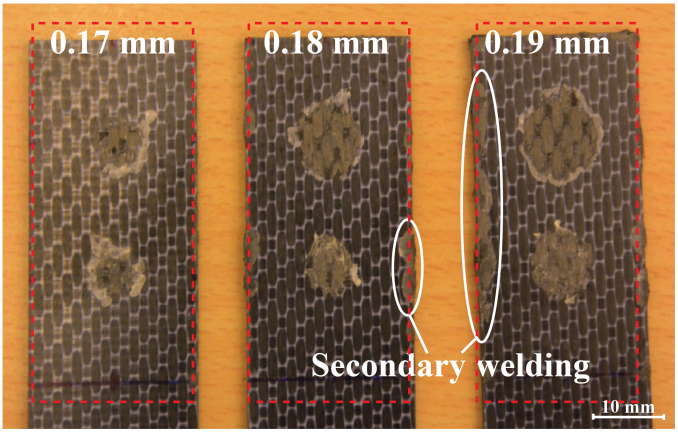

Figure 4.14: Fracture surfaces of 2SW joints welded by Sonotrode R with 0.17mm (left), 0.18 mm (middle) and 0.19 mm (right) input displacement, 52.8 μm peak-to-peak amplitude, 1500 N welding force and 1000 N/s increasing force during vibration phase. The dotted lines indicate the overlap-area of the rectangular sonotrode. Secondary welding significantly occurred when the displacement was above 0.18 mm.

not only within the welded area but also on the edges of the overlap, which was referred to as 'secondary welding'. Decreasing the sonotrode displacement, e.g. 0.17 mm, was found as an effective approach to prevent secondary welding. However, this resulted in around 30 – 40 % decrease of the welded areas for both welded spots.

4.4. DISCUSSION

4.4.1. DISPLACEMENT- VS. ENERGY-CONTROLLED WELDING

THE manufacturing of multi-spot welded joints as single spots sequentially welded after each other entails a change in the boundary conditions for each new spot to be welded. A constant welding energy can hence be expected to result in a different effective energy input in each spot. In another words, the same energy input is likely to result in individual spots with variable quality. On the contrary, displacement-controlled welding with the same displacement value for each spot could potentially lead to consistent weld quality based on our previous results.

The observations in fractographic analysis combined with mechanical testing in the research on the 2SW joints manufactured in a sequential manner validated the hypothesis above. Fibre-matrix debonding failure, which was consistently found in both spots of the 2SW-D joints (Fig. 4.6), indicates high weld quality [14]. The consistent failure mode explains their high LSS with low scatter (Fig. 4.9a). In addition, the similar spot size of the two welds, also similar to that obtained in the 1SW-D joints (Fig. 4.8), resulted in doubled UFL as compared to that yielded by the 1SW-D joints (Fig. 4.9b). Regarding the 2SW-E joints, one of the spots was found to be smaller than the other one (Fig. 4.7 and Fig. 4.8) which resulted in a lower average value of total welded areas and subsequently a lower average UFL as compared to the 2SW-D joints (Fig. 4.9b). Moreover, the distinctly different failure mechanisms (see Fig. 4.7b and c) between two spots most likely led to the high scatter in their UFL (Fig. 4.9b) and and hence in their average LSS (Fig. 4.9a).

The analysis on the output data from the welding processes highlights the robustness of displacement-controlled welding in a different way. Firstly, as indicated in [3] and in the previous chapter, the highest weld quality is consistently obtained at the optimum stage (i.e. stage 4) of the welding process. The significant dispersion of welding energy obtained from displacement-controlled welds (see Fig. 4.10) implies that, using energy-controlled welding will likely result in welds at different stages of the welding process and thus at different levels of weld quality. Secondly, the higher energy obtained in both spots in 2SW-D joints indicates the optimum welding energy for individual spot in 2SW joints is potentially higher than that for the ones in the 1SW joints, since more energy was dissipated in the longer adherends and longer overlap for 2SW samples. As a consequence, given the optimum welding energy for the 1SW joints, both spots in 2SW joints were expected to feature smaller welded areas, as observed in Fig. 4.8. Finally, the lower sonotrode displacements for producing the second spots in 2SW-E joints (see Fig. 4.10b) likely resulted in a thicker weld line and thus a resin-rich welded area, which is consistent with the resin-rich fracture surfaces shown in Fig. 4.7.

4.4.2. SEQUENCE EFFECTS IN DISPLACEMENT-CONTROLLED WELDING

The observations in Section 4.3.2 give further confirmation on the robust behaviour of displacement-controlled welding in sequential double-spot welding. It means that using displacement-controlled welding, consistent spot welds (Fig. 4.12) can be produced without necessity for considering the welding sequence. However, if energy-controlled welding is used, considering the changes in the boundary conditions induced by different welding sequences, the optimum energy for individual spot in Sequence I could be expected to differ from that in Sequence II.

4.4.3. SEQUENTIAL VS. SIMULTANEOUS DOUBLE-SPOT WELDING

The variation in between the two welded spots in the simultaneous 2SW joints most likely resulted from lack of parallelism between the top and bottom adherend, which is schematized in Fig. 4.15. Since the supporting plate (1.5 mm-thick) is slightly thinner than the adherend (1.6 mm-thick), there was an initial angle between two surfaces to be welded. As indicated in the study in the previous chapter, such a thin supporting plate is chosen to prevent blocking of the vertical movement of the sonotrode during the melting of the EDs. Although the lack of parallelism was corrected once the overlap was subjected to pressure applied by the sonotrode. The pressure distribution between two EDs was still non uniform. ED A underwent a comparably higher pressure. As a consequence, the flow front of the melted ED A could be further compressed and eventually formed a bigger welded area (see Fig. 4.13a). On the contrary, lower pressure was applied on ED B for pushing the flow front away from the original location. Since the melting time for both EDs was the same, the final welded area for Spot B was smaller. In contrast to that, sequential welding provides separate welding processes for both spots, allowing different welding time for each process. Therefore, although the second spot (the same position with Spot B, shown in Fig. 4.4) in sequential welding also underwent a lower pressure during the vibration process, the ED had sufficient time for melting and expanding to a welded spot as big as the first weld.

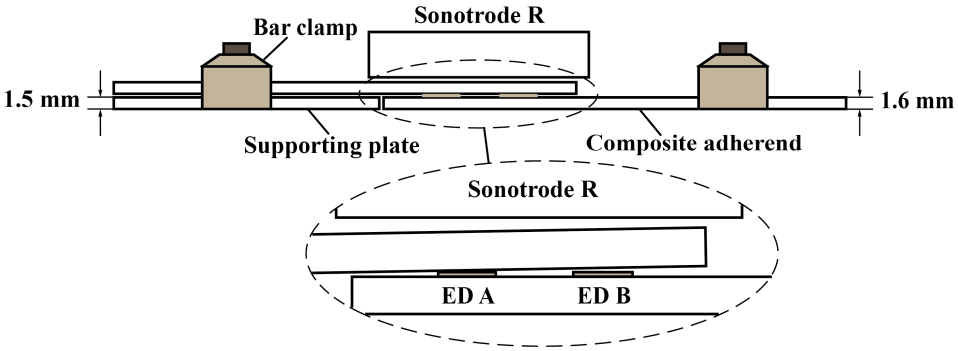

Figure 4.15: Schematic of the lack of parallelism between top and bottom adherends caused by the clamping situation during the simultaneous double-spot welding process. Dimensions are not to scale.

Regarding the void imprints observed in both welded spots, it must be noted that they were resulted from different reasons. Voids in Spot A were bigger and were found

in the uppermost layer of the adherends, which is similar to the observations from the over-heated welds in the previous chapter, as shown in Fig. 3.15b. This over-welding condition was possibly caused by the higher pressure which led to a faster heating rate [3]. In comparison to that, voids in Spot B predominantly presented on the top of resin-rich area and were formed by numerous resin tips. Owing to the lack of parallelism between two adherends, ED B was likely to be frequently compressed and stretched by the top adherend during the vibration. Hence, air was compressed into the molten ED and was kept in the resin-rich weldline.

Secondary welding was introduced on the edges of the overlap is because the surfaces of top and bottom adherends contacted to each other. Specifically, given the 52.8 μm peak-to-peak amplitude of Sonotrode R, when the sonotrode displacement was above 0.18 mm, the maximum displacement of the top adherend in the vibration phase was approximately 0.24 mm, which is almost the same with the initial thickness of EDs (i.e. the distance in between the surfaces of the top and bottom adherends). Combined with the pressure and vibration provided by the big sonotrode cross-section, secondary welding was introduced at the interface. All these observations indicates the simultaneous welding is not a proper technique for double-spot welding.

4.5. CONCLUSIONS

A series of experimental studies were carried out in this chapter to assess the quality of ultrasonically double-spot welded (2SW) joints, formed by two single-spot welded (1SW) joints through different welding strategies. The main goal was to validate the hypothesis that in sequential multi-spot welding, displacement-controlled welding is potentially capable of producing consistent welded spots with the fixed sonotrode displacement, while the welding energy has to be recalculated for each spot when energy-controlled welding is used. Apart from that, short investigations were carried out on the effects of welding sequences on displacement-controlled welding and the quality assessment of the 2SW joints created by simultaneous welding. Based on the experimental results, the following conclusions could be drawn:

- High-quality 2SW joints were sequentially produced under the same sonotrode displacement through displacement-controlled welding, featuring similar spot size and consistent failure modes (i.e. intralaminar failure with fibre-matrix debonding and fibre tearing). Both the average values of lap-shear strength (LSS) and ultimate failure load (UFL) of individual spots showed consistency with those obtained from the 1SW joints. However, two spots welded with the same input energy by energy-controlled welding showed different spot sizes and failure mechanisms. The observations indicate that in energy-controlled sequential spot welding is, the optimum energy for each spot has to be recalculated for obtaining consistent spot welds.

- Welded spots in two types of 2SW joints, which were manufactured following different sequences, showed similar spot size and consistently intralaminar failure mode, implying the sequence effects on displacement-controlled multi-spot welding are negligible.

- Regarding simultaneous welding, the two welded spots in 2SW joints featured different sizes of the final welded areas and significant void imprints were found in the fracture surfaces of both spots. The former observation can probably attributed to the pressure distribution on the two EDs not being uniform.

This chapter gave a solid validation on the robustness of displacement-controlled process in manufacturing the double-spot welded joints in a sequential manner, which was highlighted by producing consistent spot welds of high-quality with a fixed sonotrode displacement and regardless of sequence effects. Hence, displacement-controlled welding is a very promising strategy for facilitating the industrial application of sequential ultrasonic welding. In order to achieve a further improvement on the mechanical performance of double- or multi-spot welded joints, future work will focus on the effects of geometric parameters, e.g. different overlap length and different spot numbers, on the load-carrying capability of the MSW joints.

REFERENCES

[1] T. Zhao, C. Broek, G. Palardy, I.F. Villegas, and R. Benedictus. Towards robust sequential ultrasonic spot welding of thermoplastic composites: Welding process control strategy for consistent weld quality. *Composite Part A: Applied Science and Manufacturing*, 109:355–367, 2018.

[2] C. Ageorges, L. Ye, and M. Hou. Advances in fusion bonding techniques for joining thermoplastic matrix composites: A review. *Composites - Part A: Applied Science and Manufacturing*, 32(6):839–857, 2001.

[3] I.F. Villegas. Strength development versus process data in ultrasonic welding of thermoplastic composites with flat energy directors and its application to the definition of optimum processing parameters. *Composites Part A: Applied Science and Manufacturing*, 65:27–37, 2014.

[4] I.F. Villegas. In situ monitoring of ultrasonic welding of thermoplastic composites through power and displacement data. *Journal of Thermoplastic Composite Materials*, 28(1):66–85, 2015.

[5] G. Palardy and I.F. Villegas. On the effect of flat energy directors thickness on heat generation during ultrasonic welding of thermoplastic composites. *Composite Interfaces*, 24(2):203–214, 2017.

[6] T. Zhao, G. Palardy, I.F. Villegas, C. Rans, M. Martinez, and R. Benedictus. Mechanical behaviour of thermoplastic composites spot-welded and mechanically fastened joints: A preliminary comparison. *Composites Part B: Engineering*, 112:224–234, 2017.

[7] H.-M. Lu, A. Benatar, and F.-G.Cf+ He. Sequential ultrasonic welding of peek/graphite composites plates. In *Proceedings of the annual technical conference ANTEC*, volume 37, pages 2523–2526, 1991.

[8] S. Hassanifard, M. Zehsaz, and F. Esmaeili. Spot weld arrangement effects on the fatigue behavior of multi-spot welded joints. *Journal of Mechanical Science and Technology*, 25(3):647–653, 2001.

[9] Triyono, Jamasri, M.N. Ilman, and R. Soekrisno. Static and fatigue behavior of plug-welded dissimilar metal welds between carbon steel and austenitic stainless steel with different thicknesses. *International Journal of Mechanical and Materials Engineering*, 9(1):1–7, 2014.

[10] A. Benatar and T.G. Gutowski. Ultrasonic welding of peek graphite apc-2 composites. *Polymer Engineering and Science*, 29(23):1705–1721, 1989.

[11] ASTM D 1002-05. Standard test method for apparent shear strength of single-lap-joint adhesively bonded metal specimens by tension loading (metal-to-metal). *ASTM International*, 2005.

[12] E.S. Greenhalgh. Failure Analysis and Fractography of Polymer Composites. *Woodhead Publishing in Materials*, 2009.

[13] I.F. Villegas, B. V. Grande, H.E.N. Bersee, and R. Benedictus. A comparative evaluation between flat and traditional energy directors for ultrasonic welding of cf/pps thermoplastic composites. *Composite Interfaces*, 22(8):717–729, 2015.

[14] I.F. Villegas and H.E.N. Bersee. Ultrasonic welding of advanced thermoplastic composites: An investigation on energy-directing surfaces. *Advances in Polymer Technology*, 29(2):112–121, 2010.

5

A Study of the Effects of Various Geometric Parameters on the Mechanical Behaviour of Multi-spot Welded Single-lap Joints in Thermoplastic Composites

Thermoplastic composite spot welded joints are well-suited for carrying shear load rather than peel load. However, regarding the eccentric geometry of the single-lap joint configuration, secondary bending always occurs which introduces peel stress into the welded joints. A combination of experimental and analytical studies was carried out in this chapter to investigate the effects of the distance between spots and the numbers of welded spots on the secondary bending and subsequently on the load-carrying capability (LCC) of multi-spot welded joints. The latter results were compared to the LCC of joints assembled with multi-fasteners. The results indicated that, by increasing either the spot spacing or the spot number, secondary bending was effectively reduced and thus achieving an improvement of the LCC of the welded joints. In addition, owing to the reduced secondary bending, multi-spot welded joints showed a comparable LCC to that of mechanically fastened joints.

This chapter is to be submitted to Composite Part B: Engineering.

5.1. INTRODUCTION

THERMOPLASTIC composites (TPCs), which offer excellent mechanical properties (compared to metallic materials) and rapid manufacturing processes (compared to thermoset composites), are becoming increasingly attractive to aerospace and automotive industries [1–3]. Ultrasonic welding has been regarded as a very promising technique for assembling TPCs owing to its fast process and absence of foreign materials at the welding interface [4, 5]. In addition, ultrasonic welding is well-suited for producing spot welds. Our previous study [6] showed that ultrasonically single-spot welded (SSW) joints provide comparable shear strength to mechanically fastened joints assembled with a single fastener of similar size. Moreover, since welding relies on polymer autohesion at the welding interface, failure of SSW joints only takes place at the uppermost ply of the composite laminates, which results in significantly less damage in comparison to that in the mechanically fastened joints. However, due to the same reason, SSW joints show a low capability in carrying out-of-plane (i.e. peel) load [6]. Consequently, our experimental results indicate that, spot welded joints can be regarded as a composite-friendly alternative to mechanically fastened joints but it is of vital importance to minimize out-of-plane loading of the spot welded joints in their structural applications.

Single-lap joint is considered as the most typical configuration in mechanical tests for characterizing the tensile/shear behaviour of welded joints in both TPCs [4, 5, 7, 8]and metals [9–11]. However, it is well known that so-called secondary bending occurs once the joints are loaded in tension due to the eccentricity of the single-lap configuration [9, 12–17]. Bending results in out-of-plane deformation of the overlap and thus introduces peel stress into the welded joints negatively affecting the joint strength [9]. Therefore, the mechanical performance of single-lap welded joints, in particular multi-spot welded joints, is not only affected by the weld quality but it is also significantly dependent on the joint geometry, which directly affects secondary bending. Only a few research papers on metal welding discussed this point. Wung et al. [9] indicated the influence of out-of-plane warping on the weld strength and whereby a U-shape guide plate was used to restrain the rotation. However, this method is not practical for the multi-spot joints with a large overlap. Dieter [11] assessed the strength of spot welded joints in different configuration and reported the out-of-plane deformation for both single- and double-spot welded joints. Nevertheless no further details were reported on the influence of the configuration on the joint strength. To the best of authors' knowledge, little to no research was carried out on spot welded joints in TPCs considering the effect of the joint geometry as well as the secondary bending on the joint strength.

Extensive research, including both numerical and experimental work, has however been carried out on mechanically fastened joints regarding the effect of secondary bending on the strength of single-lap joints. Schijve [12, 13] proposed an analytical model, referred to as the Neutral Line Mode (NLM), to calculate the bending stress in multi-row mechanically fastened (MMF) single-lap joints. The neutral line indicates the loading path within the joints and the bending stress along the neutral line can be calculated based on the beam theory. Schijve also indicated that secondary bending can be reduced by increasing the distance between fasteners. Müller [14] proposed a modified NLM on the basis of the Schijve's model for MMF joints considering the fastener flexibility. In this modified model, the location of the neutral line is no longer at the mating

surface between two plates but being recalculated based on the load transfer by each fastener row. Ekh et al. [15, 16] studied secondary bending in multi-fastener, composite-to-aluminium joints through the analysis of the curvature of the specimen. The curvature, assessed in that study through digital speckle photography (DSP) techniques combined with finite element modelling, provides a good characterization on the out-of-plane deformation of the samples during testing and hence allows evaluating secondary bending.

In order to facilitate the application of spot welded joints, in particular of multi-spot welded (MSW) joints, in composite structures, the research in this chapter addresses the effects of different geometric parameters, namely the distance between welded spots and the number of welded spots, on secondary bending and hence on the load-carrying capability (LCC) of MSW single-lap joints. Based upon the abovementioned research on mechanically fastened joints, the LCC of MSW joints is expected to be increased by increasing the distance between spots. Likewise, owing to the increased amounts of welded area by an increased number of welded spots, the LCC is also expected to be improved. Nevertheless, owing to the non-uniform load distribution in MMF joints [14], the LCC of MSW joints is not likely to has a linear increase with the increased spot numbers. In order to validate these concerns, the experimental programme was divided into two parts: 1) welded samples formed by two single spots were used to assess the effect of distance between spots on the joint strength; 2) welded samples consisting of different numbers of welded spots at a fixed-length overlap were used to evaluate the effect of the spot numbers on the joint strength. For both parts, out-of-plane deformation, which was used to characterize the secondary bending within the joints, was captured by digital image correlation (DIC) techniques and the bending stress was calculated using the NLM. In the final part, a comparative study was carried out on the LCC between the MSW and the MMF joints.

5.2. EXPERIMENTAL

5.2.1. MATERIALS

CETEX® carbon fibre reinforced polyphenylene sulphide (CF/PPS) with 5 harness satin fabric reinforcement, supplied by Ten Cate Advanced Composites (The Netherlands), was used as the thermoplastic composite adherend material in this study. Laminates composed of six powder-impregnated composite plies with dimensions 580 mm × 580 mm and $[0/90]_{3s}$ stacking sequence were consolidated in a hot-platen press. The stacks were sandwiched between two aluminium plates and were consolidated at 320 °C and 1 MPa for 20 min. Comparing to the semi-impregnated plies used in the studies in Chapter 3 and 4, the powder-impregnated plies have higher resin portion. Therefore, the final thickness of the resulting laminates was 1.90 mm, which was relatively higher than the laminate thickness (1.6 mm) in the previous chapters. A water-cooled diamond saw was used to cut adherends into the required dimensions (based on the specific test design, Section 5.2.3) from the laminates. The adherends were cut such that the main apparent fibre orientation on their outer surfaces was parallel to their longer side (i.e. loading direction in the single-lap shear test).

5.2.2. ASSEMBLY TECHNIQUES

Sequential ultrasonic welding using a 20 kHz Rinco Dynamic microprocessor-controlled ultrasonic welder with a maximum power output of 3000 W was used to obtain the multi-spot welded joints. A 10 mm-diameter-circular sonotrode was utilized to create the individual spots in the MSW joints following the procedure explained in [6]. As shown in Fig. 5.1, both the upper and lower adherend were clamped with two aluminium bars to a base plate with a torque of 20 Nm. The upper adherend partially rested on the lower adhered (single-lap overlap area) and on a 1.8 mm-thick aluminium supporting plate. This configuration introduced a small misalignment between the surfaces of the adherends which was nevertheless corrected once the sonotrode applied pressure on the overlap. This thin, 1.8 mm-thick, base plate was selected to allow for unobstructed downward movement of the sonotrode during melting and flow of the ED. After welding of each individual spot, the sample was manually unclamped, shifted and clamped again to weld the next spot. Spot, i.e. circular, energy directors (EDs) with a 4 mm diameter were used to concentrate the heat generation at the welding interface. They were cut from the flat EDs with a thickness of approximately 0.25 mm, which were pre-manufactured in a hot platen press at 260 °C and 2 MPa for 10 min with three layers of 0.08 mm-thick neat Fortron® PPS films. Prior to the welding process, the spot EDs were manually fixed on the lower adherends using a Rinco handheld ultrasonic welder.

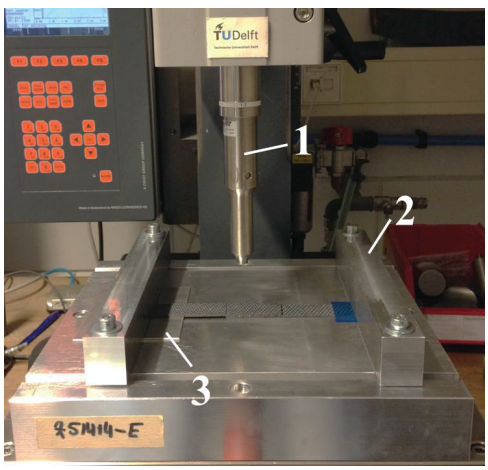

Figure 5.1: Ultrasonic welder and welding jig used in this study. 1: sonotrode, 2: bar clamp, 3: supporting plate for the upper adherend.

Regarding the welding process, displacement-controlled welding was used as the welding control strategy. The vibration stage was stopped when a pre-defined vertical displacement of the sonotrode was completed. The optimum sonotrode displacement (i.e. the displacement value resulting the maximum weld strength) and peak-to-peak vibration amplitude in this study were defined as 0.23 mm and 60.8 μm, respectively [18]. The welding force was 1500 N in the initiation of the welding and was linearly increased at a rate of 1000N/s during the vibration phase. After that, welds were kept under 1500 N force for 4000 ms for solidification based on previous experience.

Titanium HL10V6 Hi-Lok® fasteners (provided with a protruding head) were used to mechanically fasten the CF/PPS composites adherends. The pin length and diameter were approximately 4.0 and 4.8 mm, respectively. Fastened-hole were drilled in prior to the installation of fasteners by using a wooden plate underneath the composites adherends, thus minimizing the eventual drilling-induced delamination during tool entry and exit [19]. Fasteners were manually installed with a ratchet wrench, following the manual procedure in [20]. A constant clamping force could be provided during the installation of the fasteners, since the process was completed when the collar's wrenching device was torqued off.

5.2.3. TEST DESIGN AND TEST PROCEDURE

As indicated in Section 5.1, in order to evaluate the influence of the spacing between welded spots and the number of welded spots on the joint strength, the mechanical test programme was divided into two parts. In the first part, the MSW joints were formed by two single spots, referred as to 2SW joints, with a constant distance from the spot to the edge of the overlap (15 mm), but with varying spot spacing (i.e. spot-to-spot distance, SSD) (see Fig 5.2 and Table 5.1). Single-spot welded joints, which is referred to as 1SW joints, were also manufactured and tested, since they can be regarded as a special case of 2SW joints with zero spot spacing (i.e 2SW-0). In the second part, the mechanical behaviour of the MSW joints with two (2SW), three (3SW) and four (4SW) welded spots in a 70 mm-long overlap was analysed (Table 5.2). The distance from the outer spots to the overlap edge was still 15 mm. For both parts of tests, the clamped length of the welded samples was 50 mm. The free sheet length (FSL), i.e. the part from the clamp to the overlap edge, was designed to be equal to the overlap length for each case. In this way, the secondary bending of the overlap would be independent from the FSL since the latter one was fairly larger than the SSD of the samples [12]. The MMF joints assembled by two, three or four Hi-lok® fasteners, referred to as 2MF, 3MF and 4MF joints, respectively, were also tested in the second experimental part (see Table 5.2) for comparison purposes.

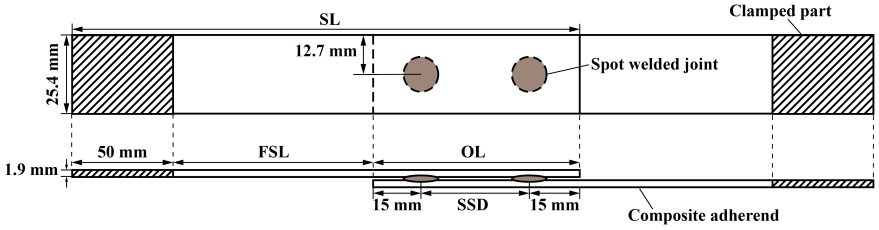

Figure 5.2: Schematic of the generic configuration of multi-spot welded single-lap shear joint specimen in this study. Dimensions are not to scale. Abbreviations are indicated in Table 5.1 and 5.2.

Single-lap shear tests were performed in Zwick/Roell 250 KN universal testing machine and in accordance with the ASTM D1002 standard [21]. Tests were initiated with a pre-load of approximately 100 N and performed at a constant crosshead speed of 1.3 mm/min. Hydraulic grips were used in this study and they were offset to ensure parallelism between the load path and the interface between the two adherends in every sam-

Table 5.1: Sample configurations with different distance between two spots.

Weld reference	Sample length (SL) (mm)	Overlap length (OL) (mm)	Free sheet length (FSL) (mm)	Spot-to-spot distance (SSD) (mm)
1SW (2SW-0)	110.0	25.4	34.6	0
2SW-10	130.0	40.0	40.0	10.0
2SW-20	150.0	50.0	50.0	20.0
2SW-30	170.0	60.0	60.0	30.0
2SW-40	190.0	70.0	70.0	40.0

Table 5.2: Sample configurations with different numbers of welded spots.

Sample reference	Number of joint	Overlap length (OL) (mm)	Spot-to-spot distance (SSD) (mm)	ED diameter (mm)	Pin diameter (mm)
2SW	2	70.0	40.0	4	-
3SW	3	70.0	20.0	4	-
4SW	4	70.0	13.3	4	-
2MF	2	70.0	40.0	-	4.8
3MF	3	70.0	20.0	-	4.8
4MF	4	70.0	13.3	-	4.8

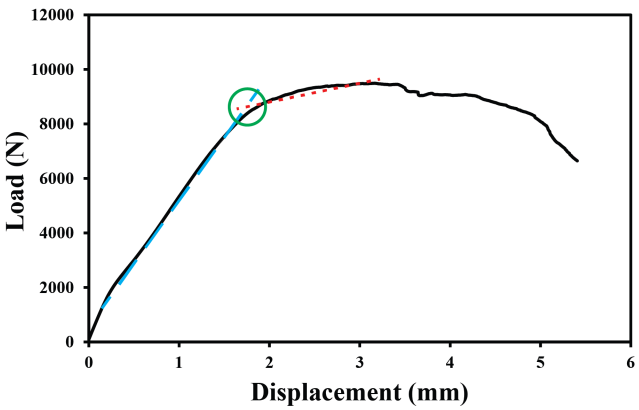

Figure 5.3: Bilinear approximation for identifying the OFL of the 2MF joints on the L-D curve. The OFL is indicated by the circle on the intersection of two fitting lines.

ple. Five samples were tested for each joint configuration. The maximum load reached during the tests, denoted as ultimate failure load (UFL) hereafter, was regarded as an indicator of the load-carrying capability (LCC) of the welded joints [6]. Regarding the mechanically fastened joints, the LCC was linked to the onset failure load (OFL) owing to the fact that it indicates the onset of bearing damage within the adherends [22]. Therefore, the LCC was calculated using a bilinear approximation [6, 23], as shown in Fig. 5.3, based on the load-displacement (L-D) curves obtained from the tests. The final welded areas (WAs) of the welded joints were visually inspected via a Zeiss stereo-microscope

and were measured using ImageJ150 (NIH). As indicated by the example shown in Fig. 5.4, the adhesive failure happened in the flow front of the ED was not taken into account when measuring the welded areas due to its negligible contribution to the weld strength. That is to say, only the area which showed failure within the composite adherends was considered as the welded area.

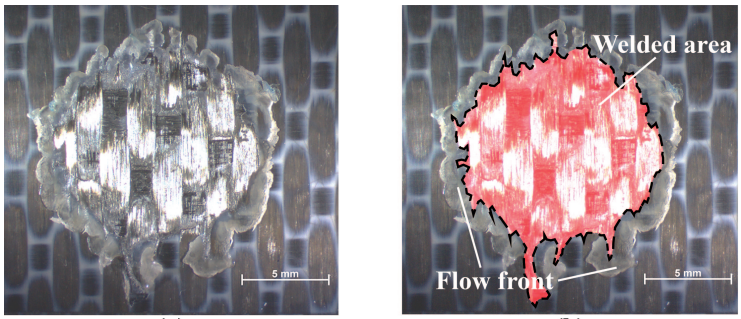

Figure 5.4: (a) Representative fracture surface of spot welded joint and (b) calculation of the WA (highlighted by the red area surrounded by the dashed line). The flow fronts surrounding the welded area are not taken into account for the calculation.

During the testing process, the Vic-3D DIC system, supplied by Limess Messtechnik & Software GmbH Inc, Germany, was used for measuring the out-of-plane deformation of the joint overlap as shown in Fig. 5.5a. Two CCD (charge coupled device) cameras combined with a light source were utilized to simultaneously track an applied surface pattern during loading by taking digital images of the surface [15, 24]. Owing to the small welded areas of the welded spots, no welds could be observed at the edge of the joint overlap. Therefore, instead of the side surface, the top surface of the overlap was chosen for the observation of the secondary bending (see Fig. 5.5b). A calibration process was performed for adjusting the position of the cameras relative to each other as well as to the samples, to assure the accuracy of the measurement. Prior to the tests, the surfaces to be tracked were individually cleaned using alcohol and were spray-painted to get a high-contrast pattern consisting of black speckles on a white background. Images of speckle pattern were captured at a frequency of 1 Hz during the tests. The first image was taken as the reference for the subsequent images and thus the accumulated strain on the tracked surface was calculated.

5.2.4. NEUTRAL LINE MODEL

The Neutral Line Model (NLM) proposed by Schijve [12], was used to calculate the bending stress at the location of the welded spots and the out-of-plane deformation of the joint overlap in this chapter. This model has been widely used in calculations for different types of mechanically fastened joints [12–14]. The NLM of a mechanically fastened joint assembled by two fasteners is shown in Fig. 5.6a. The neutral line is indicated by the dashed line, showing the eccentric loading path. The eccentricity occurs at the outer row of fasteners and the loading path is subsequently transferred to the mating interface between two adherends from the central line of the each adherend. Part I can be

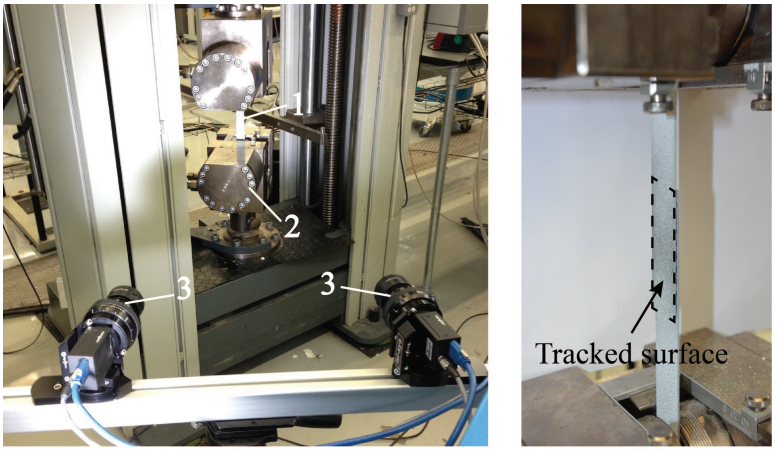

Figure 5.5: (a) Mechanical test set-up: 1, specimen, 2, hydraulic grips, 3, CCD cameras, and (b) the magnification of testing specimen. The area framed by dashed line indicates the surface being tracked during tests.

regarded as a beam once subjected to a combination of tensile and bending load due to the eccentricity, as shown in Fig. 5.6b. While the overlap part (i.e. the joint part between two fasteners) is considered as an integral beam formed by two adherends and thus has twice of the adherend thickness. Part II is defined as half of the overlap part due to the symmetrical configuration. Owing to the similar configuration to the MMF joints, the NLM is expected to be applicable for the MSW joints (see Fig. 5.6c).

Secondary bending can be analysed by considering the equilibrium of bending moment, as shown in Fig. 5.7. The detailed process for analysing secondary bending was given by Schijve in [12], which is just briefly shown in here. According to the beam theory, bending moments for both parts (M_{xi}) can be calculated with:

$$M_{xi} = E^* I_i (\frac{d^2 w}{dx^2})_i \tag{5.1}$$

where E^* is the Young's Modulus for plane bending of 2-d model:

$$E^* = \frac{E}{1-\nu^2} \tag{5.2}$$

I is the inertia moment of the cross section of the sample and w is out-of-plane deformation of the neutral line. In this way, bending stress (S_b) at the outer row of fastener/spot can be given as:

$$S_b = \frac{M_{(x_1=L_1)}}{W t^2/6} \tag{5.3}$$

W is the width of the sample, which can assumed to be 1 for plane bending.

Combined with the practical case for the MSW joints in this study, two things should be taken into account. Firstly, welded samples were clamped with offset grips during

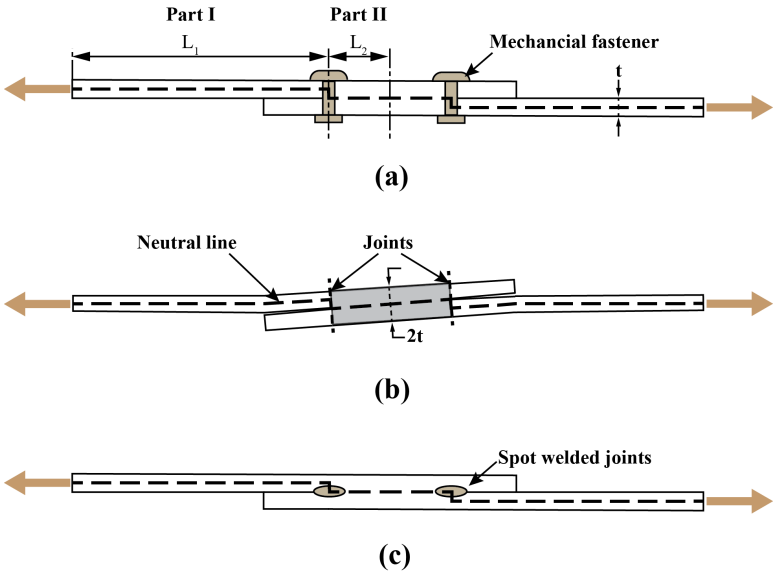

Figure 5.6: Eccentric loading path and neutral line within single-lap joints: (a) 2MF joint; (b) NLM (affected by secondary bending); (c) 2SW joint.

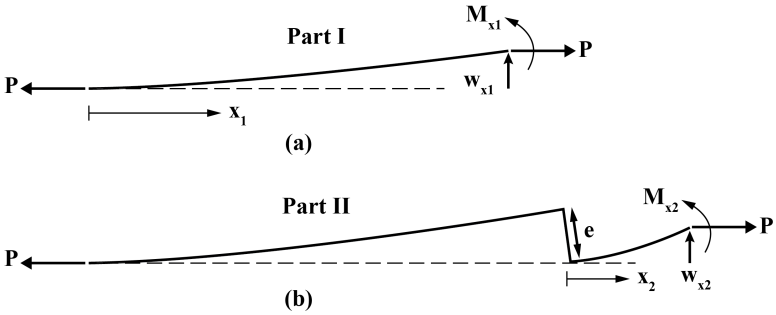

Figure 5.7: Two parts in the neutral line model: (a) Part I; (b) Part II. The eccentricity is indicated by *e*.

tests, a misalignment of 1.9 mm (equal to the adherend thickness) for the applied load should be input in the NLM calculation [12]. Secondly, joints are simplified as single lines in NLM, indicated by dotted lines in Fig. 5.6b. This is different from the practical cases for both welded spots and mechanical fasteners since they have diameters. The potential cause from this assumption will be discussed in the later text. Due to the difficulties in measuring the flexibility of mechanically fasteners and welded spots, the modified NLM model from Müller [14] cannot be used here to analyse the secondary bending in the 3SW and 4SW joints. Therefore, NLM was only used to calculate the bending stress and out-of-plane deformation of 2SW joints with different distance between spots.

5.3. RESULTS

This section presents the major results obtained from both mechanical tests and analytical calculation using the NLM for the MSW joints. It is mainly divided by three parts. In the first part, the mechanical behaviour of 2SW joints with different spot-to-spot distance (SSD) is reported. For comparison purposes, the results obtained for single-spot welded joints, i.e. 1SW joints, is also included. In order to analyse the secondary bending, bending stress of the 2SW joints with different SSD under the same loading condition is shown. Out-of-plane deformation obtained from DIC results is used to validate the analytical calculation. It should be noted that, the out-of-plane deformation was gathered from the points both inside and outside of the welded spots, in order to assess the influence of welds on the resistance to the out-of-plane deformation of the composite adherends. In addition, bending stress under the ultimate failure load (UFL) of each sample set is also provided to explain their mechanical behaviour at the maximum load condition. In the second part, the UFL as well as the welded areas of the MSW joints formed by different numbers of spots are presented. As indicated in Section 5.2.4, no NLM calculation was performed in this section due to the difficulties in measuring the flexibility of spot welded joints. In the final part, the comparison of the MSW and the MMF joints are shown in terms of load-carrying capability, out-of-plane deformation, load-displacement response and failure modes.

5.3.1. EFFECT OF THE SPOT-TO-SPOT DISTANCE

ULTIMATE FAILURE LOAD AND WELDED AREA

Table 5.3 summarises both the ultimate failure load (UFL) and the final welded areas (WAs) of the spots in both the 1SW and 2SW joints with different SSD considered in this study. Specifically, the UFL of the 1SW (reference) and of various 2SW joints are plotted in Fig. 5.8. As depicted in the figure, the UFL of the 2SW joints, in general, exhibited an increasing trend by increasing the spot spacing. A significant improvement, around 22 %, of the UFL was achieved from 2SW-10 to 2SW-20 joints. However, 2SW-30 showed a comparable, although slightly better, strength as compared to 2SW-20 joints. Regarding the scatter, 2SW-10 joints featured a relatively higher scatter in their UFL (around 8 %) in comparison to other 2SW samples (below 4 %). As a special case, the UFL of the 1SW joints was significantly lower than that of their 2SW counterparts which is reasonable taking into account that each sample had only one welded spot. To facilitate a fair comparison between the 1SW and 2SW joints, twice the magnitude of the UFL of the 1SW joint is indicated by a dashed line in Fig. 5.8. Comparing to this line, it is clear that a lower average joint strength was obtained for the lower weld spot spacing while the average strength was greater or equal to that of the 1SW joint for the larger weld spot spacings tested.

The final welded areas for the spot in the 1SW and for each spot in the 2SW joints with different SSD are shown in Fig. 5.9. Both spots in the 2SW joints, except those in 2SW-10 joints, provided similar final welded areas accompanied by low COV (from 2 % to 6 %) and all of them were comparable to that of the spot in the 1SW joints. Although the second spot of 2SW-10 samples also showed similar welded area to the reference of the 1SW joints, the variation was comparably higher (COV around 10 %). More importantly, the first spot of 2SW-10 joints presented significantly lower average welded areas,

Table 5.3: Ultimate failure load and welded area values (average ± standard deviation) of the 1SW and the 2SW joints with different SSD (COV: coefficient of variation).

Weld reference	Ultimate failure load UFL, (N) (COV, %)	Welded area, WA, (mm^2) (COV, %)	
		Spot 1	Spot 2
1SW (2SW-0)	3575.3 ± 147.3 (4.1)	90.4 ± 3.7 (4.1)	-
2SW-10	5876.1 ± 459.1 (7.8)	75.1 ± 12.7 (16.9)	85.1 ± 8.8 (10.4)
2SW-20	7084.0 ± 156.8 (2.2)	89.1 ± 1.9 (2.1)	88.3 ± 2.8 (3.1)
2SW-30	7309.1 ± 149.0 (2.0)	86.6 ± 5.5 (6.4)	83.2 ± 5.7 (6.8)
2SW-40	7776.1 ± 275.8 (3.5)	87.0 ± 4.5 (5.2)	85.3 ± 4.4 (5.2)

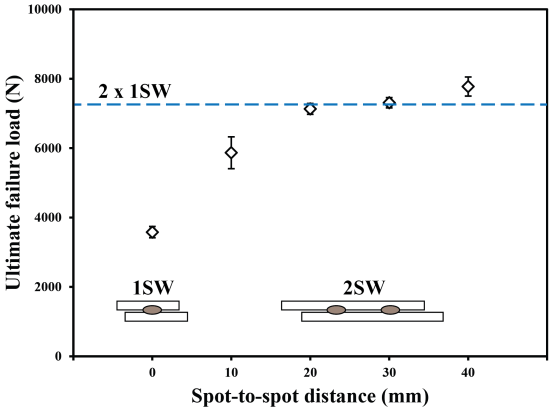

Figure 5.8: UFL of both the 1SW and the 2SW joints with different SSD. The dashed line corresponds the double of the average UFL of the 1SW joints.

approximately 12 % lower, than that of the second one, with an even higher scatter (COV around 17 %).

SECONDARY BENDING

According to the study in [12], the bending factor K_b is a typical factor for characterizing secondary bending within single-lap joint configurations. The bending factor is calculated as the ratio of bending stress, S_b, to tensile stress, S_t, at any point along the neutral line according to the following equation:

$$K_b = \frac{S_b}{S_t} \tag{5.4}$$

where S_b is calculated following Eq. 5.3 and S_t is calculated as the applied load divided by the cross-section area of the adherends.

In this research, K_b was calculated at the location of each welded spot of the 2SW joints using the Neutral Line Model (NLM). Owing to the symmetrical configuration of the welded joint, K_b should be the same at both spot locations. Fig. 5.10 illustrates the

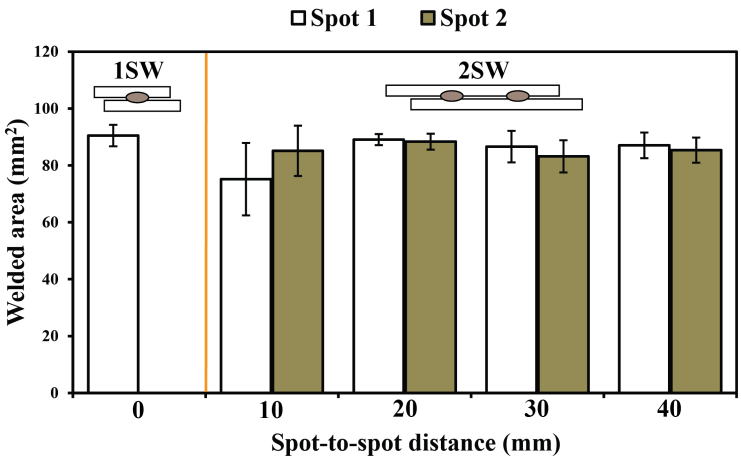

Figure 5.9: Final welded areas of individual spots in the 1SW joints and the 2SW joints with different SSD. The numbers of the spot indicate the welding sequence.

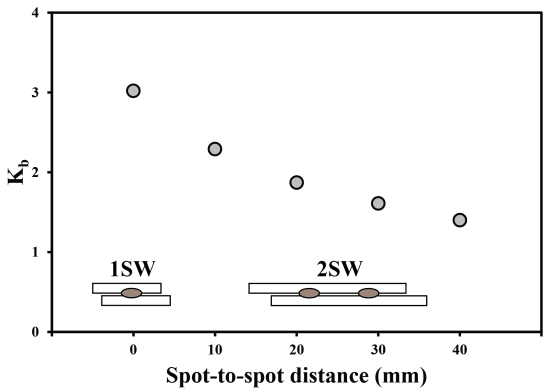

Figure 5.10: Bending factor calculated for both the 1SW and the 2SW joints with different SSD using the NLM under 3000 N load.

bending factor (K_b) for the 1SW joints and for the 2SW joints with different SSD under 3000 N load, which is just below the UFL of the 1SW joints (see Table 5.3 and Fig. 5.8). It can be clearly indicated that, by increasing the spacing between welded spots, the bending factor was effectively reduced. The highest bending factor (K_b = 3) was obtained for the 1SW joints, owing to the shortest SSD (i.e. 0 mm) they had. This result is in line with that obtained from the calculation for mechanically fastened joints with single fasteners [12]. Comparing to the 1SW joints, 2SW-10 achieved an approximately 30 % drop in K_b and 2SW-20 joints got a further 25 % decrease. The 2SW-30 and 2SW-40 joints showed around 10 % and 20 % decrease on the basis of the value of 2SW-20 joints, respectively.

The calculation of bending stress using the NLM can be validated by the observations

of the out-of-plane deformation under the same load condition (i.e. 3000 N). Fig. 5.11 showed that the out-of-plane deformation of the joint overlap calculated via the NLM and that captured by the DIC during loading process for three typical joint configurations, i.e. the 1SW, 2SW-10 and 2SW-40 joints. The results obtained by both methods displayed good agreement in terms of both trends and values. Apart from that, three interesting points were observed. Firstly, both analytical and experimental results indicated similar deformation (ranging from -0.3 to 0.6 mm in Z-axis) for different configurations. Secondly, results obtained from DIC invariably showed less deformation compared to that given by the NLM. Finally, deformation along the central line of the overlap (x = 0, points inside the welded spots) resulted in the same curvature as that obtained along the line close to the side (x = -10, points outside the welded spots).

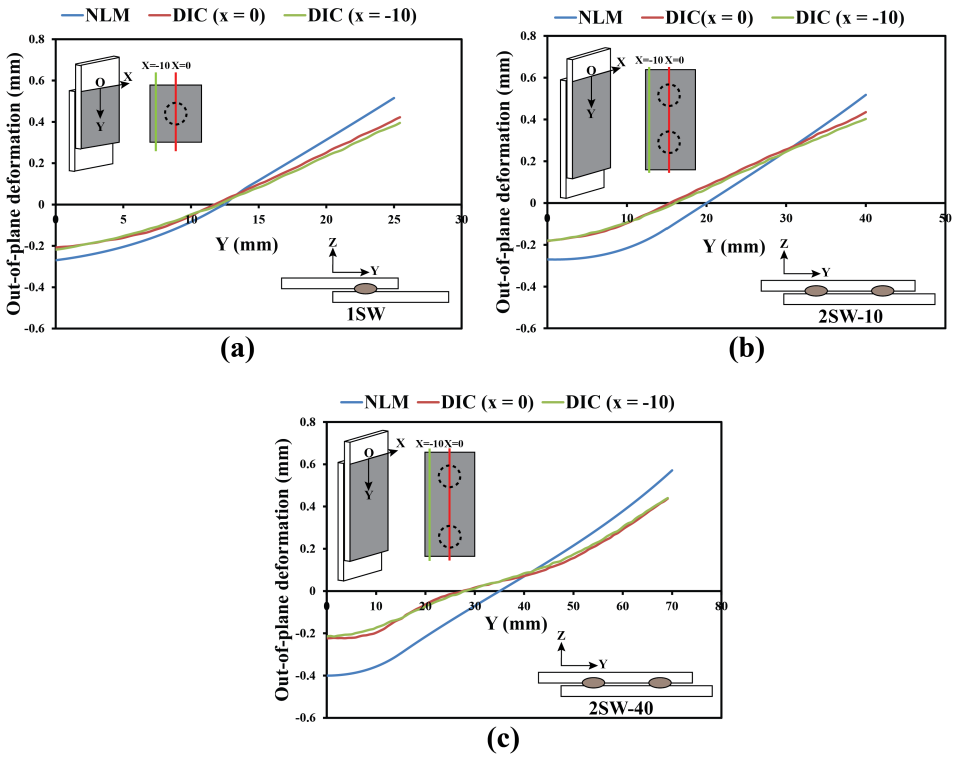

Figure 5.11: Out-of-plane deformation of the joint overlap under 3000 N load for different joint configurations: (a) 1SW joints, (b) 2SW-10 joints and (c) 2SW-40 joints.

In addition, the bending stress of both the 1SW and 2SW joints with different SSD under their UFL was also calculated and the results are summarized in Fig. 5.12. It must be noted that, even under their maximum loading condition, bending stress of the 2SW joints, excluded 1SW joints, still exhibited an approximately linear decrease, when increasing the spot spacing. The bending stress value of the 1SW was however found similar to that of the 2SW-20 joints.

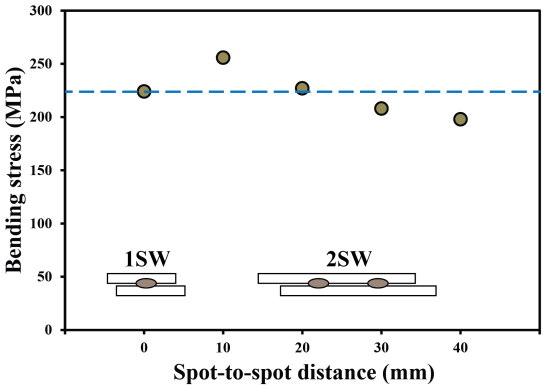

Figure 5.12: Bending stress calculated for both the 1SW and the 2SW joints with different SSD using the NLM under their UFL.

5.3.2. EFFECT OF THE NUMBER OF SPOTS

The UFL of all the MSW joint configurations, including 1SW joints, considered in this study is plotted in Fig. 5.13. The dashed lines indicate the two, three and four times of the average UFL value of the 1SW joints. The joint strength was found to be further improved by increasing the number of welded spots in the joint configuration with the largest SSD (i.e. 40 mm). On the other hand, this increase was not proportional to the increased welded spots, i.e. the increased amounts of welded area. It was found that 2SW-40, referred to as 2SW hereafter, joints achieved a slightly higher UFL, around 10 %, as compared to the twice magnitude of the UFL of the 1SW joints. The improvement of the UFL from the 2SW to the 3SW joints was around 30 %. However, the UFL of the 3SW joints was similar to three times of the UFL of the 1SW joints. Only a slight increase (around 10 %) was found in the UFL of the 4SW on the basis of the 3SW joints and the former one was obviously lower, by around 22 %, than four times of the UFL of the 1SW joints.

The comparison of the final welded areas measured for the spot in the 1SW and for each spot in the MSW joints formed by different number of spots is illustrated in Fig. 5.14. Spots in the 2SW and the 3SW joints showed similar welded areas and both values were comparable to the reference of the 1SW joints. The COV for these three cases was ranging from 5 % to 7 % of the corresponding average values. In contrast to that, the final welded areas for individual spot in the 4SW joints showed a relatively lower, by around 15 %, average value compared to that of the 1SW joints, combined with a slightly higher COV (approximately 11 %).

5.3.3. MSW JOINTS VS. MMF JOINTS

LOAD-CARRYING CAPABILITY

The load-carrying capability (LCC) of the MSW and the MMF joints assembled with either two, three, or four spots/fasteners is summarized in Fig. 5.15. From this figure, it is observed that the MSW and MMF joints exhibited similar trends in behaviour with re-

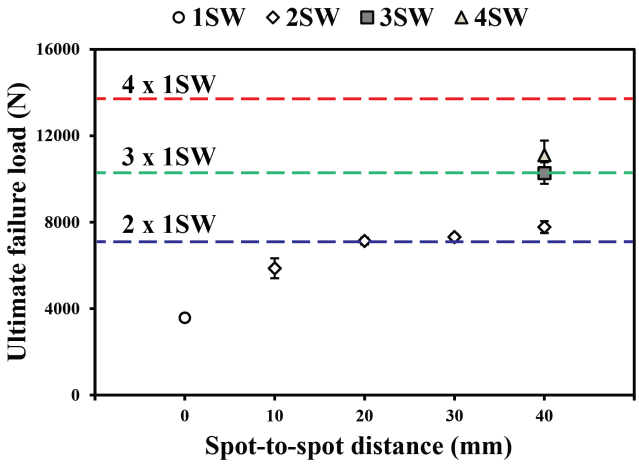

Figure 5.13: The relationship between the UFL (obtained from the mechanical tests) and the SSD and the number of welded spots in the MSW joints considered in this study. Blue, green and red dashed lines indicate the two, three and four times of the UFL of 1SW joints, respectively.

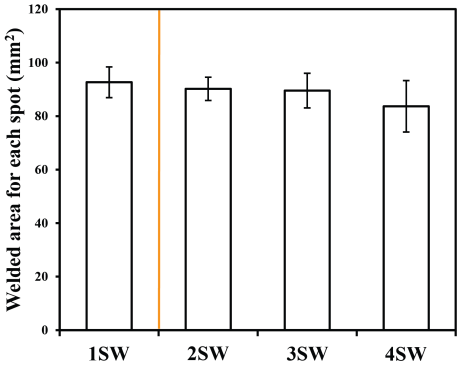

Figure 5.14: Comparison of the welded areas (obtained from the microscopic inspections) of individual spots in both the 1SW and MSW joints with different welded spots.

spect to the number of spots/fasteners. The 2SW joints showed a slightly lower value, by 9 %, than the 2MF joints. For the 3SW and the 4SW joints, their LCC was however marginally higher, by around 5 % and 4 %, than those of the 3MF and the 4MF joints, respectively. Regarding the scatter, the MSW joints showed consistent COV for the average LCC in all the three cases, ranging from 4 % to 6 %. On the contrary, a significant lower COV (approximately 2 %) was found for the average LCC of the MMF-N2 joints in comparison to that of the MMF-N3 (9 %) and of the MMF-N4 joints (8 %).

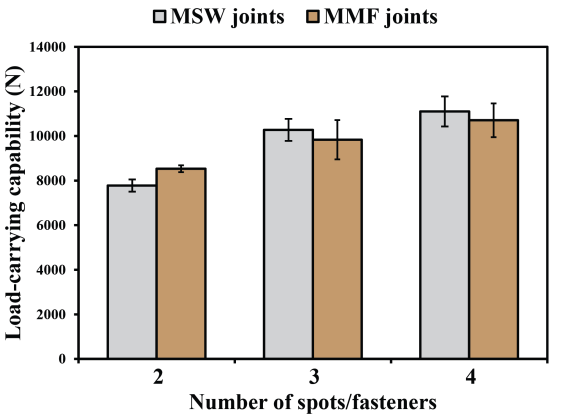

Figure 5.15: Comparison of the load-carrying capability between the MSW and the MMF joints with different number of spots/fasteners.

OUT-OF-PLANE DEFORMATION

The out-of-plane deformation of the joint overlap, which was mainly obtained from the DIC results for both types of joints (MSW vs. MMF) under 7000 N load, is plotted in Fig. 5.16. Likewise, this load level was selected since it is just below the UFL of the 2SW joints as well as the OFL of the 2MF joints. The results of NLM calculation was only shown for the 2SW and the 2MF case, as indicated by the dashed line in Fig. 5.16a. Regarding this case, the DIC results for both types of joints fitted well to the NLM results, nevertheless, the results of the 2MF joints displayed slightly better consistency than that of the 2SW joints. Focusing on the DIC results, the MSW joints invariably showed less deformation than that of their MMF counterparts for all the joint configurations. Moreover, increasing the welded spots (from Fig. 5.16a to 5.16c) was also found to decrease the out-of-plane deformation (i.e. secondary bending) for the MSW joints. However, this phenomenon was not observed in the MMF joints.

LOAD-DISPLACEMENT (L-D) CURVES

Regarding the L-D response of both types of joints, as shown in Fig. 5.17a, three points should be noted. Firstly, the MSW joints exhibited elastic behaviour during the loading process. Regarding the MMF joints, the joint stiffness, represented by the slope of the L-D curve, was significantly reduced after the initial failure, even though the joint strength was still maintained (2MF) or even increased (3MF and 4MF). Secondly, displacement between the initial and the ultimate failure was considerably reduced when more fasteners were installed. Finally, the MSW joints showed higher joint stiffness than their MMF counterparts even in the initial loading stage (see Fig. 5.17b) and no stiffness reduction was observed for the former one.

FAILURE MODES

Failure was found to only take place at the uppermost ply of the laminates for the MSW joints, featured by bare fibres, deep fibre imprints on thermoplastic resins and torn fi-

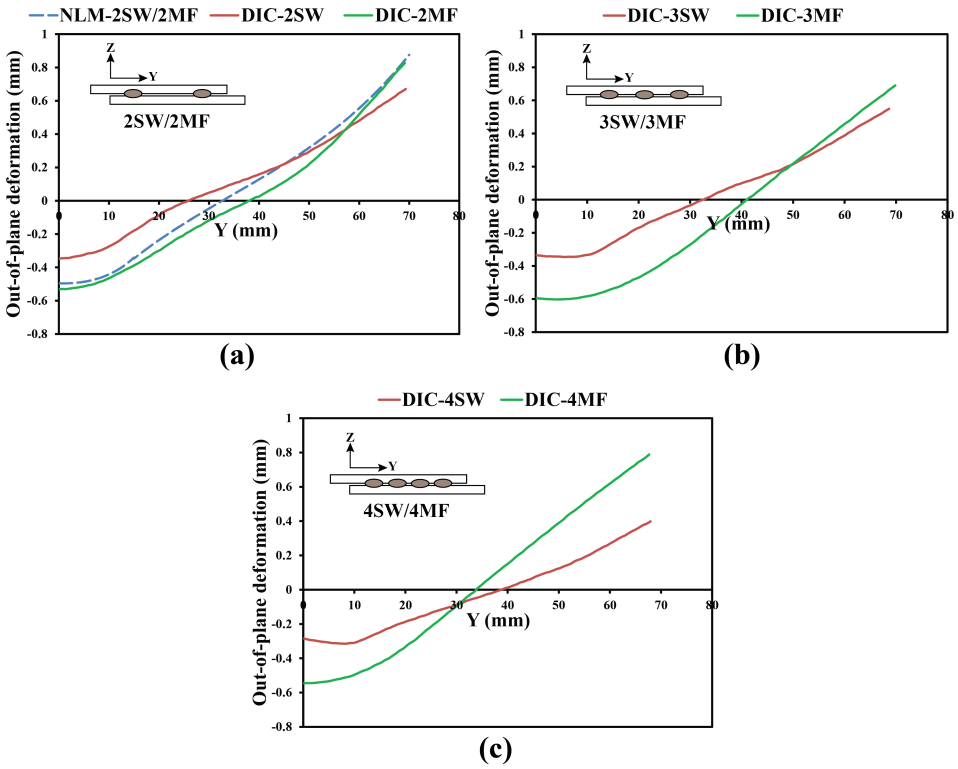

Figure 5.16: Comparison of out-of-plane deformation of the joint overlap under 7000 N load between the MSW and the MMF joints with different number of spots/fasteners: (a) 2 spots/fasteners; (b) 3 spots/fasteners; (c) 4 spots/fasteners.

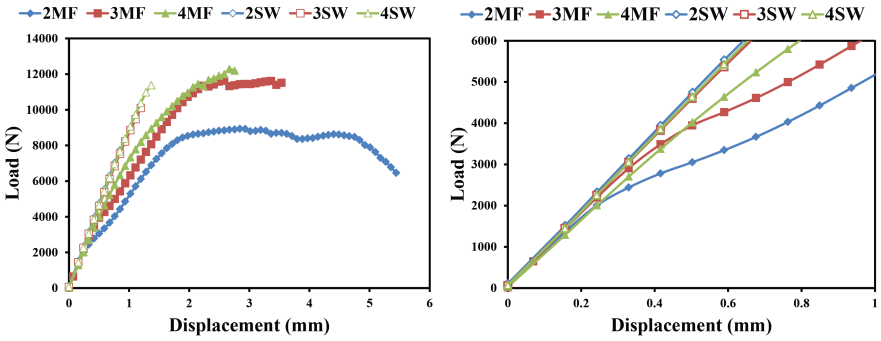

Figure 5.17: (a) Typical load-displacement (L-D) response and (b) the magnification of the initiation of loading process of two types of joints with different number of spots/fasteners.

bres, as illustrated in Fig. 5.18. This failure mechanism, namely intralaminar failure, was

invariably found for all the MSW joint configurations, indicating high weld quality [26]. In contrast to that, the 2MF joints showed a typical pull-through failure characterized by a significant rotation of the mechanical fasteners (Fig. 5.19a). A net-section failure in the composite adherends at the location of the outer fasteners (Fig. 5.19b) was however observed in the 3MF and the 4MF samples.

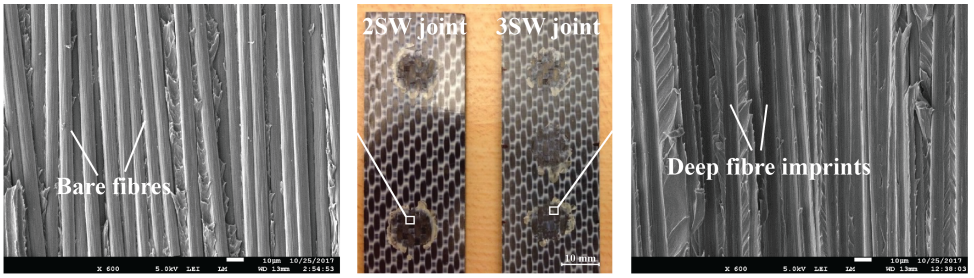

Figure 5.18: Representative fracture surfaces and the corresponding SEM details of the MSW joints in this study. The left and right SEM micrographs indicate the bare fibres and deep fibre imprints on the thermoplastic resins caused by fibre-matrix debonding. The scale bars are 10 μm for both SEM images.

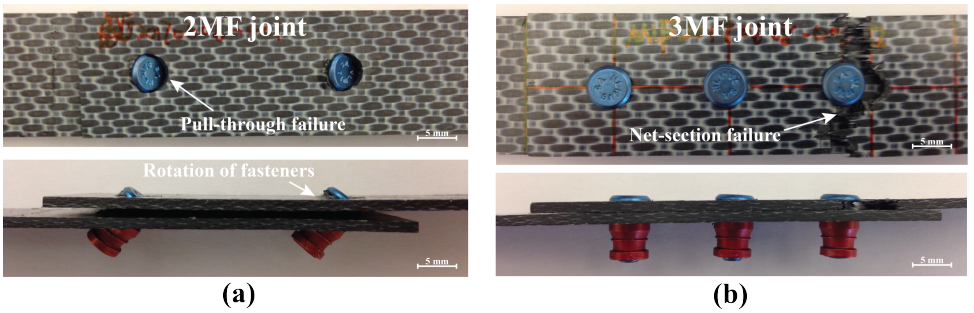

Figure 5.19: Failure mode transition from (a) the 2MF (pull-through failure) to (b) the 3MF joint (net-section failure).

5.4. DISCUSSION

5.4.1. SECONDARY BENDING AFFECTED BY DIFFERENT SPOT-TO-SPOT DISTANCE

The increase in the UFL of the 2SW joints observed in Fig. 5.8 is believed to result from the decreased secondary bending introduced into the joints, as shown in Fig. 5.10. Less bending stress (Fig. 5.10), which was achieved by increasing the distance between welded spots, essentially resulted in less peel stress introduced into the welded spots and thus improved their load-carrying capability. The highest bending factor (K_b = 3) of the 1SW joints indicates the single-row single-lap joint configuration is not an expected selection for carrying load in structure design. However, double magnitude of the UFL of the 1SW joints showed similar value to the UFL of the 2SW-20 samples (Fig. 5.8). This

is possibly explained by the similar bending stress at the moment of failure they had, as shown in Fig. 5.12. Regarding the 2SW-10 joints, the reason for their lower UFL, as compared to the double UFL of the 1SW joints, was possibly the lower value for their total welded areas, as compared to the double WAs of the 1SW joints. As shown in Table 5.3 and Fig. 5.9, the welded areas for the Spot 1 in the 2SW-10 joints was obviously smaller than that of the Spot 2 and also than that of the spot in the 1SW joints. This can be explained by the findings in fractographic analysis. As shown in the Fig. 5.20a, owing to the short spacing between two spots, i.e. 10 mm (approximately equal to the spot diameter), the flow fronts of the melted ED of the Spot 1 was hindered by the solid ED of the Spot 2 and thus resulting a smaller welded area. In addition, parts of the flow fronts of the Spot 1 was remelted when the Spot 2 was welded. As a result, these two welded spots somewhat came in contact with each other (Fig. 5.20b), which potentially led to the high scatter in their final welded areas (see Fig. 5.9).

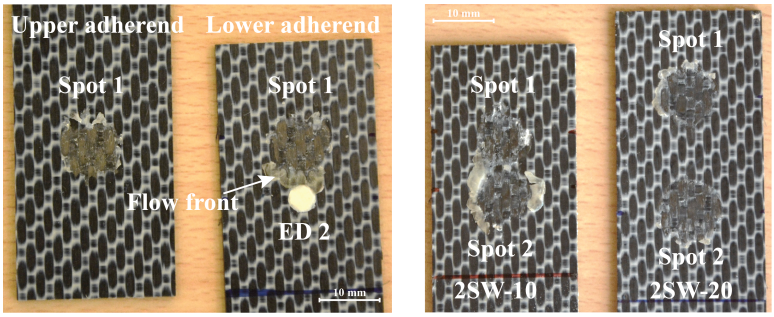

Figure 5.20: (a) Fracture surfaces of the 2SW-10 joints with only one spot welded and (b) the comparison of fracture surfaces between the 2SW-10 and the 2SW-20 joints. The flow fronts of the melted ED 1 in the 2SW-10 joints was impeded by the ED 2 and resulted in a smaller welded area for the Spot 1.

Regarding the observations of out-of-plane deformation of the 2SW joints under the same load level (Fig. 5.11), the mentioned three points in Section 5.3.1 can be explained as following. Firstly, although welded joints with different spot spacing showed similar out-of-plane deformation, it should be taken into account that various spot spacing led to various overlap length. For instance, the 2SW-40 joints have longer overlap than the 2SW-10 joints. As a consequence, the secondary bending of the 2SW-40 joints is less significant than that of 2SW-10 counterparts when they have the similar out-of-plane deformation. Secondly, joints in the NLM are simplified as single lines, as show in Fig. 5.6b. In practical case, however, welded spots have parameters (see Fig. 5.6c), which is around 10 mm specifically in this study. Owing to the spot diameters, welded joints provided more areas for load transmission and hence achieving a less secondary bending than that obtained through the model (Fig. 5.11). Finally, DIC results obtained along the central line (x = 0) consists of the maximum number of points inside the welded joints and hence it entails the maximum constraints provided from the welded spots. However, it showed similar out-of-plane deformation to the results obtained along the line close to overlap side (x = -10), which has no points inside the welded joints. This implies that, even without the constraints provided by welded joints, the composite laminates

still have enough resistance to the out-of-plane deformation.

5.4.2. SECONDARY BENDING AFFECTED BY DIFFERENT NUMBER OF SPOTS

Owing to the increased welded areas provided by the increased number of welded spots, the UFL of the MSW joints increased with increasing number of spots, as shown in Fig. 5.13, which is according to expectations. Apart from that, decreased secondary bending, following decreased out-of-plane deformation (see Fig. 5.16), for the MSW joints with increasing number of welded spots is regarded as another reason for the improvement of the joint strength. Therefore, according to the combination of the increased welded areas and the decreased secondary bending, it could be expected a more significant increase in the strength when increasing the number of spots from two to three or four.

However, when more than two spots were welded, the increase of the UFL was not as significant as expected (see Fig. 5.13). This was likely caused by a non-uniform load distribution within the MSW joints, which is known to occur in the MMF joints [14]. In the MMF joints, the outer-row fasteners always transfer more load than the inner ones. This can be obtained by considering the fastener flexibility and the displacement compatibility between two adherends. The load distribution of a 3-row mechanically fastened joint in Glare3, for instance, could be around 35 % - 30 % - 35 % for each row [14]. Hence, due to the similar joint configurations, MSW joints are believed to have the similar load distribution. However, unlike the mechanically fastened joints, spot welded joints showed a brittle failure, as indicated in both Fig. 5.17 and [6]. Therefore, the MSW joints were supposed to fail once the outer-row spots reached their UFL and therefore the increased magnitude of the UFL when increasing the number of spots was diminished (Fig. 5.13). Due to the difficulties in measuring the flexibility of spot welded joints, which is directly linked to the calculation of the load distribution within the MSW joints, no validation of the hypothesis about the non-uniform load distribution within the MSW joints was provided. This should be done in the future research. Another possible reason for the diminished increase of the UFL when increasing the number of spots from 3 to 4, as compared to the increase from the 2SW to the 3SW joints, was the reduction in the welded areas for each spot, as indicated in Fig. 5.14. Similar to the observations from the fracture surfaces of the 2SW-10 joints, the short spacing between EDs in the 4SW joints caused interferences between the flow front of each welded spot and the adjacent and resulted in smaller welded areas for each spot (see Fig. 5.21).

5.4.3. SECONDARY BENDING IN MSW AND MMF JOINTS

It is well known that both shear and peel stress are present in single-lap joints owing to their eccentric loading path. The results gathered from the pull-through tests in Chapter 2 showed that the peel strength of the 1SW joints is around 20 % of that of the 1MF joints. Consequently, it is expected that the load-carrying capability (LCC) of the MSW joints is significantly lower than that of the MMF joints in a single-lap configuration. The LCC of the MSW joints in Fig. 5.15 however showed comparable values to that of the MMF joints for all the studied configurations. This is believed as a consequence of the decreased secondary bending in the MSW joints, featured by the decreased out-of-plane deformation shown in Fig. 5.16. Specifically for the 2SW and 2MF case, it was found that a slightly better consistency between the NLM and DIC results was achieved by the latter

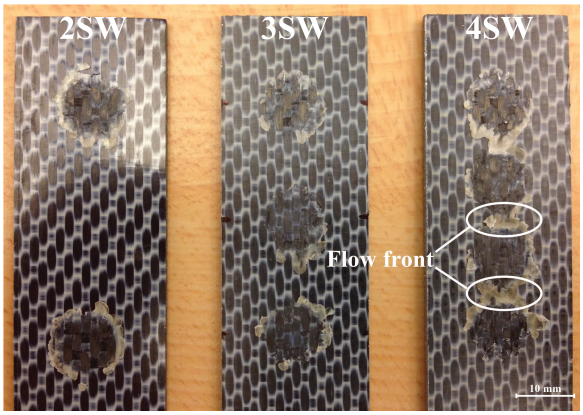

Figure 5.21: Representative fracture surfaces of the 2SW, 3SW and 4SW joints. The welded spots almost contacted to each other in the 4SW joints due to the meet of the flow fronts, which resulted in smaller welded areas for each spot compared to that of the spot in the 2SW and 3SW joints.

one (Fig. 5.16a). This is most likely attributed to the diameter of the mechanical fastener pin (4.8 mm), which is, comparing to that of the welded spots (around 10 mm), more similar to the assumed joints (0 diameter) in the NLM. Therefore, the load transmission in the 2MF joints was more similar to that in the NLM, which consequently resulted in similar out-of-plane deformation.

Decreased secondary bending or out-of-plane deformation of the MSW joints was likely caused by their higher joint stiffness than that of the MMF joints, as shown by the L-D response in Fig. 5.17. As indicated in Fig. 5.18, failure in the MSW joints only took place in the first-ply of the laminates. Owing to this benefits, no through-the-thickness damage was introduced into the adherends of welded samples and thus achieving a higher joint stiffness. In contrast, the stiffness degradation of the MMF joints was likely a consequence of the concentrated pin-load applied on the interior of the circumference of the fastened hole by the mechanical fasteners [6]. In particular for the 2MF samples, the significant rotation of fasteners (see Fig. 5.19a) resulted in a further stiffness reduction as compared to their 3MF and 4MF counterparts. Although fastener rotation was found to be prevented by the assembly with more fasteners in the 3MF and 4MF samples, the cost was a net-section laminate failure (Fig. 5.19b) and a significant reduction in the displacement during loading (Fig. 5.17a).

5.5. CONCLUSIONS

In this study, a series of mechanical tests were carried out to investigate the effects of different geometric parameters on mechanical behaviour of multi-spot welded single-lap joints in thermoplastic composites. Special attention was paid on the effects of the distance between welded spots and the number of welded spots on the secondary bending and consequently on the ultimate failure load (UFL) of welded samples. The secondary bending was, on one hand, analysed through the neutral line model (NLM). On another hand, it was also experimentally assessed via the out-of-plane deformation of the joint

overlap using a commercial 3D Digital Image correlation (DIC) system. The NLM calculation showed a good agreement with DIC results regarding the out-of-plane deformation of the welded joints. Finally, a comparative study was carried out to investigate the load-carrying capability of the multi-spot welded joints and the mechanically fastened joints with multiple fasteners. Based on the experimental and analytical study, the following conclusions can be made:

- The UFL of welded samples was increased by increasing distance between welded spots, which was likely a consequence of the decreased secondary bending within the joints.
- Increase of the number of welded spots within a fixed-length overlap provided an improvement of the UFL for the multi-spot welded joints. This was likely a result of a combination of increased amounts of welded areas and decreased secondary bending. However, the UFL was not proportionally increased with increasing number of the welded spots. This probably resulted from that a non-uniform load distribution within the multi-spot welded joints. The entire welded joints are believed to fail once the outer spots reach their UFL and hence, the increased magnitude of the joint strength was nevertheless decreased when increasing the number of spots. Due to the difficulties in measuring the flexibility of the welded spots, no validation was provided for this hypothesis.
- In spite of a combination of peel and shear load transmission of the single-lap joint configuration, multi-spot welded joints exhibited a comparable load-carrying capability compared to that of mechanically fastened joints assembled with the same number of fasteners. This was believed as a result of the decrease of the secondary bending within the welded joints, owing to the higher stiffness of the welded joints.

REFERENCES

[1] A.R. Offringa. Thermoplastic composites - Rapid processing applications. Part A: Applied Science and Manufacturing, 27(4 PART A):329–336, 1996.

[2] C. Ageorges, L. Ye, and M. Hou. Advances in fusion bonding techniques for joining thermoplastic matrix composites: A review. *Composites - Part A: Applied Science and Manufacturing*, 32(6):839–857, 2001.

[3] A. Yousefpour, M. Hojjati, and J.P. Immarigeon. Fusion bonding/welding of thermoplastic composites. *Journal of Thermoplastic Composite Materials*, 17(4):303–341, 2004.

[4] I.F. Villegas. Strength development versus process data in ultrasonic welding of thermoplastic composites with flat energy directors and its application to the definition of optimum processing parameters. *Composites Part A: Applied Science and Manufacturing*, 65:27–37, 2014.

[5] G. Palardy and I.F. Villegas. On the effect of flat energy directors thickness on heat generation during ultrasonic welding of thermoplastic composites. *Composite Interfaces*, 24(2):203–214, 2017.

[6] T. Zhao, G. Palardy, I.F. Villegas, C. Rans, M. Martinez, and R. Benedictus. Mechanical behaviour of thermoplastic composites spot-welded and mechanically fastened joints: A preliminary comparison. *Composites Part B: Engineering*, 112:224–234, 2017.

[7] I.F. Villegas, B. V. Grande, H.E.N. Bersee, and R. Benedictus. A comparative evaluation between flat and traditional energy directors for ultrasonic welding of cf/pps thermoplastic composites. *Composite Interfaces*, 22(8):717–729, 2015.

[8] I.F. Villegas, L. Moser, A. Yousefpour, P. Mitschang, and H.E.N. Bersee. Process and performance evaluation of ultrasonic, induction and resistance welding of advanced thermoplastic composites. *Journal of Thermoplastic Composite Materials*, 26(8):1007–1024, 2013.

[9] P. Wung, T. Walsh, A. Ourchane, W. Stewart, and M. Jie. Failure of spot welds under in-plane static loading, journal="Experimental Mechanics. *Experimental Mechanics*, 41(1):100–106, 2001.

[10] P. Wung. A force-based failure criterion for spot weld design. *Experimental Mechanics*, 41(1):107–113, 2001.

[11] R. Dieter, Z.Y. Zheng, and M. Walter. Local stress parameters at the weld spot of various specimens. *Engineering Fracture Mechanics*, 37(5):933–951, 1990.

[12] J. Schijve, G. Campoli, and A. Monaco. Fatigue of structures and secondary bending in structural elements. *International Journal of Fatigue*, 31(7):1111–1123, 2009.

[13] J. Schijve. Some elementary calculations on secondary bending in simple lap joints. *Technical report*, National Aerospace Laboratory, Amsterdam, 1972.

[14] R.P.G. Müller. An experimental and analytical investigation on the fatigue behaviour of fuselage riveted lap joints. The significance of the rivet squeeze force, and a comparison of 2024-T3 and Glare 3. *Doctor Thesis*, Delft University of Technology, 1995.

[15] J. Ekh, J. Schön, and L.G. Melin. Secondary bending in multi fastener, composite-to-aluminium single shear lap joints. *Composites Part B: Engineering*, 36(3):195–208, 2005.

[16] J. Ekh and J. Schön. Effect of secondary bending on strength prediction of composite, single shear lap joints. *Composites Science and Technology*, 65(6):953–965, 2005.

[17] L.B. Zhao, A. Xin, F.R. Liu, J. Y. Zhang, and N. Hu. Secondary bending effects in progressively damaged single-lap, single-bolt composite joints. *Results in Physics*, 6:704–711, 2016.

[18] T. Zhao, C. Broek, G. Palardy, I.F. Villegas, and R. Benedictus. Towards robust sequential ultrasonic spot welding of thermoplastic composites: Welding process control strategy for consistent weld quality. *Under review at Composite Part A: Applied Science and Manufacturing*.

[19] F. Gamdani, and R. Boukhili, and A. Vadean. Tensile strength of open-hole, pin-loaded and multi-bolted single-lap joints in woven composite plates. *Materials & Design*, 88:702–712, 2015.

[20] Hi-Shear. Corporation. hi-lok®;/hi-tigue® fastening systems installation instructions. 1991.

[21] ASTM D 1002-05. Standard test method for apparent shear strength of single-lap-joint adhesively bonded metal specimens by tension loading (metal-to-metal). *ASTM International*, 2005.

[22] T.L. Qin, L.B. Zhao, and J.Y. Zhang. Fastener effects on mechanical behaviors of double-lap composite joints. *Composite Structures*, 100:413 – 423, 2013.

[23] A.B. de Morais, A.B. Pereira, M.F.S.F. de Moura, F.G.A. Silva, and N. Dourado. Bilinear approximations to the mixed-mode I–II delamination cohesive law using an inverse method. *Composite Structures*, 122:361 – 366, 2015.

[24] H. Shi, I.F. Villegas, and H.E.N. Bersee. An investigation on the strain distribution of resistance welded thermoplastic composite joints. In *Proceedings of 53rd AIAA/ASME/ASCE/AHS/ASC Structures, Structural Dynamics and Materials Conference 2012*, Honolulu, Hawaii, USW, April 2012.

[25] J. Schijve. Fatigue of structures and materials. *Springer Science + Business Media, B. V.*, 2009.

[26] I.F. Villegas and H.E.N. Bersee. Ultrasonic welding of advanced thermoplastic composites: An investigation on energy-directing surfaces. *Advances in Polymer Technology*, 29(2):112–121, 2010.

6

CONCLUSIONS AND RECOMMENDATIONS

This chapter summarises the main conclusions of ultrasonic spot welding and mechanical characterization of spot welded joints obtained from Chapters 2-5, which systematically provide answers to the scientific questions proposed in Chapter 1. In addition, effects of manufacturing issues and experimental design on the outputs of the experiments and the mechanical tests are discussed. Based upon that, recommendations are provided for future research, in order to facilitate the application of spot welded joints in thermoplastic composite structures.

6.1. OVERVIEW OF RESEARCH

As indicated in Chapter 1, the objectives of the research presented in this thesis are to: 1) define a procedure for manufacturing (multi-)spot welded joints with consistent quality, and 2) gain insight into the mechanical behaviour and failure mechanisms of (multi-)spot welded joints in different load conditions as compared to that of mechanically fastened joints. Therefore, the research in this thesis mainly focuses on two aspects: manufacturing and mechanical characterization of ultrasonic spot welded joints. Aiming at achieving these objectives, several scientific questions were proposed:

1 How to define a distinct procedure which is well-suited for ultrasonic spot welding to produce a single spot?

2 What is the in-plane (shear) and out-of-plane (peel) mechanical behaviour and failure modes of the created single-spot welded joints?

3 How is the above-mentioned mechanical behaviour and failure modes of spot welded joints compared to that of mechanically fastened joints with a single fastener?

4 What is the optimum welding procedure to obtain multi-spot welded joints with consistent quality taking into account the change in boundary conditions introduced by every new spot in the sequential welding process?

5 In multi-spot welded single-lap joints, how is the effects of different distance between spots and numbers of welded spots in a fixed overlap on the joint strength?

6 How is the mechanical performance of multi-spot welded joints as compared to mechanically fastened joints with multiple fasteners regarding a single-lap configuration?

A series of investigations on manufacturing and mechanical characterization of ultrasonic spot welded joints were systematically carried out to address these questions. The major parts of the research in this thesis were completed by experimental studies, mainly including ultrasonic welding, mechanical tests and fractographic analysis. Some modelling work was performed in Chapter 5 to analyse the secondary bending in the multi-spot welded single-lap joints.

As a conclusion of the entire thesis, this chapter systematically summarizes the answers to each of the scientific questions. Specifically, the first three questions will be addressed in Section 6.2. The fourth and fifth questions will be answered in Section 6.3. Section 6.4 will focus on the last two questions. Finally, regarding the potential effects of the manufacturing issues and the experimental methods on the research outcomes, some recommendations for future work will be given.

6.2. MANUFACTURING AND MECHANICAL BEHAVIOUR OF SPOT WELDED JOINTS

A welding procedure was defined to weld single spots as compared to the traditional one for creating joints with fully-welded overlap. Firstly, spot, i.e. circular, flat energy

directors (EDs) with a diameter of 4 mm were used to produce the spot welded joints, as shown in Fig. 2.7. Prior to welding, the spot EDs were manually fixed on the bottom adherends. During welding, they were melted and flowed and finally formed spot welded joints with an average diameter of approximately 10 mm. Secondly, due to the small area of the spot EDs (as compared to the area of the overlap, i.e. 25.4 × 25.4 mm^2), secondary welding was observed when a big sonotrode, e.g. a 40 mm-diameter sonotrode, was used in the welding process, as shown in Fig. 2.5. To overcome this problem, a sonotrode with smaller cross-section, i.e. 10 mm diameter, was employed and the results indicated the secondary welding on the overlap edges was effectively prevented. Finally, owing to the presence of a displacement plateau (see Fig. 2.6), an energy-controlled welding instead of displacement-controlled welding was adopted for the spot welding process.

The in-plane and out-of-plane mechanical behaviour of the single-spot welded joints and of mechanically fastened joints with single Hi-Lok fasteners was characterized via double-lap shear and pull-through tests, respectively. Regarding the in-plane performance, spot welded joints showed similar load-carrying capability, ranging from 94 % to 112 %, as compared to the mechanically fastened joints. Moreover, the joint stiffness of the welded samples was found to be considerably higher, by around 88 %, than that of the mechanically fastened joints, which was negatively affected by the pin-load applied by the mechanical fasteners on the fastened holes. Failure of welded samples was found only at the outermost ply of the laminates, featured by fibre-matrix debonding and torn fibres. In contrast to that, severe through-the-thickness damage, featured by delamination and matrix cracking, was introduced into the laminates of the mechanically fastened joints.

Regarding the out-of-plane behaviour, the spot welded joints showed a lower load-carrying capability and however a slightly higher joint stiffness as compared to those of the mechanically fastened joints. Likewise, welded samples still displayed first-ply failure, showing fibre-matrix debonding and laminate tearing. However, through-the-thickness damage was invariably foMutlund in the laminates of the mechanically fastened joints.

6.3. DEVELOPMENT OF THE WELDING PROCEDURE FOR SEQUENTIAL SPOT WELDING

ALTHOUGH energy-controlled welding was successfully used in producing single-spot welded joints in Chapter 2, according to the study by Benatar [1], welding energy is likely not only used to create the spots but is also dissipated in the surroundings, such as the adherends, clamping jigs and welding base, during the welding process. Therefore, one concern for the adoption of energy-controlled welding in sequential multi-spot welding is that a constant energy input will possibly result in different weld quality for each spot. To validate this concern, different welding jigs were used to provide different boundary conditions and thus the effect of boundary conditions to the welding of single spots on energy-controlled welding was assessed.

The optimum welding energy was found to be significantly different when different welding jigs were used. Even given the optimum welding energy, some variations of the weld quality, e.g. under-welded and over-welded spots, were observed on the

welds created by energy-controlled welding. These observations confirmed our expectation that energy-controlled welding is sensitive to the changes in boundary conditions. On the contrary, when displacement-controlled welding was used, the optimum sonotrode displacement was found to be the same for both welding jigs. In addition, the displacement-controlled welds provided comparable weld strength as compared to that of the energy-controlled ones, with however more consistent weld quality, featured by more consistent failure modes.

It should be noted that displacement-controlled welding was enabled for ultrasonic spot welding by increasing the welding force during the vibration phase of the welding process. The flow fronts of the melted ED were further compressed under the constantly increased welding force, allowing a continuous increase of the sonotrode displacement. As a consequence, the optimum displacement value was able to be identified. Based on the results of the comparative study on the effect of boundary conditions on the welding process, displacement-controlled welding was identified to be a promising approach for sequential ultrasonic spot welding.

The results obtained in Chapter 3 primarily indicated that displacement-controlled welding is a more appropriate procedure, as compared to energy-controlled welding, for sequential spot welding. However, changes in the boundary conditions introduced by the welded spots in multi-spot welding were likely different from that provided by different welding jigs. Therefore, displacement-controlled welding and energy-controlled welding were comparatively assessed regarding their applicability to the producing of double-spot welded joints.

High-quality double-spot welded joints, featured by consistent spot size and failure modes in the two spots, were found when using displacement-controlled welding. The optimum displacement values for both spots in double-spot welding were the same and were also consistent to that for welding of single spots. On the contrary, two welded spots created using energy-controlled welding with a constant energy input showed significantly different spot sizes and failure modes. This observation indicated that the first welded spot indeed affect the energy required to obtain a second spot of similar quality. If energy-controlled welding is used, the optimum energy has to be recalculated for each spot.

Given different welding sequences in the sequential welding process, the two welded spots produced using displacement-controlled welding still showed consistent quality, i.e. similar spot size and consistent failure mode. This provided a further confirmation that displacement-controlled welding is a robust procedure for sequential multi-spot welding.

6.4. MECHANICAL BEHAVIOUR OF MULTI-SPOT WELDED JOINTS

AIMING at diminishing peel load introduced into spot welded joints, the effects of the distance between welded spots (in double-spot welded joints) and the number of welded spots (in multi-spot welded joints) on the mechanical behaviour of multi-spot welded single-lap joints were investigated. A comparative study was performed regarding the load-carrying capability of multi-spot welded joints and mechanically fastened joints with multiple fasteners.

It was found that, by increasing the distance between welded spots, the secondary

bending of the joint overlap was effectively reduced, which eventually resulted in an increase in the load-carrying capability of the double-spot welded joints. In addition, maintaining a constant overlap length, the load-carrying capability of multi-spot welded joints was also improved by increasing the number of spots, i.e from two to three and four spots. This was likely a consequence of the combination of the increased welded areas (owing to the increased number of welded spots) and the decreased secondary bending of the joint overlap. On the other hand, the increase of the load-carrying capability of the multi-spot welded joints was found less and less significant with increasing the number of welded spots. This was believed to be attributed to the non-uniform load distribution among the welded spots when more than two spots were used, which is similar to the case of mechanically fastened joints assembled with more than two fasteners.

The multi-spot welded joints showed a comparable load-carrying capability to the mechanically fastened joints assembled with the same amounts of Hi-Lok® fasteners in a single-lap joint configuration. This was a consequence of the reduced secondary bending, which resulted from the high joint stiffness of the spot welded samples as compared to that of their mechanically fastened counterparts.

6.5. FINAL CONCLUSION

THE results presented in this thesis showed that displacement-controlled welding is a very robust welding procedure for sequential ultrasonic welding, featured by producing welded spots with consistent quality under the same sonotrode displacement. In addition, the created (multi-)spot welded joints showed similar load-carrying capability but higher joint stiffness and less damage affected zone (no through-the-thickness in the adherends) as compared to those of mechanically fastened joints. The obtained results, on one hand, successfully fill in the current knowledge gaps (Section 1.5) of ultrasonic spot welding in thermoplastic composites, providing attempts to achieve the upscaling of ultrasonic welding. On another hand, the conclusions highlight the superiority of spot welded joints to traditional mechanically fastened joints, displaying a possibility of the widespread applications of the former joints as an alternative to the latter ones in composite aircraft structures.

6.6. RECOMMENDATIONS

THIS thesis is a preliminary study on ultrasonic spot welding in thermoplastic composites. Further research is necessary to be done based on the present work to achieve the final goal mentioned in Section 1.5. This section will present some manufacturing issues and limitations on the experimental design in the research presented in this thesis. Based on these, several recommendations will be given for the future research.

6.6.1. MANUFACTURING OF SPOT WELDED JOINTS

Spot flat energy directors (EDs) were used for creating spot welded joints in the research throughout this thesis. Prior to the welding, the 4 mm-diameter spot EDs were manually fixed on the surface of the bottom adherend to be welded. This manual installation is not only labour intensive, but is also less precise for fixing the spot EDs at pre-defined

locations. To help circumvent this issue, some automated technologies, e.g. moulding [2] or 3D printing [3], are expected to be used in future to achieve an integral assembly of EDs on the adherends.

Additionally, the fixation procedure is normally completed by partially melting the periphery of the spot EDs using a Rinco handheld ultrasonic welder with a 5 W power output. The pre-melt tend to introduce more constraints on these points and thus hinder the surface friction during the vibration phase, which potentially slow down the process. As it is a necessary step to fix the spot EDs on the adherends, investigating the influence of attaching the EDs on adherends on the welding process is believed to be helpful for researchers to gain more insights into the ultrasonic welding process.

6.6.2. EXPERIMENTAL DESIGN OF SPOT WELDED JOINTS

The research in this thesis mainly focused on the spot welded joints produced using 4 mm-diameter EDs. The diameter of the final welded area was approximately 10 mm except that for some special cases, e.g. the 2SW-10 and 4SW joints in Chapter 5. However, it must be noted that the size of the final welded area is also associated to the sonotrode cross-section. Therefore, it is interesting to know the influence of the geometry of spot EDs as well as the sonotrode on the final welded area of the joints.

Regarding to the welding process, in order to facilitate a stable welding procedure, only one set of welding parameters, i.e. 1500 N welding force and 60.8 μm peak-to-peak vibration amplitude (for the most frequently used 10 mm-diameter circular sonotrode), was used. A parametric study would be interesting for the future research to investigate the influence of different welding force and amplitude on the weld quality and a processing window would be helpful to the industrialization of ultrasonic spot welding.

With regards to the multi-spot welded joints, the samples in this thesis were only designed with a multi-row, single-column configuration. However, according to the structural design for mechanically fastened joints, the fastener pitch (i.e. the distance between the fasteners in a row) is also an important parameter, affecting the mechanical behaviour of the joints. Hence, the influence of the spot pitch as well as other geometric parameters on the strength of multi-row, multi-column spot welded joints is also expected to be investigated in future research.

REFERENCES

[1] A. Benatar and T.G. Gutowski. Ultrasonic welding of peek graphite apc-2 composites. *Polymer Engineering and Science*, 29(23):1705–1721, 1989.

[2] C. Broek. Optimising ultrasonic welding of carbon fibre pekk composites by investigating integrated energy directors, displacement ceilings and displacement-controlled welding strategies. *Master thesis of Delft University of Technology*, 2015.

[3] T. Kerssemakers. Investigating the use of Fused Deposition Modeling as Energy Director application method for Ultrasonic Welding of Thermoplastic Composites. *Master thesis of Delft University of Technology*, 2018.

ACKNOWLEDGEMENTS

My PhD study and this thesis cannot be completed without the support I received from many people during the past four years. In the end of this book, I would like to express my sincere gratitude to all of those who helped me to achieve this goal.

First of all, I would like to acknowledge my co-promotor as well as my first daily supervisor Dr. Irene Fernandez Villegas. Thank you for your kind help and encouragement with great patience. I still remember the life was tough in the beginning of my PhD but you didn't abandon me. Instead, you were always enthusiastic and energetic on our (little) progress, which provided me numerous confidence on our work. You taught me more than just how to do research independently, but how to be more critical in the way of thinking. Without your great effort and guidance, I can never reach this end. Thank you, Irene!

I would like to thank my promotor Prof. Rinze Benedictus. Thank you for accepting me to become a PhD researcher in Structural Integrity & Composite group and giving me another chance when I failed in my first Go/No Go Meeting. I also want to thank my second supervisors, Dr. Calvin Rans and Dr. Marcias Martinez. Thank you for your precious knowledge and patient guidance on both English writing and presentations.

I am grateful to Gemma. Thank you so much for taking care of all kinds of paper work, including employment contract, hospitality form and travel booking, etc. Franca, also thank you for helping me with the issues about Visa, housing and health insurance, etc.

A substantial amount of experimental work was involved in my thesis, all of which could not be achieved without the help of the technician group and the lab secretary. I would like to thank Marianne, Berthil, Gertjan, Johan, Misja, Bob, Cees, Frans, Fred, Victor, Bart and Lijing for all your kind help and support.

The Aerospace Welding Laboratory was established together with my PhD life by a group of smart, creative and 'crazy' people. I am so proud to be one 'crazy' member of you: Huajie, Genevieve, Nikos, Eirini, Bram, Yannos, Kim and Michiel. Thank you for all the help and jokes in the lab and nice feedback on my presentations and manuscripts. A special thanks to Huajie and Genevieve. Thank you for your selfless help, including the discussion and the guidance on my research.

The wonderful life is always formed by 'crazy' guys together with kind-hearted colleagues and friends. Thank you, Maria, Fabricio and Big Adrian, for forming such a nice and warm office family. Your kind care diminish my scary and transfer me from an isolated person to 'the man from the east'. Megan, Maro, Morteza and Julian, thank you all for joining us and forming a big office together. Our communication brings me so much fun, letting the academic life less boring. In addition, I also want to thank Small Adrian, Andrei, Arianna, Aydin, Bernhard, Chirag, Chelsey, Cornelis, Daniel, Davide, Derek, Dimitrios, Frank, Freek, Freddy, Hans, Ilias, Ilhan, John-Alan, Jesse, Jos, Julie, Kostantin, Leila, Lucas, Luis, Marcelo, Maria Pia, Mayank, Michiel, Nakash, Nat,

Nick, Nicolas, Niels, Nitesh, Otto, Ozan, Paola, Pedro, René, Rob, Roger, Romina, Sofia, Sonell, Sotiris, Vassilis, Vincent, Vincentius, Zahid, and anyone I have forgotten to mention (sorry!) in our group, for all the birthday parties, cakes, dinners, BBQs and jokes. Without you guys, my life in Delft will be black and white. Special thanks go to John-Alan, Pedro and Megan for your helpful comments on several chapters of this thesis and the propositions and to Bram, Niels and Julie for your nice translation. Last but not least, the Chinese Mafia should never be forgotten. Thank you Lei, Hao, Liaojun, Ping, Zhinan, Yuan, Chunsen, Hongwei and Yuzhe for coming to our group. It is my great experience to work with you in Delft. Wandong, although they are always doubting your nationality, I will definitely choose to trust you! Thank you so much for your company and your help on everything.

Thanks to all my friends I met in Delft: Lu Zhang, Yan Ni, Jianting Deng, Liwei Duan, Peng Wei, Cuijie Feng, Xueqing Zhang, Bowei Huang, Gang Liu, Xuedong Zhang, Hongxiao Guo, Lei Xie, Yan Xie, Fan Feng, Minghe Shan, Chuang Yu, Zenan Yang, Jie Zhou, Zixuan Zheng, Yang Lv, Zhi Hong, Yili Mo, Jiachen Zhu, Yupeng Zhao, etc. Thank you for appearing in my life and making it so colourful.

Last, but most importantly, I would like to express my greatest gratitude to my family. Without their support, it is impossible for me to survive in a foreign country, regarding less to finish the PhD study. Thank you my parents and my grand-parents to contribute everything you have to support my study. It is a great honour to be your son and grandson! Thank you my sister for companying and taking care of our parents when I was absent. Finally, I would like to thank my girlfriend, Qi. For me, you are a miracle. People can hardly understand the difficulties on dating with a guy from 8000 km away combined with a time difference of 7 hours for two years, but YOU MAKE IT! Your endless love, understanding and encouragement are like the lighthouse at night, showing the home path for me, a sailing in an enormous ocean. Thank God Allah for bringing you to me.

CURRICULUM VITÆ

Tian ZHAO

The author was born on the 26th of September 1987, in Yangquan, Shanxi Province, China. After graduating from high school in 2006, he moved to Beijing and entered China University of Mining & Technology (Beijing), Faculty of Mechanics and Civil Engineering. The author obtained his Bachelor degree in Engineering Mechanics in 2010 and subsequently started his study as a master student in the same university without entrance examination. He worked on the numerical and experimental investigations of the mechanical behaviour of glass fibre reinforced epoxy matrix composites under the supervision of Prof. dr. H.W. Zhou. In 2013, he got his Master degree in Engineering on the topic: the effects of environmental moisture on the mechanical performance of glass fibre reinforced epoxy composites. In the same year, he started his PhD research at Delft University of Technology, Faculty of Aerospace Engineering, Structural Integrity & Composite research group in mid October, with the sponsorship of China Scholarship Council. Under the supervision of Prof. dr. R. Benedictus as promotor and Dr. I. F. Villegas as co-promotor and daily supervisor, he focused on the investigations of manufacturing and mechanical characterization of ultrasonic spot welded joints in thermoplastic composites. The results of this work are presented in this thesis. Since October 16, 2017, the author was appointed as a researcher in the same group.

LIST OF PUBLICATIONS

JOURNAL PAPER

3. **T. Zhao**, I. F. Villegas, C. Rans and R. Benedictus, *A study on the effect of various geometric parameters on the mechanical behaviour of multi-spot welded single-lap joints in thermoplastic composites*, to be submitted to Composite Part B: Engineering.

2. **T. Zhao**, C. Broek, G. Palardy, I. F. Villegas and R. Benedictus, *Towards robust sequential ultrasonic spot welding of thermoplastic composites: Welding process control strategy for consistent weld quality*, Composite Part A: Applied Science and Manufacturing, **109**, 355-367 (2018).

1. **T. Zhao**, G. Palardy, I. F. Villegas, C. Rans, M. Martinez and R. Benedictus, *Mechanical behaviour of thermoplastic composites spot-welded and mechanically fastened joints: A preliminary comparison*, Composite Part B: Engineering **112**, 224-234 (2017).

CONFERENCE PAPER

3. **T. Zhao**, I. Tsakoniatis, C. Rans, I. F. Villegas and R. Benedictus, *Multi-spot ultrasonic welding of thermoplastic composite single-lap joints: effect of overlap length and number of spots on weld strength*, to be submitted to the 18th European Conference on Composite Materials (2018), Abstract accepted.

2. **T. Zhao**, G. Palardy, I. F. Villegas and R. Benedictus, *Towards high-quality multi-spot welded joints in thermoplastic composite structures*, in: Proceedings of the 21th International Conference on Composite Materials (2017).

1. **T. Zhao**, G. Palardy, I. F. Villegas, C. Rans and R. Benedictus, *Comparative analysis of in-plane and out-of-plane mechanical behaviour of spot welded and mechanically fastened joints in thermoplastic composites*, in: Proceedings of the 17th European Conference on Composite Materials (2016).